Conjugate volcanic passive margins in the austral segment of the South Atlantic – Architecture and development

François Chauvet, François Sapin, Laurent Geoffroy, Jean-Claude Ringenbach, Jean-Noël Ferry

Conjugate volcanic passive margins in the austral segment of the South Atlantic – architecture and development

François Chauvet[a,b], François Sapin[c], Laurent Geoffroy[b], Jean-Claude Ringenbach[c], Jean-Noël Ferry[c]

[a] SEDISOR, IUEM, 29280 Plouzané, France

[b] Univ Brest, CNRS, IUEM, UMR 6538 Laboratoire Géosciences Océan, Place Nicolas Copernic, 29280 Plouzané, France

[b] TOTAL SA, CSTJF, Pau

Abstract

The thorough interpretation of the South Atlantic long offset seismic lines provides a new view of the magmatic and crustal architecture and of the evolution of the conjugate volcanic passive margins (VPM) along the austral segment of the South Atlantic Ocean. In this study, we make the synthesis of previously published and unpublished seismic profiles that are reinterpreted consistently, and, for the first time, displayed in a conjugate view. The seaward dipping reflector sequences (SDR) expose here three main structural types (inner, outer and intermediate) that can be distinguished based on both the curvature of the reflectors and the topography displayed at their downdip terminations. We observe a specific correlation between the thinning profile of the crust and the geometric attributes of SDR. This correlation suggests a genetic relationship that is discussed in-term of rheological evolution of the crust during the magma-assisted lithospheric break-up. The South Atlantic margins architecture also featured a moderate but significant asymmetry, with a relative difference estimated to about 60% for the margin width, the total volume of SDR and their spatial distribution. A change toward a more symmetric architecture is however observed when approaching the highly magmatic area of conjugate Walvis Ridge and Rio Grande Rise. The influence of the pre-rift inheritance, the mode of rifting and the coeval mantle dynamic are put into balance to explain this global architecture. In the asymmetric domain, the extrusive sequences show evidences for westward rift jumps that participate to develop a wider margin on the African side. We propose that an asymmetric thermal structure controlled by the profile of the lithosphere asthenosphere boundary may have promoted the formation of a wider African margin. The focusing of the last rift axis is associated to the development of the thickest SDR wedges above an ultimate necking zone of the crust. Conversely to the early stages of the rift which appears

segmented and diachronous, the final localization of the tectono-magmatic activity appears coarsely synchronous, at least, along the northern half of the austral segment. A further higher thermal gradient than elsewhere associated to a thicker and a weaker preexisting continental crust and a more intense magmatic input is inferred to have promote the development of symmetric and very wide conjugate margins close to the Walvis Ridge and Rio Grande Rise.

1. Introduction

The SE-Brazil/Uruguay and Namibia conjugate Volcanic Passive Margins (VPM) developed during the opening of the South Atlantic Ocean austral segment (Fig. 1) and the emplacement of the Early Cretaceous Paraná-Etendeka Large Igneous Province (LIP; Hinz, 1981; White and McKenzie, 1989; Courtillot et al., 1999; Buiter and Torsvik, 2014; Foulger, 2018). As elsewhere, the development of these VPM is related to the formation of a set of spectacular wedges of seaward-dipping reflectors sequences (SDR). Where outcropping (eastern and western Greenland) or drilled (ODP 642 Norway, Kudu and Murombe wells in Namibia; Florianópolis High in SE Brazil), the SDR consist of subaerial volcanic flows interbedded with minor volcano-detrital and continental sediments (Planke et al., 2000; Larsen et al., 1998; Wickens and McLachlan, 1990; Bueno et al., 2007).

Two main conceptual models are invoked in the formation of VPM. The SDR structure would be controlled by a system of landward dipping detachment faults (Clerc et al., 2015; Geoffroy, 2005; Geoffroy et al., 2015) or by flexural subsidence from each side of a magmatic spreading axis (Mutter et al., 1982; Buck, 2017; Morgan and Watts, 2018). The first model implies the volcanic wedges are contemporaneous with the syn-rift necking and thinning of the continental basement. The second implies that most of the SDR wedges is the post-rift product of an in-excess magmatism associated to spreading and continental drift.

Previous studies on Namibia and Uruguay/Brazil VPM have essentially identified the successive SDR wedges and characterized their along-strike segmentation (Clemson et al., 1997; Hinz et al., 1999; Franke et al., 2007, 2010; Koopmann et al., 2014a). Thanks to the recent high quality deep multi-channel seismic profiles, the imaging of both the base of the crust, the crustal fabric and the SDR internal organization can be approached (Stica et al., 2014; Clerc et al., 2015; Geoffroy et al., 2015; McDermott et al., 2015, 2018; Reuber et al., 2019; Suppl. Mat. Table I). The quality and density (50-100km of spacing, Fig. 1) of these datasets offer an opportunity to evaluate the organization of the SDR structure both along dip and strike directions, allowing to perform a

precise mapping of their architecture and to discuss first order elements such as the along-dip crustal deformation and the along-strike propagation of the lithospheric break-up.

Similarly to other margins (Sapin et al., accepted), the structural evolution of VPM may be impacted by many different factors such as rheological heterogeneities (Callot et al., 2002; Gac and Geoffroy, 2009), the thermal architecture of the lithosphere (Simon et al., 2009; Armitage and Collier, 2018), the rift history (Armitage et al., 2010; Guan et al., 2018), the structural inheritance (Franke et al., 2007; Corner et al., 2002; Chenin et al., 2015; Petersen and Schiffer, 2016; Peace et al., 2018; Phillips et al., 2018; Reuber & Mann, 2019), the kinematic and obliquity of the rift system (Schiffer et al., 2019; Brune et al., 2018), the buoyancy forces (Bellhasen et al., 2013) and the mantle drag on the lithosphere (Clerc et al., 2018; Jolivet et al, 2018).

The development of a significant asymmetry in conjugate VPM architecture has been pointed out in several places (Eldholm et al., 2000; Mohriak et al., 2002; Mohriak & Fainstein, 2012; Becker et al., 2014). It has generally been related to similar mechanisms observed in magma-poor margins, such as crustal-scale detachment fault in a simple shear mode of deformation (Blaich et al., 2009; Becker et al., 2014, 2016), rift jumps (Buck, 2017; Norcliffe et al., 2018), or to asymmetric magmatic accretion (Reuber et al., 2019).

In this paper, we focus on a rigorous description of: the SDR wedges, the crustal thinning profile and the tectonic structures observed within the crust, on both conjugate margins. The internal structure of SDR is described and used to re-qualify the « Inner » vs. « Outer » usual nomenclature introduced by Planke et al. (2000). The evolution of the shape and of the thickness of SDR are analyzed and mapped out together with the shape and architecture and the deep crustal reflections (lower crustal package, Moho reflection(s), etc.).

The integration of the crustal structure and the SDR packages organization together within a comprehensive synthesis on the pre-rift inheritance of the austral South Atlantic domain puts the basis of a re-evaluation of the primary factors controlling its opening, the rheological behavior of the crust and the apparent asymmetry of the finite architecture of these margins.

2. Geological setting

The studied conjugate VPM developed between the Agulhas-Falkland (AFFZ) and Florianópolis (FFZ) Fracture Zones, as the result of the SW Gondwana break-up and opening of the austral segment of the South Atlantic Ocean (Moulin et al., 2010; Fig. 1). This ocean opened between the Rio de la Plata (RdlP), Kalahari and Congo cratons and throughout two generations of orogenic belts: the Late Precambrian Pan-African/Brasiliano belts to the north and the Late

Paleozoic Gondwanides to the south, comprising the Ventana and Cape Foldbelts (Figs. 2 & 3a; Pangaro & Ramos, 2012; Paton et al., 2016). The break-up axis is strongly oblique to the E-W compressive structures of the Gondwanides and to the NNE-SSW trending structures of the Pan-African Damara Belt. But elsewhere, the break-up axis appears as coarsely parallel to the N-S structural grain of the Pan-African/Brasiliano orogenic belts (de Wit et al., 2008; Fig. 3a).

The austral South Atlantic opening is contemporaneous with Early Cretaceous voluminous magmatism found onshore, in conjugate dykes swarms (Fig. 1; Almeida et al., 2013; Will et al., 2016; McMaster et al., 2019), a set of intrusive centers identified onshore Namibia (Corner et al., 2000, 2002) and in the Paraná and Etendeka continental flood basalts (Peate et al., 1992; Turner et al., 1994). Offshore, this magmatism was drilled at the top of the high-frequency seismic reflectors packages forming the so-called sequences of SDR (Hinz, 1981; Wickens and McLachlan, 1990; Gladczenko et al., 1997, 1998; Hinz et al., 1999; Franke et al., 2007; Koopmann et al., 2014a; Soto et al., 2011; Stica et al., 2014; Gordon et al., 2017; Fig. 2).

Assuming the geological time scale of Gradstein et al. (2012), the magnetic anomalies identification ascribed to the oceanic crust domain by previous works (Fig. 2) suggests that drift of conjugate plates initiated around 135 Ma (Late Valanginian/Early Hauterivian times) north of the AFFZ (M11 anomaly for Hall et al., 2018; M10r anomaly for Collier et al., 2017) and around 129 Ma (M2 anomaly) south of the Rio Grande Rise/Walvis Ridges (Franke, 2013; Collier et al., 2017; Fig. 2), meaning a 6 Myr northward propagation along a nearly 2500 km long segment.

The Rio Grande Rise (RGR) and Walvis Ridge (WR) form conjugate volcanic plateaus that lies on an anomalously thick crust (20-25 km in Fromm et al., 2017; Graça et al., 2019) where some relicts of continental basement were recovered (e.g. Foulger, 2018; Graça et al., 2019). They are classically considered as the remnants of the post-breakup continuation of the excess of magmatism related to the trail of the Tristan da Cunha plume (Fig. 1, O'Connor and Duncan, 1990; Peate et al., 1990; Ryberg et al., 2015).

North of the RGR/WR, the oceanic realm developed entirely within the Cretaceous Magnetic Quiet Zone, posterior to 126 Ma M0 anomaly (Moulin et al., 2010; Collier et al., 2017). In this central segment of the South Atlantic, the onset of the seafloor spreading is considered as Late Aptian, around 112-113 Ma, following the deposition of the salt province (Karner & Gambôa, 2007; Torsvik et al., 2009; Moulin et al., 2010; Perez-Diaz and Eagles, 2014). This indicates over 16 Myr delay for the connection between the tip of the austral and the central segments of the South Atlantic. This delay is accommodated both in the buffer zone of the Santos Basin (Fig. 2, Moulin et al., 2013) and in the highly magmatic conjugated segments of the WR/RGR (e.g. Stica et al., 2014).

2.1. Pre-rift basement

2.1.1. Proterozoic orogeny

The Pan-African/Brasiliano orogenic belts cover the northern two third of the austral South Atlantic continental margins. They outcrop in the Kaoko, Damara, Gariep and Saldania belts in Africa, and along the Dom Feliciano, Ribeira and Araçuaí belts in South America (Fig. 3a). The Pan-African/Brasiliano orogenic axes form a « triple junction » characterized by the NNW-trending belts along the Cretaceous margins (Brasiliano, Kaoko and Gariep belts) and a NE-trending arm across the Africa (Damara, Zambezi, Mozambique and Lufilian arc belts; Gray et al., 2008, Miller, 2013).

These mobile belts developed during the Neoproterozoic-Cambrian amalgamation of the Gondwana and the eastward subduction of the Adamastor Ocean (Heilbron et al., 2008). The Precambrian tectono-stratigraphic units involved in these orogenic belts can be correlated on either side of the South Atlantic (Fig. 3a). They include a long-lived and huge calc-alkaline continental magmatic arc, a wide back-arc basin and the inverted sequences of the passive margins developed on the fringes of the Congo, Kalahari and Rio de la Plata cratons (Fig. 3a; Gray et al., 2008; Frimmel et al., 2013; Heilbron et al., 2008, 2017; Oriolo et al., 2018; Basei et al., 2018). The widespread post-collisional magmatism and the presence of some metamorphic core complexes testify of a possible NS extensional collapse of the belt between the Cambrian and the Ordovocian (Heilbron et al., 2008; Goscombe et al., 2018; Hueck et al., 2018; Lehmann et al., 2016).

The main oceanic suture would be located on the American side (Fig. 3a) and, according to the works of Frimmel et al. (2011 & 2013), Will et al. (2014) and Will & Fimmel (2018), the South Atlantic Ocean would opened preferentially through the relics of the closed back-arc basin located south of the Kaoko belt. But, northward, the break-up axis cut through the huge magmatic arc (Fig. 3a).

2.1.2. Paleozoic to Jurassic

Following the Precambrian orogeny, Cambrian to Jurassic sedimentary successions were deposited in subsiding areas (Congo, Paraná & Chaco-Paraná, Karoo basins; Milani et al., 2007; Linol et al., 2015). Along the southwestern fringe of the Gondwana, the coeval sequences deposited in a back-arc setting during the subduction of the Panthalassa Ocean beneath the SW Gondwana (Claromeco, Ventana, Cape basins; du Toit, 1937; Milani & de Wit, 2008; Pankhurst et al., 2006; Uriz et al., 2011, 2016; Tankard et al., 2012; Lovecchio et al., 2020). These basins were then inverted in the Permian forming the Cape and Ventana Fold Belts which represent the northern front of the Gondwanides orogeny (Fig. 3a; Hansma et al., 2016).

During the Early-Middle Triassic, a set of localized rifted basins develop further North, along a coarsely E-W trending transtensional corridor which reactivated pre-Cambrian orogenic structures including those of the Damara Belt (Daly et al., 1989; de Wit et al., 1988; Zerfass et al., 2005). In the Waterberg Basin in Namibia, the coeval syn-rift successions do not exceed 700m, demonstrating a very limited stretching (Fig. 3b; Wanke et al., 2000; Smith and Swart, 2002).

From the Triassic up, a global aridification led to development of a giant desert through SW Gondwana. The Botucatu and Etjo fluviatile and aeolian sands are found beneath and intercalated at the base of the Paraná and Etendeka flood basalts (Jerram et al., 1999, Waichel et al., 2006). These sands are inferred to be Jurassic to Early Cretaceous in age (e.g. Wanke et al., 2000; Milani et al., 2007).

2.2. Mesozoic rifting

Several rifted basins are found along the southern half of the austral South Atlantic margins: the Outeniqua, Malvinas, North Falkland, San Jorge, Rawson, Valdes, Colorado, Salado and Punta del Este basins (Fig. 3b). These early basins trend obliquely to the South Atlantic axis and are related to polyphase Jurassic extensional events that predate the South Atlantic margins development (e.g. Franke, 2013; Frizon de Lamotte et al., 2015; Lovecchio et al., 2018 & 2020). The trend of these early rifts is strongly controlled by pre-existing orogenic structures (Fig. 3b; Jacques, 2003; Pangaro and Ramos, 2012; Chernicoff et al., 2014; Franke, 2013; Autin et al., 2013; Salomon et al., 2017; Lovecchio et al., 2018; 2020). For instance, the Salado and Punta del Este basins are localized along a 2.1 Ga suture zone embedded within the Rio de la Plata Craton (Reuber and Mann, 2019; Fig. 3b). The undated syn-rift volcano-sedimentary units infill WSW-ENE-trending half-grabens which may exceed 6km in thickness (Stoakes et al., 1991; Tavella and Wright, 1996; Ucha et al., 2004; Tugend et al., 2018).

The South Atlantic rift is classically presented as ranging from Late Jurassic/Early Cretaceous to Hauterivian and the post-rift deposits as starting in the Barremian (Jungslager, 1999; McMillan, 2003; Cartwright et al., 2012; Broad et al., 2012). This timing was mainly defined in the poorly developed grabens and hemi-grabens, trending parallel to the margin along the South Africa and southern Namibian shelves (Fig. 3b). The associated syn-rift infill is less than 3 km thick (McMillan, 2003). The top of the syn-rift successions is dated Valanginan-Hauterivian (140-130 Ma; McMilan, 2003, Broad et al., 2012) and the base was never drilled. Off South Africa, these successions consist in continental sediments (fluvial claystones, sandstones, and pebble beds), volcaniclastics, and volcanics in places (Broad et al., 2006; McMillan, 2003).

On the Argentina conjugate margin, Franke et al. (2007) note the lack of major rift structures developed in the upper crust. Northward in Uruguay-Brazil, syn-rift structures are also poorly developed and form small basins of about 1 km thick (Stica et al., 2014; Morales et al., 2017; McDermott et al., 2018). The major part of the Pelotas basin (Fig. 2) would thus be floored by the Dom Feliciano basement and the Pelotas batholith. The Permo-Triassic pre-rift sequences of the Paraná Basin were however drilled at the base of the Punta Del Este rift and in the northern part of the Pelotas Basin (Verovlasky et al., 2004; Bueno et al., 2007; Stica et al., 2014).

2.3. South Atlantic VPM development

The most conspicuous phase for South Atlantic magmatism corresponds to the emplacement onshore and in a very short time of the Paraná-Etendeka traps: 131-133 Ma according to Renne et al. (1992, 1996a, b) recently reevaluated to 134-135 Ma by Baksi (2018). Onshore Namibia, the Etendeka traps lie either on Karoo sediments or directly on the Damara basement, indicating that the Karoo cover was largely eroded before the Cretaceous events (Dauteuil et al., 2013). The widespread Paraná Traps reach about 2 km in the central part of the Paraná Basin. The volcanic sequences pinch-out toward the South Atlantic margins where Precambrian rocks crop out near the coastline (Bueno et al., 2007; Gordon et al., 2017).

A younger and voluminous magmatic activity is evidenced in the same area. The different generations of dyke swarms that outcrops in Namibia and SE Brazil (Fig. 2) span from 135 to 113 Ma (e.g., Almeida et al., 2013, Will et al., 2016). The recent works of Will et al. (2016) and McMaster et al. (2019) document the petrogenetic evolution between three main generations of tholeiitic dykes. The two older generations exhibit very similar compositions with the Parana-Etendeka basalts and would be contaminated by an enriched component (lithospheric mantle or continental crust). By contrast, the younger generation of dyke shows a more 'primitive' composition deriving from a depleted asthenosphere source. These results suggest the progressive thinning of the lithosphere between 135 and 113 Ma (Will et al., 2016; McMaster et al., 2019). Offshore, the seaward dipping volcanic sequences drilled in the northern part of the Pelotas Basin range from 125 to 118 Ma (Fig. 2, 1-RSS-003 well in Bueno et al., 2007) and up to 113 Ma on the Florianópolis High (Curumim Fm., Dias et al., 1994; Bueno et al., 2007; Gordon and Mohriak, 2015; Stica et al., 2014). A Late Aptian age was also obtained on basaltic flows erupted on the northern flank of Walvis Ridge (Fig. 2, 114 Ma, Rohde et al., 2013).

SDR wedges are found almost all along the conjugate margins of the austral South Atlantic (Fig. 2). Subaerial basalts were drilled off Namibia (Kudu wells in Fig. 2, Wickens and McLachlan, 1990; Clemson et al., 1997), at the top of inner SDR. Only the southernmost segment of South

Atlantic margins appears free of SDR (Fig. 2; Koopmann et al., 2014a, b). The pioneer works on seismic data covering the Atlantic VPM (Gladczenko et al., 1997, 1998; Clemson et al., 1997; Abreu, 1998; Hinz et al., 1999) suggest that SDR sequences form a coarsely continuous band of about 100 km wide all along the austral South Atlantic margins. Gladczenko et al. (1998) propose a wide (>100 km) Late Jurassic–Early Cretaceous volcano-sedimentary rift zone covered by the SDR. In Namibia, Bauer et al. (2000), using reflection and refraction seismic data, identify two main wedges of seaward-dipping reflectors separated by flat lying flows sequences. The available refraction data and gravity modelling show the existence of high-velocity and dense lower crust beneath the SDR sequences (Bauer et al., 2000; Blaich et al., 2009, 2011, 2013, Schnabel et al., 2008; Hirsch et al., 2009; Becker et al., 2014; Fromm et al., 2017; Planert et al., 2017).

Franke et al. (2007, 2010) in Argentina, Soto et al. (2011) in Uruguay, Stica et al. (2014) in SE Brazil and Koopmann et al. (2014a) in South Africa and Namibia emphasize a significant along-strike segmentation of the margin and of the earliest volcanic successions. Franke et al. (2007) divide the Argentina margin in three main segments that would be bounded by the Falkland, Colorado, Ventana and Salado transfer zones (Fig. 2). Soto et al. (2011) introduce the Rio de la Plata transfer zone (RPTZ) that lies between the Punta del Este Basin and the Polonio High (Fig. 2). Northward, Stica et al. (2014) divide the Pelotas Basin into three segments whom the boundaries locate coarsely in the continuation of the oceanic fracture zones: Meteor FZ (for the RPTZ), Chuí FZ, Porto Alegre FZ and the Florianópolis FZ (Fig. 2).

In Argentina, Franke et al. (2007) observed significant lateral offset in SDR distribution from each side of the previously quoted transfer zones. The authors observed that the width and volume of SDR tend to decrease from S to N, within each individual margin segment. They further proposed that South Atlantic break-up propagated by successive jumps, each transfer zones acting as rift propagation barriers. In their view, the decreasing in SDR width from S to N in each segment would sign a passive decompression of the mantle rather than the direct influence of a mantle plume. Franke (2013) hence proposes three successive breakup events at ~137 Ma between the Falkland TZ and Colorado TZ, 133 Ma between the Colorado and Salado TZ and 128 Ma for the segment north of the Salado TZ.

Conversely, in SE Brazil, Stica et al. (2014) observed a net increase in thickness and width of SDR toward the north. They also argue for a strongly diachronous and segmented opening between the Salado TZ and the FFZ. They note that the M2 and M0 anomalies rest on oceanic crust south of the Chui FZ, that only the M0 rest on the oceanic crust south of the Porto Alegre FZ (PAFZ in Fig. 2). They finally propose that the rifting of the northernmost segment between the PAFZ and the FFZ lasted much longer, at least till the end of Aptian. The Ar-Ar age of 113 Ma obtained on the

last SDR sequence of this northernmost segment indeed suggests a slower evolution of the rifting (Stica et al., 2014).

On the conjugated margin, Clemson et al. (1997), Blaich et al. (2011 & 2013) and Koopmann et al. (2014a) observe that gravity and magnetic data and the thickness and distribution of SDR are also influenced by transverse-to-the-margin fractured zones, called, from S to N: Hope, Namaqua, Orange, Lüderitz, Oystercliffs, Cape Cross and Walvis (Fig. 2). These transfer zones correspond to inherited structures which are reactivated during rifting and SDR emplacement (Clemson et al., 1997; Koopmann et al., 2014a; Corner et al., 2002; Corner and Durrheim, 2018). In line with the Autseib and Omaruru major Pan-African structures, the Cape Cross TZ offsets the landward boundary of SDR of about 160km (Fig. 2). The line of onshore intrusive complexes Brandberg, Messum, and Cape Cross are also emplaced along these reactivated structures (Figs. 2 & 3b). The Orange TZ also significantly offsets the proximal structures of the Namibian margin. This transverse structure was tentatively correlated to an inherited structure, the Kuboos-Bremen lineament, by Clemson et al. (1997).

3. Data & methods

In order to constrain the 3D architecture of the conjugate South Atlantic VPM, we reinterpreted 2D ION GXT long-offset seismic profiles (Fig. 1 and Suppl. Mat. Table I) and additional 2D seismic surveys (Fig. 1) provided by TOTAL S.A. to pick the key horizons of the Moho, the base- and the top-SDR.

The primary picking/mapping is done in the time domain of the seismic datasets. Regional time-depth conversion laws were used to build isopach maps on each conjugate margin. In Uruguay-Brazil this conversion law was built using a 3D-seismic survey from TOTAL S.A. It consists in : $Z = 0.843.t + 1.46^{-4}.t^2$ (with Z equal to the depth below seabed and t equal the tow-way travel time below the seabed). The extrapolation of this law to the entire Uruguay-Brazil margin generates some deviations of less than 3 km in depth for the Moho and the base SDR relatively to the same horizons determined on pre-stack depth migrated (PSDM) dataset from ION Geophysical. We consider these discrepancies as suitable to analyze the first-order architecture of the margin. In Namibia, the time-depth conversion law corresponds to a 5-layers model that was compiled to fit perfectly both the Moho and the top-SDR horizons from the PSDM sections from ION Geophysical.

The thickness maps of the crustal basement and of the SDR define the first-order architecture of conjugate margins. Due to the variable qualities of the seismic data, the Moho and

base-SDR horizons have only been determined in Namibia and Uruguay-SE Brazil. But the facies and internal structure of SDR were also mapped in the Argentina and South Africa conjugate margins.

The Moho interface was coherently picked as lying below the deepest powerful reflections that lie at the crust base of the studied margins. The available refraction data were used to control our interpretation, especially for the Moho picking. A maximum of 4 km of difference is met between our interpretation of the Moho depth and those inferred from the available refraction data in Namibia (Bauer et al., 2000; Fromm et al., 2017). This difference was checked on five crossovers between studied lines and the published refraction lines. No refraction data is currently available along Uruguay/SE Brazil margin.

The GPlates (2.1.0) software (Müller et al., 2018) was used with the paleogeographic model of Moulin et al. (2010) in order to locate the conjugate profiles (Fig. 2), and to better assess the tectono-stratigraphic variability along strike before break-up. The Moulin et al's (2010) rotation poles were preferred mainly because they honor the intra-oceanic fractures zones. Moulin et al.'s (2010) reconstitution use microplates which boundaries perfectly match with the main transfer zones recognized such as the RPTZ (Fig. 3a & 2). The Moulin et al.'s model generates also the tightest fit between the oceanic fracture zones and magnetic marginal anomalies. We further observe that the Gondwanides northern orogenic front fit perfectly using this reconstitution (see Fig. 3a). It is convenient to note that the use of other palinspastic reconstructions can lead till up to 150 km of latitudinal offsets between these different features.

Based on our GPlates reconstruction, three conjugate seismic profiles are selected to represent the conjugate architecture of the southern, central and northern segments (# IV, V & IV in Fig. 2) of the Uruguay/SE Brazil and Namibian margins (Figs. 4 to 6, see also the reconstruction in the inset map in Fig. 7). The Moho, Base-SDR and Top-SDR are reported together with the internal fabric of both the crustal basement and of the intra-SDR reflections. Interpretations obtained on depth-converted seismic profiles are reported in the Fig. 7 for the entire 2D survey as plotted on the inset maps in Fig. 7.

The quality of the seismic data varies between the Uruguay-SE Brazil and Namibian lines. In general, intra-basement reflectivity is poorer in Uruguay-Brazil. Moreover, the thick post-rift sedimentary wedge of the Rio Grande Cone affects the seismic resolution of the deepest level of the margin (e.g. Line 040 in Fig. 5a). Such sedimentary features decrease strongly the accuracy of the base-SDR determination and the analysis of their internal reflectivity.

In both margins, the base-SDR is the most difficult interface to interpret. This is particularly true for the base of the innermost SDR which is often diffuse and badly defined, even more when it

rests on a roughly concordant seismic unit (e.g., line 6000, Fig. 6b) or in an intensively injected basement (e.g., line 6050, Fig. 7). Considering the difficulties to distinguish SDR from the underlying strongly intruded pre-rift basement, our interpretation was primarily guided by the geometric relationships. All seismic units mapped as SDR exhibit clear lateral variations of thickness (blue sequences in Figs. 4 to 7). When they occur, the underlying sequences of which the lateral variations of thickness are really equivocal are reported in dotted blue lines in interpretations (Figs. 4 to 7). Seismic units that do not show lateral variations of thickness are considered as pre-rift and reported in purple. The syn-rift reflector sequences that lie on the proximal continental shelf and which are disconnected from the SDR domain are reported in green. The reflections crosscutting the surrounding basement fabric, a layered sequence or the Moho are interpreted as magmatic injections (red lines in Figs. 4 to 6) or major faults. It is however highly likely that the SDR sequences comprise a large amount of intrusions.

4. Thinning profile of the crust

The crustal architecture of the South Atlantic conjugate VPM was identified on the basis of first order features that represent analogous elements on the conjugate profiles (Fig. 8). One of the most prominent conjugate structure is the seaward flexural hinge displayed by the top basement (Figs. 4 to 7). This key structure, called the Necking Line (NL, Fig. 8), corresponds to the onset of the significant thinning of the continental crust (Fig. 7 & 9a) and coincides almost everywhere with the landward edge for the successive SDR packages (Fig. 7). Morphologically, the NL is marked by a wavecut surface in the continent side (Fig. 4 to 7). Seaward, the thinned continental basement is almost entirely caped by SDR (Figs. 7). In that sense, the SDR domain marks the transition between the thick proximal continental crust and the thin distal crust (Fig. 8).

Moreover, when integrating the topography of Moho, the resulting crustal thickness profiles appear divided in different domains. Each of these crustal domains is delimited by more or less conspicuous inflexions of the slope of the Moho, the Proximal and Distal «Moho hinge lines » (PMHL and DMHL in Figs. 4 to 8). These Moho hinge lines are used to delimit the crustal domains namely Proximal Domain, Proximal Necking, Thinned Domain, Distal Necking and Distal Domain (Fig. 8). It is noteworthy this terminology is essentially descriptive here and only related to the main Moho hinge lines that are observed on the studied seismic lines. Therefore, it does not made references to the nomenclature developed for magma-poor passive margins, or to the associated specific tectonic processes (Jammes et al, 2009; Mohn et al., 2010; Sutra et al., 2013; Tugend et al., 2015). Also, in some locations, additional MHL lie between the distal and proximal necking areas.

These intermediate MHL are also mapped and described, to be as accurate as possible (Figs. 7 & 9b).

4.1. Proximal Domain

The seismic image of the Proximal Domain informs us on the pre-rift crustal basement thickness and fabric. In Namibia, the thickness of the most proximal continental crust varies from 22 to 43 km (Fig. 9a). A domain of particularly thin crust is located between the Cape Cross and Lüderitz segment boundaries. There the crust ranges between 22 and 26 km in thickness (from lines 5000 to 6050 in Fig. 7). In southern Namibia and off the Gariep Belt, the continental crust recovers a more classical 30-36 km thickness.

In Uruguay-Brazil, the continental crust ranges from 32 to 35 km thick all along the Proximal Domain. However, the proximal crust in the southern part of the Pelotas Basin is not covered by the data (Fig. 9a). North of the CFZ, the continental crust thickened over 40km and its base is not imaged by the seismic data (lines 90 in Fig. 4a & line 70 in Fig. 7).

The conjugate profiles indicate, thus, that the crust tends to thicken when approaching to the northernmost segment of the studied margins. They also show that the Proximal Domain is never associated to a significant thinning of the crust (Fig. 7).

4.2. Proximal Necking

In both conjugate margins, the Proximal Necking is marked by a conspicuous convergence of the top-basement and the Moho (Figs. 4 to 7). The NL as previously defined is most often located within the Proximal Necking domain and in general close to onset of Proximal Necking (Fig. 9b). At the end of the Proximal Necking, the Moho's slope evolves from landward dipping to a flat or gently landward dipping slope. This inflexion (PMHL 2) is more tenuous and not systematically observed, especially on Namibian side (Fig. 7). But it is particularly noticeable on the southern Namibian and Uruguayan margins (Figs. 6 & 7).

This inner necking most often coincides with the onset of the SDR (Fig. 7), however it tends to be more landward south of the RPTZ-Lüderitz conjugated transfer zones. Here, the thinning of the crust onsets prior to the SDR domain (Fig. 9b & lines 6500, 7000, 7500 in Fig. 7) and the Proximal Necking is located beneath the proximal rift structures. The most obvious example lies on the line 7500 where the continental crust thins from 40 to 30km before the NL and the onset of SDR (Fig. 7). This thinning lies beneath a seaward dipping major fault which bounds a small half-graben developed at the top of the crust (2-3 km thick). This extension is associated with a local crust

thinning of about 5 km (Fig. 7). A similar configuration is observed into the conjugate Punta del Este basin (Fig. 9b and line drawing from Tugend et al., 2018, in Fig. 7). Here the syn-rift succession reaches up to 6-7 km and its age is unknown but supposedly Upper Jurassic/Lower Cretaceous (Tavella and Wright, 1996; Ucha et al., 2004; Morales et al., 2017; Lovecchio et al., 2018; Tugend et al., 2018). This likely early rift offsets the Proximal Necking and the NL from about 120 km relatively to the northernmost segments of the margin (Fig. 9b).

4.3. Thinned Domain

Seaward of the Proximal Necking, the crust never exceeds 22 km and is most generally lower than 15 km. With the exception of the northern area, the South American margin presents a narrow Thinned Domain (inexistent to 60 km between the RPTZ and PAFZ) and the Namibian side possesses a wide Thinned Domain of 50 to 170 km within the segments III to V (Fig. 2). In the northernmost segment VI, it is much more extended, forming a domain from 200 to 340 km wide (Fig. 9b) on both sides.

In Namibian northern segments (V & VI), noticeable changes of the slope of the Moho lie beneath the Thinned Domain. These slights inflexions of the Moho are distinguished as "intermediate hinge lines". They were tentatively distinguished on northern Pelotas Basin profiles but are less noticeable there (Lines 70 – 90 in Fig. 7 and Fig. 4a). In map (Fig. 9b) this intermediate ramp of the Moho merges with the DMHL 1 toward the south, and this, on both conjugate margins. Intermediate Moho hinge lines are also observed on the conjugate southernmost segments (III, Figs. 7 & 9b). In Uruguay, they lie between the Punta del Este Basin and the SDR wedges. In this segment the proximal rift structures testify that the crust undergone a significant stretching landward of the SDR domain (Tugend et al., 2018; Fig. 7). In such configuration, the Proximal Necking records an earlier rifting stage and the intermediate MHL record the syn-SDR thinning of the crust.

4.4. Distal Necking

The DMHL 1&2 delimit a significant necking of the crust in the outer domain of the margin (Figs. 7 & 8). The DMHL 1 corresponds to a significant increasing, sometimes abrupt, in the slope of the Moho toward the Distal Domain (Fig. 6a-b, 5b). In Uruguay, the average slope of the Moho is close to 3-4° beneath the Thinned Domain and increases brutally to reach between 10 and 15° in the Distal Necking (lines 4500 & 4700 in Fig. 7). In Uruguay-SE Brazil, South of the PAFZ, the onset

of the Distal Necking is located between 60 and 140 km from the NL (Fig. 9b). In Namibia, it lies further offshore, between 120 to 340 km from the NL.

The outermost Moho slope inflexion (DMHL 2) is the most conspicuous one and lies between the Distal Necking and the Distal Domain (Fig. 8) which is characterized by either a sub-horizontal Moho or a downward bulge-like topography (Figs. 5 to 7). The DMHL 2 is less noticeable toward the north and the conjugate Florianópolis High-Walvis Ridge (Figs. 4 & 7). In this highly magmatic area, the base of the crust stays at a greater depth than in the south precluding a clear differentiation between various Moho slopes. South of the influence of the WR/RGR magmatism, the end of the Distal Necking (DMHL 2) corresponds to a minimum of the basement thickness (Fig. 4 to 8). This area is thinner than the crust located seaward and has been called the crustal thin point (CTP) (Geoffroy et al., 2019).

South of the PAFZ, the distance between the NL and the crustal thin point ranges from 80 to 180 km in Uruguay-Brazil, and between 160 and 260 km in Namibia (Fig. 9b). The same distance increases dramatically in northern Pelotas Basin where it reaches 340 km (line 090, Fig. 4a). On the conjugate profile, south of Walvis Ridge, a distal Moho inflexion is not clearly observed (Fig. 4b). Either this distance is even larger than in Brazil either the huge magmatism of Walvis Ridge would preclude the formation of a similar distal necking.

5. Seaward-Dipping Reflectors description, typing and distribution

The top-SDR unconformity is a high-amplitude seismic marker. In the distal part of the margins, it merges with the top of the flat-lying flows (Figs. 4 to 7). This unconformity represents a very smooth depositional surface onlapped by the post-rift sediments (Fig. 10). The uppermost reflections of SDR packages are generally flat (e.g. Fig. 10a-b-c) or present apparent toplaps up dip terminations (e.g. Fig. 10d). But in detail, it is very hard to demonstrate the erosional character of these terminations which most likely characterize the landward thinning of the flow sequences.

The base-SDR horizon is of unknown nature. It has been consistently picked as the base of the seaward wedges independently of its possible nature (fault, detachment, level of intrusion, facies/composition lateral variation, etc.).

From 4 to 7 different wedges of SDR can be individualized. Each sequence is bounded either by a seismic unconformity or a noticeable contrast in the acoustic impedance or internal architecture (Fig. 10). The detailed mapping of each succession was not possible due to the wide spacing of available seismic lines. The volcanic sequences are thus regrouped into three types of SDR which were distinguished on their internal structure (Fig. 10).

5.1. Seismic facies

5.1.1. SDR sequences

The seismic facies of SDR sequences show a great variability along-dip of the margin, as well as within a single sequence (Fig. 10). The first emplaced SDR wedges are generally made of packages of thick, long and high-amplitude reflections (Fig. 10a, b, c). This facies contrasts with the SDR lying on the outer domain of the margin. Their internal reflectivity tends to be much lower (Fig. 10d, e, f) with relatively continuous low amplitude reflections in between which high amplitude and long reflectors can be intercalated (Fig. 10d). Theses outermost SDR show a higher amount of intrusion figures such as saucer-shaped and transgressive sills (red arrows in Fig. 10d). This higher frequency of intrusions must be taken with caution. It can only be due to a higher contrast of impedance between intrusions and the volcanic host rocks or to the dip of the sequence at the age of the intrusion. It is also possible that the concordant high-amplitude reflections could also correspond to large sills intruded within a relatively homogeneous pile of lava flows.

This two-fold classification between the highly reflective and poorly reflective proximal (inner) and distal (outer) SDR (also in Planke et al., 2000) is far from representative of the intrinsic variability of internal facies. The majority of inner-most SDR wedges present alternating high and low amplitude reflectors packages (Fig. 10a, b, c). Moreover, lateral facies variations are also frequently observed with high-amplitude units passing laterally to a transparent facies without any peculiar structural discontinuities (Fig. 10c). This evolution of seismic properties from high to low amplitude reflections could either sign a change in the type of volcanic constructions (quantity of sediments intercalated, sub-marine or continental lava emplacement, etc.), a change of rocks petrology as it was evidenced in Norway (between the Vøring Lower and Upper SDR Series; Abdelmalak et al., 2016b); or can be due to an acoustic blanking effect caused by the overlying flows (like in Fig. 10c). On that point, the seismic reflection data only is not conclusive. In addition to the flat-lying packages (Fig. 10d, e), some distinctive geometries may be observed within the SDR wedges.

5.1.2. Lava deltas

Lava deltas are breccias of volcanic glass formed where flows reach the water and are thus the most relevant volcanic construction to constraint the base-level elevation at the time of the volcanic activity (Planke et al., 2000 & 2017; Abdelmalak et al., 2016a). Though rare in the south Atlantic, such lava deltas are observed on the southward-dipping flank of the Walvis Ridge (Fig.

11a and line 3000 in Fig. 7) and Florianópolis High conjugate volcanic plateaus (Fig. 7 line 070, ~ km 150; line 3000, km 200 to 250, from 4 to 8 km in depth). In Namibia, the 3D seismic view (Fig. 11b) indicates the delta prograded toward both the SE (off the WR) and the NE (landward), in a maximum of 1000m deep basin. This observation shows that the margin segment localized south of Walvis Ridge (n°V in Fig. 2) was partially drown during the development of the northward-most subaerial SDR (Fig. 11a). On the Florianópolis High (Fig. 2), similar hyaloclastite deltas develop at the top of SDR in a basin of a maximum of 400m depth (line 070 in Fig. 7). The Walvis/Florianópolis Ridge marked thus an important barrier separating a subaerial realm in the north from a subaqueous domain in the south up to the Aptian/Albian transition (Stica et al., 2014; Bueno et al., 2007).

More reduced volcanoclastic deposits are also inferred at the landward edge of some sequences flows but also in large sag-type basins developed in central part of the Namibian thinned crust. These sag basins form between two topographic highs, the Necking Line and the seaward coeval SDR (Fig. 10g, h and in Fig. 7, lines 3000-3500-4500-5000-5500-6500). These depot-centers (~100 km wide and maximum of 2-3 km thick) likely derive form a flexural deformation of the lithosphere during the subaerial development of the outer-more wedges. It is worth notice that shallow marine invasion could have begun in the proximal domain prior to the distal domain where continental SDR wedges were forming.

5.1.3. Volcanoes and eroded volcanic edifices

Volcanic edifices are locally preserved within SDR packages (Fig. 10g). They are always featured by an area (in 2D section) of chaotic internal seismic facies and by an inflexion of surrounding reflections (Fig. 10g). A high density of intrusions is often observed in their neighborhood. Such edifices are observed within and at the base of SDR, but also within flexural-shape basins (line 5500 and 4500 in Fig. 7). A seismically highly disrupted zone underlies these edifices. The associated chaotic facies may reach the lower crust suggesting the overlying edifices could be seated on long-lived magmatic injection area (Fig. 10g).

5.2. Geometric attributes

In addition to the seismic character, the geometry of the wedges must be considered in order to be more accurate in their typing. By doing so, three main types of SDR can be distinguished based on both the curvature of the reflectors and the topography displayed at their downdip terminations (Fig. 12). Two highly different patterns were found (inner-type vs. outer-type) and a third, which is the most widespread (intermediate-type) that shows intermediate characteristics. The

outer-type has been also divided into two sub-types (outer-types 1 and 2) to be as accurate as possible.

5.2.1. Inner-type: Planar-diverging wedges

These sequences systematically correspond to the innermost and oldest emplaced SDR. They show repetitive and coherent seismic pattern characterized by a seaward thickening wedge with planar-diverging reflections (Fig. 10a, b, c and 12). Internal reflections pinch out landward toward a single point (Fig. 12). The length of reflections corresponds roughly to the length of the wedge. But this length may strongly vary, from 10 km (line 7500) up to 80 km (lines 7000 – 6500 in Fig. 7). The typical thickness of these wedges ranges from 2 to 4 km and locally up to 6 km in northern Pelotas half-grabens (Figs. 5a and 7).

Their geometric character, a fan-shaped package associated to a single rotation point, suggest that they develop as tilted blocks bounded by continent-ward dipping normal fault. The wavelength of the panels would be controlled by the detachment depth (in accordance with inner-SDR development model of Geoffroy, 2005; Paton et al., 2017; McDermott et al., 2018). These normal faults are not always identified on seismic profiles, but some independent features point clearly to their presence. They are often underlined by powerful reflections cross cutting the basement fabric and interpreted as magmatic injections or hydrothermal alteration within the damage zone of the fault (e.g., Fig. 10b, d). When the fault plane is not clearly imaged, it is inferred by significant inflexions and/or truncations in the deeper crustal reflections (Fig. 10a, b, c).

5.2.2. Intermediate-type: Arcuate-diverging wedges

This sequence is characterized by more arcuate internal reflections with downward terminations dipping from 10 to 20° seaward (Fig. 10d). The landward tip of these intermediate SDR is often very close to the pinch out of the inner wedges. This argues for a very smooth and low relief of the margin during their development.

Intermediate SDR organizes in successive wedged sequences, with the up-dip tip of individual wedges migrating seaward (Fig. 10d, 12). All together, they form systematically larger and thicker volcanic wedges than the inner-type (Figs. 4 to 6). Their length ranges from 50 to 200 km (Fig. 13). Their thickness reaches up to 18 km in the northernmost segment (VI in Fig. 2, Figs. 4 and 7) but typically ranges from 6 to 10 km in the southern segments (Fig. 13). The related sequences seal the underlying units which can be over-tilted and eroded (Fig. 5, 5, 9d). The base of these SDR packages is unclear and the identification of single and large detachment fault even more

567 doubtful. The global curvature of the wedges does not seem consistent with the functioning of only
568 one growth fault. We however recognize several fault-type offsets of seismic markers in the
569 underlying and highly intruded basement. These packages are thus likely controlled by a set of low
570 angle normal faults (Fig. 10d) strongly intruded. The progressive rotation and the apparently
571 sequential deformation of the hangingwall likely forces the successive sequences of flows to offset
572 seaward indicating important horizontal displacement.
573 Locally, these arcuate intermediate-SDR form «laterally confined volcanic successions»
574 recently described by Norcliffe et al. (2018) in the northern Orange Basin. The lines 7500 (Fig. 7)
575 and 6500 (Fig. 10h) in Namibia features this type of structures, which exhibits double-verging
576 sequences (DVS) of volcanic wedges (Fig. 12). A conspicuous DVS is also imaged in the distal part
577 of the northernmost seismic lines of Namibia (Fig. 4b and lines 2700 and 3000 in Fig. 7). This DVS
578 can be mapped as a coarsely NS-trending axis which abuts against the FFZ and/or the Walvis Ridge
579 (Fig. 13b). Similar but less well-developed DVS are recognized in lines 4500 & 5000 (Fig. 7).
580 These structures resemble to aborted rifts (Fig. 11). The presence of such structures shows
581 that an important hesitation in rift localization must have accompanied the South Atlantic opening.
582 Outside of these aborted volcanic rifts, the stratigraphically coeval volcanic sequences form
583 « classical » inner-type seaward dipping volcanic wedges. It is noteworthy that sag-type volcanic or
584 volcaniclastic basins tend to develop above these fossil rifts, after or during the transient stage of
585 the rift jump (Fig. 10h and Fig. 7).
586
587 *5.2.3. Outer-type 1: Strongly arcuate-diverging wedges*
588 The outer-SDR are poorly to not really defined in the literature, mainly because of the
589 poorly resolved and scarce available seismic images of these distal-most sequences (Hinz, 1981;
590 Hinz et al., 1999; Planke et al., 2000; Berndt et al., 2001). Planke et al. (2000) define outer-SDR as
591 being separated from the inner-SDR by an outer-high, which would correspond to a volcanic mound
592 or a rotated fault block delimited by a continent-ward dipping fault against which the inner-SDR
593 develops. According to the same authors, outer-SDR would correspond to sequences of deep marine
594 sheet flow or pillow-basalt volcanics which would contrast with the subaerial flood basalts
595 emplaced in the inner-SDR. They also point that outer-SDR are smaller and weaker with less
596 prominent internal reflections. Franke et al. (2007) use terminology of outer-SDR as exclusively
597 related to highly arcuate pattern of thin and discontinuous reflections located in the outermost part
598 of the Argentina margin. The authors show that such shape of SDR are not exclusively found in
599 relation with outer highs. In accordance with Planke et al's (2000) interpretations, Franke and

coworkers (2007) infer that these outer wedges have been emplaced under subaquatic conditions due to the progressive subsidence of a volcanic-magmatic crust.

The definition of outer-SDR can be reevaluate in the light of the impressive quality of the ION south Atlantic seismic dataset. Indeed, the geometric attributes of the outer-type 1 are very peculiar and they must be distinguished from the inner-most and much less arcuate outer-type 2.

The outer-type I SDR present diverging reflections which are more arcuate than intermediate SDR, with apparent maximum dip ranging from 20° to 30° seaward (Fig. 10e). The downdip termination of reflectors dim on a seismically badly defined basal surface which corresponds to a sub-horizontal to continent-ward low-dipping irregular discontinuity (Figs. 10e and 5b). Powerful and discontinuous reflections interpreted as intrusions occur beneath the basal contact indicating this contact corresponds to a preferential injection zone of magma. These wedges not only growth seaward but also subsides all along with time as suggested by backstepping landward onlaps (mimicking in seismic aggrading foresets as observed in sedimentary basins; Fig. 10e). This suggests a distinct isostatic or/and flexural behavior of the underlying crust.

5.2.4. Outer-type 2: Planar to lowly arcuate and poorly diverging wedges

The most distinctive attributes of the outer-type 2 are their location in the outermost part of the margin, and the noticeable decrease of the coeval magmatic production (Fig. 10d, e, f). They form sequences of generally lower than 2 km in thickness (Fig. 10d) outside of the influence of the highly magmatic northern segment. When approaching this northern area, the outermost sequences represent very wide (~100km) and slightly thicker unit (< 4 km) of planar or poorly arcuate reflections (Figs. 10f, line 3000 in Fig. 7).

In the 2/3 south of the Namibian margin, they form thinner seismic units (<2km thick) which are difficult to distinguish from flat-lying isopach sequences of flows (Fig. 10d, e). They frequently onlap the previously emplaced outer-type 1 or intermediate-type wedges indicating that the corresponding flows or volcano-detrital material tend to fill a residual low formed at the end of the previously emplaced SDR (Fig. 10e). As they most often merge laterally with the flat-lying flows (Fig. 10d, e) they also can be considered as passively flexured coeval flows (Fig. 10d and 12). They thus bring an ambiguity regarding the identification of the seaward boundary of the SDR domain. In this study, the criteria used to localize the seaward boundary of the SDR domain is the inflexion displayed by the top of volcanics (Fig. 12). Landward of the SDR seaward boundary, outer-type 2 sequences are slightly but significantly tilted seaward. Their base is generally poorly tectonized (Fig. 10d, e, f). Seaward of the SDR end, the coeval sequences became flat-lying or

633 slightly tilted continent-ward. The SDR seaward boundary is the most often coinciding with a
634 paleo-scarp, not necessarily associated to a fault, that isolates a marginal basin passively infilled
635 with post-rift sediments (Fig. 10d, e).
636 In Namibia as in Uruguay-Brazil, the outermost volcanic successions are characterized, in
637 accordance with Planke et al.'s (2000) descriptions, by a chaotic, low amplitude facies but also by
638 either some short and thin wedges of lava (Fig. 10e, f), or by very long and relatively thin seaward
639 tilted sequences of planar-diverging flows (Fig. 10d). Everywhere, they override the footwall of the
640 intermediate-SDR and merge seaward with the flat-lying flows sequences.
641
642 **5.3. SDR distribution in space and time**
643 On maps, the distribution of the SDR types (Fig. 13b) corresponds to the horizontal
644 projection of their downdip termination, except for the first wedges of SDR for which all the area
645 covered by the corresponding lava flows is mapped (Figs. 4 to 6).
646
647 *5.3.1. Along-dip distribution*
648 In the South American plate, the inner-SDR form a band of 30 to 80 km wide where the
649 volcanic sequences reach 4 to 8 km thick (Fig. 13a, d). Conversely, where the crustal thinning is
650 more distributed and progressive as along the Namibian margin, the inner SDR developed along a
651 much wider domain, ranging from 80 to 150 km (Fig. 13b).
652 The distribution of the intermediate-type SDR forms a relatively symmetrical conjugate
653 domain ranging from 30 to 70 km wide, with a thickness ranging from 4 to 10 km south of the
654 PAFZ (Fig. 13a, d). When approaching the FFZ, they cover a much wider domain of about 200 km.
655 In this area, the intermediate SDR constitutes the thickest volcanic successions reaching up to 15-20
656 km thick (Figs. 13a & 7).
657 A failed magmatic rift tends to develop only on the Namibian side (Fig. 13b). The
658 corresponding sequences emplace generally after the first wedges of inner-SDR (Fig. 7) and before
659 the thick intermediate SDR wedges developed seaward of these aborted rift (lines 5000, 5500, 6500
660 & 7500 in Fig. 7). Therefore, each of them is sealed by a new sequence of intermediate SDR which
661 developed seaward and above of the basement block presently located in outer position. This last
662 block which is underlain by continental-type seismic fabric, should represent the uplifted shoulders
663 of the previously developed volcanic rift (6500 in Fig. 7).
664 The highly arcuate outer-type 1 are emplaced on the same conjugate segment of the margin,
665 confined north of the Cape Cross and Chui conjugate segment boundaries (Figs. 9d). The outer-type
666 1 structure evolves to outer-type 2 toward the south (Fig. 13b). This evolution of the internal

667 structure is correlated to a net decreasing of the SDR thickness, from close to 8 km thick (in line 70)
668 to less than 4 km thick (in line 40). In Namibia, outer-type 2 SDR are not always developed and the
669 flat lying flows tend to directly onlap the seaward flexure of the intermediate-SDR, between the
670 Cape Cross and Lüderitz TZ (Figs. 7 & 9d).
671
672 *5.3.2. Along strike segmentation & timing*
673 The period of activity of the transfer zones together with the SDR age strongly vary along
674 the margin.
675 The Rio de la Plata transfer zone (RPTZ) corresponds to a 100km along-strike area without
676 clearly developed SDR (Soto et al., 2011; McDermott et al., 2018; Fig. 13a). The line 4300 which
677 cross cuts this transfer zone shows SDR only at the foot of the present-day continental slope (Fig.
678 7). South of the RPTZ, the distalmost SDR of the segment #III (Fig. 2) are dissected by a set of
679 northward-dipping normal faults (Soto et al., 2011) which are not observed in the conjugate
680 segment. Here, the intra-continental RPTZ is thus clearly prolongated by an intra-oceanic fracture
681 zone along which some isostatic or kinematic readjustments occurred after the Argentina's SDR
682 development.
683 The magnetic anomalies map of Moulin et al. (2010) indicate a strong landward offset of the
684 M4 north of the RPTZ (Fig. 2). South of the RPTZ, the M4 is located in the outermost margin
685 domain whereas in the north, it is the M2 which lies at the SDR seaward boundary. This might
686 signify that SDR north of RPTZ could be younger due to a significant delay of the rift propagation
687 through the transfer zone (Stica et al., 2014). Franke et al. (2007) localized the major transfer zone
688 along the Salado TZ. Our mapping together with the offsets of the magnetic anomalies pattern
689 suggests that the segment comprised between the Salado and Rio de la Plata TZ may have
690 constituted another « buffer kinematic » as proposed for the Santos Basin north of the FFZ (Moulin
691 et al., 2010).
692 On the opposite margin, the SDR form en-echelon lens-shape basins of 300 to 400 km long,
693 which are offset by about 70 km from each side of the Lüderitz TZ (Fig. 13a). Therefore, South of
694 the Cape Cross & CFZ conjugate transfer zones, the SDR architecture is divided in two first-order
695 segments which coarsely correspond to the segments III & IV (Fig. 2). But, conversely with the
696 previously described RPTZ, the Luderitz TZ seems to inactivate just after the inner SDR
697 development. We observe that a double verging sequence of volcanic wedges developed in each of
698 the previously described segments, but only on the Namibian side.
699 With the exception of the RPTZ, the outer SDR successions of segments III & IV are much
700 less segmented along strike than the inner SDR (Fig. 13b). The corresponding sequences tend to

show horizontal, parallel and almost isopach sequences of reflections in parallel-to-the-margin profiles.

On both conjugate margins, the SDR distribution is dominated by a considerable widening of their extension toward the north, in segments V and VI (Fig. 13b). In SE Brazil, the SDR seaward boundary is noticeably shifted to about 150 – 200 km toward the sea, only north of the PAFZ (Fig. 2, Stica et al., 2014). In Namibia, the same offset is observed but more progressively and begins north of the Cape Cross TZ (Fig. 13b).

The lines 4000 and 4500 cross over the Cape Cross transfer zone (Fig. 7). In these two lines, the volcanic sequences of the northernmost and highly magmatic segment are strongly condensed. They seal an unconformity that lies at the top of the over-tilted and eroded younger SDR (Fig. 7 and Fig. 5b). Along strike, these first sequences of inner SDR are also controlled by a set of oblique-to-the-margin normal faults related to the Cape Cross TZ. These transverse faults do not propagate in overlying SDR, indicating that this major transtensional boundary has played during the emplacement of the firsts inner-type SDR and that it was inactivated during the rest of the VPM formation (also in Koopmann et al., 2014a). This along strike segmentation is less noticeable across the conjugate CFZ.

Northward, the segment VI constitutes a large volcanic plateau supported by thick SDR packages of 15 to 20 km thick (Fig. 4, 11a, 13). This plateau constitutes a morphological barrier isolating the austral and central segments of the South Atlantic (Figs. 2 & 11a) and delimiting the southern extend of the Aptian salt province (Torsvik et al., 2009; Chaboureau et al., 2013). In this northern segment, the wide and thick intermediate SDR are observed both tilted toward the sea and toward the PAFZ and Walvis conjugate TZ that form crustal-scale large-offset transfer fault zones (Abreu, 1998; Elliot et al., 2009; Cartwright et al., 2012; McDermott et al., 2018). The internal reflectors dip toward the sea up to 20° in Namibia and up to 30-35° in the northern Pelotas basin (Fig. 7), and the same wedges dip up to 10° toward the N and toward these EW-trending conjugate transfer zones (Fig. 11a).

The stratigraphic markers correlated through the Namibian northern profiles (orange marker in Fig. 7 and 11a) evidence that the development of the outer-type 1 of the line 4000 (Fig. 7) is coeval with formation of the intermediate-SDR in the northernmost lines (Line 3000 & 2700, Fig. 7). This implies that both, the successive SDR wedges tend to rejuvenate toward the north, but also that the magmatic activity may have continued in the north, well after the break-up of the rest of the margin (Fig. 11a) which is confirmed by the ages of the drilled volcanics. In the two northernmost profiles of Namibia (segment VI), a conspicuous double-verging magmatic structure (Fig. 4b and

734 lines 3000 and 2700 in Fig. 7) forms an early magmatic spreading center likely coeval with the
735 incipient formation of an oceanic-type crust in segment V and further south (Fig. 4b).
736 The age of the SDR wedges in this segment VI is almost unknown but would be bracketed
737 between 124 and 113 Ma according to the correlation proposed by Stica et al. (2014) and Bueno et
738 al. (2007, Fig. 2). The Walvis Ridge was formed on the northern flank of this wide volcanic plateau
739 (Fig. 11a). The ridge is characterized by an EW alignment of circular shape volcanoes. The oldest
740 Ar-Ar ages obtained on the WR is 114 Ma (Fig. 2, Rohde et al., 2013). They come from the N flank
741 of the ridge and outside of the seismic survey used in this study. Nevertheless, a similar age (113
742 Ma) was obtained on the topmost volcanic succession of the Florianópolis High (e.g. Bueno et al.,
743 2007 and Stica et al., 2014). In accordance with the tectonic calendar proposed by Stica et al.
744 (2014), it is thus likely that the SDR of the northernmost segment of the austral South Atlantic were
745 forming during all the Aptian (Segment VI, Fig. 2 and 11a).
746

747 ## 6. SDR and basement coeval structuration

748 In the following section, we emphasize the apparent genetic relationships that link the
749 evolution of (1) the crustal basement mode of deformation and thinning, (2) its seismic
750 characteristics, and (3) the SDR types throughout the identified crustal domains. Where they are
751 available, the density and velocity properties of each domain are integrated to this description, to
752 more accurately characterize basement nature.
753

754 ### 6.1. Proximal Domain and Necking

755 On both conjugate margins, the proximal grabens and half-grabens, located landward of the
756 NL, are scarce and limited both in depth and width, indicating the minor stretching recorded in the
757 inner part of the margin.
758 In Namibia, the only well-developed proximal graben develops against the southern branch
759 of the Cape Cross TZ (Clemson et al., 1997; Corner et al., 2002; Fig. 2) which obliquely crosscuts
760 the 4500 seismic line (Fig. 7). A well reaching the uppermost succession of this graben (2313-05-1)
761 indicates that the succession comprises basaltic flows and volcanodetrital sediments. Elsewhere in
762 Namibia, the proximal syn-rift successions are generally thinner than 2 km (see also McMillan,
763 2003; Jungslager, 1999; Broad et al., 2012). It is noteworthy that the different extensional structures
764 observed on the Namibian shelf tend to develop against normal faults that trend parallel to the
765 basement's fabric and which dominantly dips toward the sea. This is well displayed in Namibian

766 lines 4000 (Fig. 5b), 6000 (Fig. 6b), and 6500 (Fig. 7). This strongly suggests a dominant control of
767 the structural inheritance during the early stretching of the margin.

768 In Namibia, the upper crust in the Proximal Domain and Proximal Necking displays the
769 seismic characters of a strongly deformed basement with what appears to be tectonically stacked
770 thrust sheets and folds. This is well evidenced in line 7000 where a fold of 15 km wavelength lies in
771 the middle crust above a barely deformed package of strong reflections. Between lines 7500 and
772 6500, the proximal domain is thus the most likely composed of the deformed units of the Gariep
773 Belt (Fig. 3a). Between the Luderitz and Cape Cross segments boundaries, orogenic structures are
774 less pronounced (Fig. 5b and lines 6000 to 5000 in Fig. 7). We inferred that this apparently less
775 deformed upper crustal fabric reflects the change of orientation of the orogenic fabric. In the
776 offshore prolongation of the Damara belt, seismic lines would be parallel to slightly oblique to the
777 main orogenic fabric. North of Cape Cross, along the Kaoko Fold Belt, the upper crust displays
778 some tight fold in a layered upper crustal unit (Fig. 5b). Further northward, the Proximal Necking
779 and the NL tends to get closer to the coastal zone (e.g., Fig. 9b) precluding a relevant description of
780 inherited structures.

781 In Uruguay-Brazil, proximal rift structures are also very seldom and mainly represented by
782 landward dipping normal faults associated to limited vertical offset. The upper part of the
783 continental crust is quite transparent and appears as little deformed (Fig. 4a to 6a). It rests onto a
784 typical strongly reflective and layered middle and lower crust (Mooney & Mesner, 1992). The
785 seismically homogenous character of the upper crust is almost constant from the Polonio High in
786 Uruguay until the FFZ to the north. In northern Pelotas Basin, an isopach package of mildly
787 powerful reflectors reaching 2-3 km in thickness is interpreted as a pre-rift succession preserved at
788 the top of the crust (purple reflectors sequence in lines 70 & 60 in Fig. 7). The corresponding
789 succession is discordant on the underlying basement fabric. It is also tilted against a set of
790 continent-ward dipping normal faults. As formerly proposed by Stica et al. (2014), it is likely these
791 isopach seismic units correspond to the offshore equivalent of the pre-SDR Paraná basaltic plateau.

792 When approaching to the NL and beneath the firsts inner SDR, the upper crustal fabric tends
793 to become more reflective in both conjugate margins (Fig. 10a, b, c). The basement fabric is often
794 seen tilted against a dense network of normal faults which accommodate the strong flexure toward
795 Thinned Domain (e.g. lines 40, 4700, 90 in Fig. 7). It is also common to observe a dense network of
796 subvertical to slightly tilted high-amplitude reflections cross-cutting the background fabric (Figs. 4a
797 & 5a). These reflections are interpreted as sheeted-dyke complexes emplaced in the top of the crust.
798 Some analogous highly injected flexure zones are well documented in SE Greenland and
799 Mozambique coastal flexures. In these two cases, more than 50 % of magmatic dilatation is

associated with extensional faulting to accommodate the syn-SDR flexure of the upper part of the continental crust (Klausen and Larsen, 2002; Lenoir et al., 2003; Klausen, 2009).

The inherited continental crust of the Proximal Domain can also be intruded both by some decakilometric intrusive complexes that are well evidenced in Namibia (e.g. Fig. 3). Off these intrusive centers, the velocity vertical gradient of the upper and lower continental crust seems preserved with available Vp and density values that range from 5.9 to 6.8 $km.s^{-1}$ and from 2.7 to 2.9 between the surface and the Moho respectively (Fig. 15a, Bauer et al., 2000 & 2003). Under the Messum and Cape Cross complexes, the authors estimate the density ranges from 2.9 to 3.0 and they found the velocity increases of ~0.3 and ~0.5 km/s relative to the host rock, but with a similar gradient till the Moho (Bauer et al., 2003). Similar igneous centers with dyke swarms lie all along the W and E Greenland coastal flexure (Callot et al., 2002) and they denote the beginning of a pervasive but heterogenous modification of the composition of the pre-rift crust. Off these localized igneous centers, the proximal continental basement keeps its original characteristics till the Proximal Necking and the entrance into the SDR domain (Fig. 14b).

Therefore, Proximal Domain and Proximal Necking are always associated with brittle upper crust deformation expressed either by clear grabens filled with volcanic and detrital sediments or by innermost SDR. The mechanical behavior of Uruguayan (line 4500) and SE-Brazil (line 90) lower crust was described and analyzed by Geoffroy et al. (2015) and Clerc et al. (2015). Clerc et al. (2015) observed numerous high amplitude reflections within the middle/lower crustal layers around which the surrounding crustal fabric is deflected. They proposed that the resulting sigmoidal geometry characterizes the occurrence of ductile shear bands (yellowish intra-crustal lines on our interpretations). The 2D convolution seismic modelling performed by Wrona et al. (2019) consolidate the Clerc et al.'s conclusions, showing that several seismic reflections converging in the same direction and forming large-scale lenses are characteristics for kilometric-scale shear zones. The studied conjugate seismic lines exhibit similar structural pattern in both Proximal Domains and Necking (Fig. 14). The internal deformation of the lower crust fabric suggests the occurrence of a simple shear fabric. The middle/lower crust displays curved reflections that define dome- or lens-shape structures which are also consistent with a ductile behavior (Figs. 7 & 14). This ductile strain appears distributed through all the lower crustal section more than localized along single crustal-scale detachment.

From all these observations it can be concluded that the tectonic evolution of the Proximal Domain and Proximal Necking are controlled mainly by active faulting that tends to be more magmatic with the appearance of the inner-type SDR and strong, sheared reflections within the

lower crusts. The inner SDR rests on an intruded upper crust crosscut by landward dipping normal faults that flatten atop or into a ductily deformed middle-lower crust (see the brittle/ductile transition line in Figs. 4 to 7). Moreover, the Proximal Necking is a domain relatively symmetric on both margin with a variable width of 30 to 80 km (Fig. 9b).

6.2. Thinned Domain

In both conjugate margins, the Thinned Domain is always covered by inner and also partly by intermediate SDR (Figs. 7 & 16). We also recognize some packages of arcuate diverging reflectors developed within aborted volcanic rift. These DVS are always located in the Thinned Domain and exclusively on the Namibian margin (Figs. 7 & 16).

In this central domain of the studied VPM, the basal lower crust tends to show very high amplitude and long reflections that could be isolated or formed 1 to 4 km thick packages of either stacked reflectors or parallel to the Moho shearing. The most impressive example likely occurs in the northern Pelotas basin (line 090, Fig. 14 and 4a) or in southernmost profiles of Namibia (lines 7000 and 7500 in Fig. 7). In the northern Pelotas profile, Geoffroy et al. (2015) distinguish these stacked powerful reflections as a specific mafic lower crust (LC2, Fig. 14) from the overlying and highly deformed fabric of the ductile middle-lower crust (LC1).

Along the margin, the basal highly reflective LC2 is nor as evident neither as thick as in the previous examples. These reflections could also be strongly disrupted or totally absent (km 200 of the Fig. 6b), perturbating the Moho identification. These silent areas often coincide with evidences for volcanic edifices emplaced in upper part of the crust. But when it occurs, the LC2 type reflections are tectonically disconnected form the overlying LC1-type lower crust or is used as a level of rooting for the LC1 shear bands (Fig. 14). This is consistent with the noticeable absence of strong offsets of the Moho along the studied profiles. The base of the continental crust appears thus as a decoupling layer between the middle/lower crust and the upper mantle (Clerc et al., 2015; Geoffroy et al., 2015).

In the northern part, these lower crustal shear zones define some kinds of extensional duplexes (Figs. 4 and 13). But in central and southern Namibia, the lower crust structure is rather dominated by boudinage and an even more distributed shear (Figs. 5b, 6b and lines 5500, 6050 and 6500 in Fig. 7).

Our interpretation indicates that the inner SDR wedges development is concomitant with thinning processes of the continental crust (Fig. 7 and Figs. 4 to 6). We observe that this thinning is accommodated by brittle faulting of the upper crust and ductile shearing of the middle and lower

crust and a non-quantifiable proportion of magmatic dilatation. The seismic characteristics of the upper and lower crust are the most often coherent all along Thinned Domain, resembling the previously described layering from the Proximal Domains (Figs. 4, 5, 6).

Similar conclusion could be reach when regarding the velocity structure of the Thinned Domain gave by the available refraction data (Bauer et al., 2000; Fig. 15b). Indeed, the velocity structure appears as coherent all along the Thinned Domain and characterized, from the top-SDR to the Moho, by a much higher velocity gradient than in the Proximal Domain. The Vp pass from 5 to about 7 $km.s^{-1}$ throughout the extrusives package (Fig. 15b). Below, the crust shows high Vp ranging from 6.9 to 7.6 $km.s^{-1}$ and characteristic of the so-called HVLC of VPM. This HVLC is frequently presented as a two layer unit, with a 8-10 km thick upper layer with a relative low velocity gradient (from 7.0 to 7.3 $km.s^{-1}$), overlying a thinner (2-6 km) lower layer with Vp > 7.3 and around 7.6 to 7.8 $km.s^{-1}$ (Bauer et al., 2000; Fromm et al., 2017; Becker et al., 2014). Along the intersection between the Bauer et al.'s (2000) Transect 1 and the Namibian line 4500 (Fig. 15b), the "upper HVLC" includes both the brittle upper crust and the top of the LC1 ductile crust (Fig. 15b). Their high velocities must thus be linked to the high amount of magmatic intrusions. Downward, the "lower HVLC" corresponds to the highly reflective seismically layered LC2 (Fig. 15) but also includes a limited thickness of the silent area which characterizes the uppermost mantle in our interpretation. It is therefore likely that the upper part of HVLC in VPM correspond to an intensively injected and sheared lower crust, with possible lenses of inherited high-Vp lower crustal units (as it is expected in Norway; Gernigon et al., 2006; Nirrengarten et al., 2014). Their lower part might more composed of underplated magmatic mafic bodies.

6.3. Distal Necking

The Distal Necking is always associated to the intermediate and outer-type SDR (Fig. 16). In both conjugate margins, the onset of the Distal Necking (DMHL 1, Fig. 16) well corresponds to the onset of intermediate SDR south of the PAFZ and Cape Cross TZ (Figs. 16 & 7). When they occur, outer SDR develop prior to crustal thin point which lies at the end of the Distal Necking (DMHL 2 in Fig. 16), except in the northern segments where they develop after.

In South American profiles, the crustal seismic fabric of the Proximal and Thinned Domains tends to be replaced by a noisier and much less reflective facies throughout the Distal Necking (Fig. 5a and 6a). The nature of this crust is thus difficult to constrain from seismic reflection profiles only. Conversely in the Namibian profiles, we clearly recognize that intermediate SDR lie above the same LC1 and LC2-type facies than in the Thinned Domain (Figs. 5 to 7). The most often, the LC1-

type fabric appears tilted toward the sea, the downdip terminations of the strongest reflections showing some ductile drag against the LC2-type basal crust (Figs. 5, 6 & 7). These observations were done all along the Namibian margin and suggests that continental basement is still within part of the Distal Necking (Fig. 7).

The strong and seaward dipping reflections tend to root in the top mantle and may crosscut the entire crustal basement (e.g., line 5000, 5500, 7500 in Fig. 7). These reflections are interpreted as large-scale intrusions tardily injected within the lower crust and sheared with the host-rock (e.g. Fig. 6b), during the seaward tilt of the crustal basement. The brittle upper part of this basement the most often displays an opposite fabric, i.e., with powerful reflections inclined toward the continent. The corresponding reflections are considered as intrusions injected in the footwall of the overlying intermediate- and outer-type SDR (e.g. Fig. 6b).

In available refraction data, the "Lower HVLC" characterized by $7.3 < Vp < 7.8$ km.s^{-1} tends to pinch-out along the Distal Necking (Fig. 15c). With the exception of this noticeable structural closing, the velocity structure of the Distal Necking does not show peculiar difference with the velocity profiles of the oceanic crust from White et al. (1992, Fig. 15e). This indicates that if a certain proportion of continental crust does persist in this distal domain, it is blind for the refraction data from Bauer et al. (2000).

6.4. Distal Domain

Off the crustal thin point which lies at the end of the Distal Necking (DMHL 2), the crust is overlain directly by flat lying flows sequences (Fig. 5) in segments II to IV and by outer-SDR in segments V and VI. The transition to the distal crust is characterized by a Moho presenting a downward bulge-like topography that became flat lying and sub-horizontal further seaward (Fig. 7). Along-strike, its thickness varies between 6 and 12 km (also in Taposeea et al., 2017), the thickest crust lying in the highly magmatic northern segments (Line 3000 in Fig. 7).

The transition from the outermost SDR to the flat lying flows sequences (FLF) often lies at the onset of this Distal Domain. The FLF are associated to a very smoothed topography of the seafloor. At around 100km from the crustal thin point, the volcanic units tend to be progressively tilted toward the continent against a dense normal fault network (Fig. 7). These closely spaced fracturing gives rise to a much more rugose seafloor and a classical pattern of oceanic crust with landward tilted blocks against oceanward dipping normal faults. This last type of crust is also characterized by a thickness close of the worldwide average of the "normal oceanic crust" (6-7km according to compilations of Christeson et al., 2019 and White et al., 1992, Fig. 15e).

From the end of the Distal Necking, the basement is generally invaded by powerful oblique reflections interpreted as magmatic intrusions and/or shear bands (Becel et al., 2015; Ding et al., 2018). They either display a X-shape geometry, or an alternance of areas of landward or seaward dipping reflections. The coeval transformation of the seismic fabric is systematic along the margin and very likely due to the overpassing of a threshold in the proportion of magmatic input.

The nature and origin of this distal domain is unclear so far. It may well represent a very particular type of oceanic accretion or alternatively a kind of mixed mafic/continental crust (Geoffroy et al., 2019, 2020).

7. Asymmetry level of the conjugate VPM

The observations made on the conjugate South Atlantic margins exhibit a significant asymmetry, both in the crustal architecture, the SDR types repartition and the total volume of SDR.

7.1. Margin width

The margin width is one of the criteria used to evaluate the asymmetry level of a pair of conjugate passive margins. The main boundaries of the continental passive margin s.s. in the case of VPM are difficult to evaluate due to a lack of consensus in their formation and the definition of a strict COB can be subject to strong debate (McDermott et al., 2018; Reuber et al., 2019; Geoffroy et al., 2020). In this context, we consider more relevant to use some empirical but robust observations, common in most lines, rather than to follow an a-priori genetic definition of the successive crustal domains.

The Necking Line (i.e., the top-basement flexural hinge in Fig. 8), together with the DMHL 2 (i.e., crustal thin point) represent the most evident and repetitive features observed on most of the studied seismic survey (Figs. 4 to 7). The Necking Line corresponds together to the onset of the crustal necking and of the SDR domain. This clear feature can thus be used to delimit the onset of the volcanic passive margin s.s. On the other hand, the DMHL 2 is used as a proxy for the end of the volcanic passive margin. This boundary cannot be firmly interpreted as the seaward-most end of the continental crust. Nevertheless, it represents a specific boundary in the thinning profile that marks the transition between an in-thinning continental crust, and a crustal domain which is observed as invaded by the magmatic seismic fabric. These two crustal lines constitute thus good markers to evaluate the margin width, despite the lack of definitive explanation of their genesis.

VPM widths measures were performed along 5 conjugate lines spaced 200 km and trending perpendicular to the average trend of the margins (Fig. 16 and Table 1). The profiles #2 to 5 are all located south of the PAFZ and of the influence of the high magmatic supply of the northernmost segment (profile #1 in Fig. 16 & Table I).

The margin width is of 109 ± 22 km in the Uruguay-Brazil, while the width of the conjugate Namibian margin is 190 ± 40 km. This relative difference of about 60% outline the significant asymmetry in the conjugate VPM (Fig. 9b & 16). Conversely, North of the PAFZ, the margin width reaches close to 300km on the Florianópolis Plateau and about 310 km on the southern flank of Walvis Ridge (S of the line 2700). Here, the margin width is thus symmetric (Table 1).

Looking at the different neckings (both proximal and distal), the thinning profile of the basement of the South Atlantic margins is significantly asymmetric. The top-basement and Moho define a strong necking of the continental crust in Uruguay/SE Brazil. This is noticeable in the central and northern segments of the Pelotas Basin where the continental crust thins of more than 50 % in less than 70 km and still less locally (in 30km for line 040, Fig. 5a) and the two Necking Domains are nearly contiguous with narrow to undifferentiated Thinned Domain (Figs. 7, 9b, 16).

On the opposite margin, the necking of the crust is much gentle. Off the Necking Line, the crust exhibits rather a progressive and distributed thinning with local failed rifts (Figs. 7 & 9a). An ultimate zone of necking lies in the outermost part of the conjugate profiles. Between the DMHL 1 & 2, the Moho slope suddenly increases before it reaches the shallowest depth. In Uruguay/SE Brazil, this Distal Necking is much less noticeable than in Namibia, and when it is observed (Uruguayan lines), it lies in a much more proximal location (Figs. 7, 9a & 16).

7.2. SDR distribution

When comparing now the distribution of the different types of SDR (Figs. 13b & 16), it is remarkable that the asymmetry is bared by the inner and intermediate SDR which cover a much wider area in Namibia than in the opposite margin (Table 1).

South of the PAFZ, the inner SDR define a domain with an average width of 43 ± 9 km in Uruguay-Brazil against 119 ± 42 km in Namibia. These values do not change significantly in the northern highly magmatic segment (Table I). This 1:2 ratio in the conjugate distribution of the inner-type SDR is related to the highly different conjugate thinning gradients, characterized by the strong crustal necking in Uruguay-Brazil and the more distributed thinning in Namibia (Fig. 7 & 9).

South of the PAFZ, the intermediate-type SDR plot on a band of relatively similar width on both margins whose average is about 45 ± 10 km (Table I). However, the Namibian side presents

997 the segmented failed axis (DVS) developing local intermediate-type within the inner-type (Fig. 7).
998 Independently of the width of the domain, this intermediate-type can be considered as another
999 asymmetric element into the SDR distribution. Their extent increases dramatically to reach 180 km
1000 in northern Pelotas basin and 140 km in northern Namibia. Once again, the asymmetry in the SDR
1001 distribution tends to vanish toward the northern segment of the conjugate margins.
1002 The outer-types SDR distribution is more hazardous to compare when considering the
1003 difficulty to distinguish the outer-type 2 from the outermost flat-lying sequences of lava (Fig. 12 &
1004 7). A relative symmetry seems to occur between outer-type 1 SDR of the two conjugate margins
1005 (Fig. 16, Table I). This is not the case for the outermost sequences of outer-type 2 which, in the
1006 central and southern segments, are developed on a wider area on the American plate than on the
1007 African plate (Fig. 16 & Table I). This is particularly well evidenced in the central segment of the
1008 Namibian margin where flat-lying flows directly onlap the last intermediate-type SDR and their
1009 thinned crustal basement (line 5000, Fig. 7).
1010
1011 **7.3. SDR volume**
1012 The base- and top-SDR horizons were used to calculate the thickness and estimate the SDR
1013 volume developed from the FFZ to the southern Namibian border and on the conjugate VPM. For
1014 these conjugate areas which correspond to the 2:3 of the total length of the South Atlantic VPM, the
1015 estimated SDR volume reaches 1.82 x 10^6 km³ in Namibia and 1.15 x 10^6 km³ on the South
1016 American margin. The Namibian margin would thus contain about 60 % more of erupted magma
1017 than its conjugate. Peate et al. (1992) and Milner et al. (1992) have estimated the volume of the
1018 Etendeka and Paraná Continental Flood Basalts to 0.07 x 10^6 km^3 and 1.2 x 10^6 km^3, respectively.
1019 Assuming that the SDR consist entirely of volcanic material, and considering that our
1020 estimation concerns only the 2:3 of the margin, the total volume of melt reaching the surface during
1021 the formation of South Atlantic VPM would be three time the estimated volume for the present-day
1022 preserved onshore Paraná-Etendeka traps.
1023 At the scale of the South Atlantic VPM, these results imply that the asymmetry in the
1024 magma volume and the asymmetry in the margin width are of an equivalent level, estimated by a
1025 relative difference of about 60 %.
1026
1027 ## 8. Discussion
1028 Our interpretations of long offset seismic lines provide a new view of the magmatic
1029 elements, crustal architecture and evolution of South Atlantic VPM. We propose a new definition of

1030 the SDR packages, their distribution (Fig. 13b) along dip and strike of the margin and their
1031 correlation to the thinning profile of the crust. This allows us to propose a sequence of breaking up
1032 of the crust in this hyper-magmatic environment. In addition, the new maps of the types of SDR,
1033 their thickness profile (Fig. 13a), together with the thickness of the underlying basement (Fig. 9)
1034 and its seismic character (Fig. 4 to 7) add new elements to the already observed asymmetry of the
1035 conjugate margins. These systematic observations raised several questions on the parameters that
1036 may influence this asymmetry.
1037
1038 **8.1. Crustal deformation and SDR formation**
1039 The definition of an intermediate facies of SDR allows to propose a refined scheme of the
1040 mode of formation of the successive SDR packages. The specific relationship between the thinning
1041 gradient of the crust and the geometric attributes of the SDR suggests a likely genetic relationship.
1042 The change from inner SDR to intermediate SDR coincides with the initiation of an ultimate
1043 necking of the crust (Fig. 16). The outer SDR domain is intimately associated to the transition from
1044 this ultimate necking to the thinner and more magmatic crust of the Distal Domain (Figs. 8 & 16).
1045 Therefore, intermediate SDR tend to develop during a transitional tectono-magmatic regime,
1046 between inner and outer SDR.
1047 The Proximal Necking is related to a mechanical thinning of the crust as in any other
1048 margins (Sutra et al., 2013; Tugend et al., 2015), where active faulting of the upper crust controls
1049 the formation of extensional basins. Here they are filled with wedged volcanic sequences, qualified
1050 as inner SDR (Fig. 10). These inner SDR rest on an intruded brittle upper crust faulted by syn-
1051 magmatic landward dipping normal faults that flatten on a ductile middle-lower crust of continental
1052 nature as suggested by the velocity profiles from refraction data (Bauer et al., 2000). The middle-
1053 lower crust is intruded and sheared as imaged by multi-channel data (this study; Clerc et al., 2015).
1054 The diverging and mildly arcuate shape of the intermediate SDR suggests they are related to
1055 a more advanced stage of rifting relatively to the inner SDR stage. Their large flexuration, the
1056 sheared structures observable in the lower crust and the appearance of a lower crustal unit in
1057 refraction and multi-channel data tend to suggest a much higher amount of magmatic material in
1058 association to a stronger thinning of the crust. The increase of internal curvature and the seaward
1059 migration of their pinch-out (Fig. 10) also implies a loss of flexural strength of the crust during their
1060 development (White & Smith, 2009). The arcuate shape of SDR together with the seaward
1061 migration of the successive wedges might be explained by the symmetrical development of flexural
1062 basins on each side of a sub-aerial spreading axis (Hinz, 1981; Mutter, 1982; Corti et al., 2015;

Buck, 2017; Morgan and Watts, 2018). However, the seismic profiles exhibit some low-angle normal faults forming small tilted blocks (Fig. 10d) associated to the development of the intermediate SDR. This observation would suggest a sequential extensional faulting of continental basement associated to a migration of the magmatic activity (Gibson and Love, 1989; Eldholm et al., 1995; Geoffroy, 2005; Mjelde et al., 2007; Stica et al., 2014; Geoffroy et al., 2015, 2020; Clerc et al., 2015) on top of a heavily intruded and sheared ductile crust that tends to shallow beneath these sequences (Fig. 7).

Along most of the margin, intermediate SDR are followed by outer SDR type 2, or in few places, directly by FLF sequences. This progressive thinning of the outermost extrusives is the likely diagnostic of the coeval decrease of the magmatic production. This evolution coincides with the transition between the Distal Necking and the Distal Domain which seems to be nearly to fully composed of magmatic material as suggested by refraction data (Fig. 15c; Bauer et al., 2000) or gravimetric inversion (Maystrencko et al., 2013).

The outer SDR type 1 are confined to the northern area (Fig. 16). It is thus obvious that some specific genetic conditions are met for their development. The high curvature of these SDR suggests that the lava pile is deflected on a partially molten or a very weak basement. This is also inferred by the very low dip of the structural discontinuity which separates the SDR from lower unit (Fig. 5b & 10e). A higher thermal gradient and/or magmatic production than southward is likely, due to the proximity of the Walvis Ridge and Rio Grande Rise. The weak behavior of this outer basement could derive from a pervasive partial melting of the continental basement (Kjøll et al., 2019) and from the total replacement of the continental crust by a gabbroic mush, at the manner of the oceanic crust (Pindell et al., 2014; Quirk et al., 2014).

One of the major unresolved questions concerning VPM formation is whether the outer SDR developed after the continental breakup and are therefore oceanic (Hinz, 1981; Mutter, 1982; Corti et al., 2015; Buck, 2017; Morgan and Watts, 2018), or above a heavily intruded continental crust (Eldholm et al., 1995; Stica et al., 2014; Geoffroy et al., 2015, 2020; Clerc et al., 2015; Senkans et al., 2019). The final breakup point that defines the end of the continental crust (or Continent-Ocean Boundary, COB) is therefore highly debated. The lithospheric extension that forms the VPM is not iso-volumetric. Massive magma accretion/intrusion accompanies the tectonic stretching of the continental crust since the earliest SDR emplacement. Onshore field analogues demonstrate that the crustal dilatation caused by diking can reach up to 50 % in the most proximal SDR (Klausen and Larsen, 2002). The refraction data (Bauer et al., 2000) indicate the velocity/density of the underlying crust evolve from usual continental velocity trends from the Proximal Domain to much faster velocity beneath the Thinned Domain, suggesting an increasing magmatic content in the

crust. But, despite this magmatic input, the analyzed seismic data show that the lower crustal (LC1 and LC2) fabric of the Proximal and Thinned Domains (dark gray reflectors on our interpretations) stays consistent till beneath the domain of the intermediate SDR (Fig. 7). This suggests that the continental basement is engaged during the intermediate SDR formation and the part of the Distal Necking.

Considering this compositional and rheological evolution of conjugate VPM, the occurence of a boundary between the continent and the ocean is highly unlikely and define its precise location is, for the least, highly model-driven. The composition of the basement under outer SDR and FLF stays an opened question. These extrusives could be related to a higher magmatic production than for a typical oceanic crust, above a fully magmatic crust, or to the continuation of the ductile stretching of the continental lower crust associated to a continuous magmatic dilation (e.g. W Indian VPM; Geoffroy et al., 2019, 2020).

A peculiar and consistently observed, element is the Crustal Thin Point (CTP). It is always located at the end of the Distal Necking (Fig. 7). In the north (segment V and VI), it coincides with the transition from intermediate to outer SDR. South of the Cape Cross FZ, the CTP is more located either at the transition between outer SDR and FLF domains or directly within the FLF domain. In the exception of the northernmost segment, the CTP is parallel to the magnetic anomalies trend (slightly seaward of the M4 anomaly, DMHL 2 in Fig. 16), suggesting that this geological feature could be a synchronous event along the margin, bracketed between 131 and 129 Ma for the segments III to V (Fig. 17). The geodynamic model from Moulin et al. (2010; Fig. 17) demonstrates a strain acceleration, from less than 1 to 7 cm/yr full spreading rate, between 133 and 128 Ma. Between 128 and 124 Ma, the strain decreased to stabilized around 1.5 cm/yr full spreading rate. This would suggest a genetic correlation between the CTP formation and the strain evolution. The fact that the CTP line crosscuts the different SDR and FLF domains tend to demonstrate that the coeval strain acceleration (Fig. 17) would result from the complete strength release between the South Atlantic conjugate margins at the final breakup of the northern segments of the margin. This strain acceleration would therefore be inherent to the VPM formation but would have been delayed till the final rupture of the South Atlantic segment. At austral South Atlantic scale, we therefore propose to use the Crustal Thin Point as the edge of the South Atlantic conjugate VPM.

8.2. Austral South Atlantic VPM asymmetry and forcing parameters

Using the CTP as the a priori edge of the studied VPM, their conjugate architecture appears rather symmetric between the Porto Alegre FZ and the Florianópolis FZ (Fig. 2). Conversely, from the Ventana TZ to the Porto Alegre FZ (Fig. 2), the architecture of South Atlantic conjugate VPM is characterized by a significantly narrower margin along the American plate than along the African plate. The observed asymmetry is moderate, reaching an average value of 60 % for the margin width and the SDR total volume and distribution (Table I). Some aborted rift zones are preserved on the Namibia/South Africa wide margin only (Figs. 13b, 16; Norcliffe et al., 2018). Outside these failed volcanic rifts, the extensional structures show an opposite dip on the two conjugate margins (Clerc et al., 2018). More generally, our observations show that the tectono-magmatic development of these conjugate VPM do not operate on a single and major fault. The upper crustal faults are seen decoupled on the ductile lower crust, which itself, underwent a distributed shear.

South of the Ventana TZ, the SDR-types distribution and their global extension suggest a possible inversion in the polarity of the asymmetry. Some DVS are found on the wide American margin side (Fig. 13b). These structures were not observed at crustal scale due to the lack of deep seismic profiles in this area and are thus not included in our discussion.

The general asymmetry of the South Atlantic VPM has already been highlighted in previous studies (Mohriak et al., 2002; Mohriak & Fainstein, 2012; Blaich et al., 2009, 2011 and 2013). Becker et al. (2014) also noted that the HVLC is much more voluminous and long beneath the African margin than beneath the American plate. Becker et al. (2016) also observe that SDR cover a wider area on the African margin. More recently, McMaster et al. (2019) observed that the Florianópolis Dyke Swarm on the Brazilian side is restricted to a 50 km wide coastal strip, while the dykes along Namibia are found up to 250 km away inland.

The development of asymmetric VPM is an old issue that was also evidenced in NE Atlantic. The conjugate profiles of the SE Greenland and Hatton Bank display a similar level of asymmetry comparatively to South Atlantic VPM, with a coarsely 1:2 to 1:3 ratio in SDR width and total volume of extrusive (Hopper et al., 2003; Smith et al., 2005; White and Smith, 2009). White and Smith (2009) consider that the NE Atlantic asymmetry would be most likely caused by the initial continental stretching. They proposed that the asymmetric stretching of the continental crust is inherited from previous stretching events (Permo-Triassic, Late Jurassic-Early Cretaceous) prior to the final event in the Upper Cretaceous-Paleocene. Alternatively, Hopper et al. (2003) suggested a more autogenic/magmatic phenomenon inspired from the continuous oceanic ridge migration process proposed for asymmetric seafloor spreading. This mechanism was recently inferred by Reuber et al. (2019) in the austral South Atlantic.

A significant pre-magmatic thinning cannot be proposed for the asymmetric development of Austral South Atlantic VPM. Even if some Mesozoic extensional events are known in the south of the austral South Atlantic, they develop oblique rifts that have not thinned the lithosphere in the trend of the margin (Fig. 3b; Frizon de Lamotte et al., 2015; Lovecchio et al., 2020). The last documented and significant thermal event is the collapse of the Pan-African belts in the Ordovician (Helibron et al., 2008) evidenced by the emplacement of granites and associated exhumation.

Despite of the absence of major rifting events prior to the Lower Cretaceous one, it is admitted that crustal or lithospheric-scale compositional heterogeneity are present within ancient orogenic belts, where different paleogeographical units have been accreted together. However, the works of Frimmel et al. (2013), Will et al. (2014) and Will & Frimmel (2018) suggest that the opening of the South Atlantic occurred along the same paleogeographic unit corresponding to the axis of the Neoproterozoic Marmora back-arc basin (purple units in Fig. 3a). In our study, we observed that the tectono-magmatic asymmetry is still significant when the rift crosscuts the northern Gondwanide front and the related Paleozoic fold belts (Paton et al., 2016; Fig. 3). It is thus unlikely that crustal-scale heterogeneities would be continuous across two diachronous and perpendicular orogenic belts and therefore control the global asymmetry of the conjugate margins.

Several recent works in thermomechanical modeling (Brune et al., 2014 and 2016a; Theunissen & Huismans, 2019) demonstrated that a weak behavior of the continental crust might favored, to a certain point, an asymmetric development of passive margins independently of the presence of inheritance. Brune et al. (2014 and 2016a) evidenced that the asymmetry in the central South Atlantic passive margins is mainly promoted by the process of lateral rift migration (Ranero & Perez-Gussinye, 2010) and that the width of the wider margin increases linearly with rift velocity (i.e., southward). This process requires the formation of a low-viscosity pocket at the rift side. Also, in their models, extremely weak crusts (i.e. with a thick ductile layer) tend to develop extremely wide and symmetric conjugate margins because of the absence of any localization of the crustal thinning.

The observations made in this paper, such as the symmetrical sheared lower crust, the large, flat-lying, detachment faults and the inability to locate the deformation (as evidenced by the westward rift axis shift), tend to support the globally weak behavior of the crust during the breakup of the Austral South Atlantic. This raises the question of what may control the weakening of the crust and the general localization of potential low-viscosity pocket toward the South American side (narrow margin). We recognize an architecture that may fit the extreme weak rheological configuration of the Brune et al.'s models (2016a) for the northernmost segment (VI in Fig. 2), characterized by the development of symmetric and very wide conjugate VPM. However, along the

2500 km long margins of the austral South Atlantic, the studied profiles do not exhibit significant variations in width. Thus, we do not observe the correlation that Brune et al.'s (2014) observe between the plates velocities and the margin width. Moreover, lateral migration of active rift axis was observed and modelled in the context of magma-poor margins. This process does not involve the input of magma nor the melt migration through the lithosphere. This difficult task is often neglected or not properly modelled in passive margin simulation, whereas, in the context of VPM, it is very likely a dominant control factor which influences the mode of deformation and the rheology of the rift (Yamasaki and Gernigon, 2009, 2010).

Our interpretation suggests that the architecture of South Atlantic VPM is acquired during their development and would thus be mainly caused by an asymmetric stretching of the continental crust controlling the asymmetric repartition of the extrusives. The observed failed rifts (DVS in Figs. 7, 13b & 16) and the related westward rift jump have accompanied the enlargement the deformed zone on the African side at least, within the segments III & IV (Fig. 2). This hesitation in the main rift localization ends with the development of a conjugate, coarsely symmetric, thick and long intermediate SDR.

We propose that the westward dipping inherited crustal orogenic fabric could have helped to promote the development of primary west dipping half graben observed in the Proximal Domain of both conjugate margins (Fig. 7). This structural reactivation must be limited to the Precambrian basement domain and is highly speculative south of the Gondwanide orogenic front.

Then, it is inferred that the general and early asymmetric development of the Atlantic rift is essentially the result of the globally weaker rheological behavior of the South African lithosphere due to an more intense thinning of the lithosphere under the Africa, resulting in an asymmetrical thermal regime. This would have promoted the higher magma production under the Africa and the asymmetric distribution observed of both the HVLC (Becker et al., 2014) and dyke swarms (McMaster et al., 2019).

A recent geochemical study suggests that the Parana-Etendeka traps related melts must have been generated beneath a highly attenuated lithosphere of about 50km in thickness (Jennings et al., 2019). This implies that the LAB topography could have been highly instable and very shallow since the earliest Cretaceous on the American side in the northernmost part of the Austral South Atlantic. A more efficient thermal erosion and the shift of the magmatic activity toward the present-day location of the breakup axis might be favored by compositional or structural heterogeneities is the lithospheric mantle inherited from either or both the Pan-African orogeny north of the Gondwanide front and the Karoo-Ferrar LIP in the southernmost segments. This mechanism has

been proposed to explain geochemical and lava emplacement heterogeneities of the CAMP over Florida, West Africa and northern South America (Nomade et al., 2002).

In summary, the early stages of crustal deformation and lithospheric mantle erosion might be driven by the Pan-African inheritance. The late westward rift jump that characterizes the asymmetrical development of the austral South Atlantic might derive from the progressive enlargement of the thinning area of the lithospheric mantle beneath the rift axis and from a westward shift of the magma pathway throughout the upper mantle (e.g., Mittelstaedt et al., 2008 & 2011; Yamasaki & Gernigon, 2010). In one hand, the general weakening of the crust, consequence of a strong thermal regime associated to the early intense lithospheric mantle erosion, might be enough to explain the autogenic development of the asymmetry as suggested by the thermomechanical models (Brune et al., 2016a). In another hand, in the highly magmatic systems, the distribution of the deformation is thought to be strongly influenced by the distribution of the magma (Corti et al., 2002, 2004, Yamasaki and Gernigon, 2009).

The migration of the magmatic activity can promote a significant weakening of the lithosphere away from the previous rift axis and induce a delocalization of the deformation toward the future break-up axis (Yamasaki and Gernigon, 2010). Also, the combination of thermal relaxation of the thinned crust and associated volume of magma may also conduct to a rheological strengthening of the early rift system delocalizing the deformation to another zone of weakness (VanWijk & Cloetingh, 2002; Yamasaki and Gernigon, 2009).

Of course, these two mechanisms, could have played all together to promote a rift jump. In another hand, the development of multiple rift axes could be considered as an autogenic evolution of the highly thinned and hot lithosphere. But in this case, what would have controlled their coalescence and consistent westward migration?

Obviously, a relative motion of the lithospheric plates above the hot asthenosphere would represent a seductive explanation. Unfortunately, we did not have found consistent kinematic models that would be suitable for the observed rift jump. Moreover, the published models concerning the location of a hypothetic South Atlantic plume or hot spot are often contradictory (compare Fromm et al., 2017 and Reuber et al., 2019 for instance).

When considering that the location of the magmatic activity is constrained by the area of significant thinning of the lithosphere, there is no peculiar reasons to generate a sudden and consistent westward offset of the magma pathway from an in-development initial zone of rifting.

Therefore, it is likely that the assumed very wide thinning zone of the lithosphere may favorize, by thermal relaxation of its eastern corner, the progressive abandon of the initial rift axis.

Then the westward offset of the new deformation area would help to focus the magmatic activity at the locus of the final break-up.

The asymmetry of the VPM tends to vanish north of the PAFZ (segment VI, Fig. 13). This quite symmetric architecture also occurs where the margins are the widest. This architecture coincides with the areas where the magmatic input in the crust appears as the highest (Figs. 4b and 13a). Thus, a higher than elsewhere thermal gradient related to mantle anomaly is inferred both by the eruption of the Paraná-Etendeka CFB, the thick SDR development, the large amount of underplating and by the higher thicknesses of the oceanic crust (Line 3000 in Fig. 7, Taposeea et al., 2017). This high thermal gradient may have strongly weakened the crust, thickening its ductile part to an extreme level. This mechanism does not exclude a combination to other factors such as a chemical change of the crust or lithospheric mantle nature (magmatic arc in Fig. 3).

We propose that this highly magmatic area of the segment VI and of the associated WR/RGR may have played a dominant role in the asymmetric architecture of the southern domain. The hot and very weak northern area could have played the role of mechanical barrier, preventing the initial rift propagation and promoting its progressive cooling. The resulting rift jump would have been eased toward the west, because of an already thinned lithosphere, resulting in a higher thermal gradient.

Numerous questions remain to accurately deconvolute the forces involved in the 4D development of this VPM. What is the thinning amount of the lithospheric mantle when the traps and first grabens develop at the surface? The evolution of the shape of a thermal anomaly while the lithosphere is extended, is clearly mysterious. Also, is the mantle dynamic related to the South Atlantic opening dominated by one thermal anomaly which could have been channelized southward, or by an elongated upwelling zone related to a first-order convective cell (e.g. Husson et al., 2012), or again by a hotter than normal ambient upper mantle due to the Pangea related continental insulation (Coltice et al., 2007)?

Moreover, despite a better imaged crustal architecture, the precise timing of the N-S propagation of the Atlantic rift suffers from the lack of absolute dating on the successive SDR wedges.

9. Conclusions

The recent long offset seismic profiles of the austral South Atlantic conjugate volcanic passive margins evidence that the different geometries and internal structures of SDR are directly

related to the thinning mode of the underlying crustal basement and to the co-evolution of its rheological behavior.

In addition, the studied seismic profiles evidence a clear asymmetry both in the SDR distribution and crustal domains. This asymmetry is mainly bore by inner SDR and the newly defined intermediate-type SDR. The observable Moho slope inflexions and the overlying crustal thickness profiles also define a significant asymmetry characterized by a wide African margin facing to a narrow South American margin. Double verging sequences of flows also reveals that westward rift jumps have accompanied the development of a wider African margin.

Using these new and extensive observations we propose an evolution scheme for the formation for the South Atlantic austral segment VPM (Fig. 18) sketched here for the segment V (Fig. 2):

a) The rift emplaced over the re-equilibrated Pan-African orogenic crust (Fig. 18a). This crust is considered to be 25-30 km thick prior to the rifting (more than 300 Ma after the last thermal event) and quite heterogenous both along-dip and -strike with the presence of several inherited structural domains from the Pan-African and Gondwanide Orogeneses (magmatic arc, back-arc, retro wedge and foreland; Basei et al., 2018). The Atlantic rifting located in a dominantly W-dipping pervasive orogenic fabric, thought to be at the front of the E-dipping suture zone and the overlying magmatic arc (Fig. 3a; Will and Frimmel, 2018; Basei et al., 2018).

b) Uppermost Jurassic/Lowermost Cretaceous: The old foldbelt was stretched and affected by the first normal faults (Fig. 18b). Along dip, the structural inheritance can explain the asymmetric vergence of the early and proximal grabens which are dominantly developed by negative inversion of W-dipping orogenic fabric along both conjugate margins (Figs. 5 & 6). Considering the Mid Mesozoic rifts that developed through the SW Gondwana (in Argentina, Malvinas and Outeniqua areas) the Mid/Late Jurassic stretching phase of the Atlantic rift developed more likely in reaction to far-field stresses than to active mantle upwelling (Frizon de Lamotte et al., 2015; Lovecchio et al., 2020). However, the Latest Jurassic-Early Cretaceous grabens, from a second extensional phase, are filled with continental detrital and volcanodetrital sediments. During that period, the lithospheric mantle is thinned at least by two in order to produce the melt for the large traps (Jennings et al., 2019) and dyke swarms that emplaced during the Berriasian/Valanginian. The continental crust seems to be barely thinned during that period.

c) 135-133Ma (M10-M9): The crust began to thin (Proximal Necking, Fig. 18c). This thinning is recorded by brittle deformation in the upper-crust and the emplacement of the inner-type SDR. Meanwhile, the lower crust is strongly intruded. It suffered coevally a strong shear evidenced by ductile shear lenses imaged in seismic lines. The structural inheritance seems to no longer

influence the fault pattern which shows an opposite dip on the two conjugate margins. At that stage, the lithospheric thinning was preferentially located beneath the African side, participating to the global warming and consecutive weakening of the overlying lithosphere.

d) 133-132Ma (M9-M7): The intermediate-type SDR began to emplace while the continental crust was drastically thinning (Fig. 18d). During this period, the deformation and magmatism failed to focus, deserting proto-rift axes in the east. The dominant factor controlling this westward rift jump is not clearly defined. The inability to locate both deformation and magmatism could be characteristic of weak crust rifting related to a high thermal regime and likely a shallow asthenosphere. It could also be the consequence of a progressive cooling and strengthening of the initial rift resulting in a westward shift of the tectono-magmatic activity.

e) 132-131Ma (M7-~M4): during the onshore emplacement of the late intermediate- and first outer-type 1 SDR (Fig. 18e), magmatism and associated deformation definitely shift westward and localized close to the South American side leading to the observed asymmetry. This moment could be considered as the break-up initiation of the conjugate margins as the magmatism finally localized at a constant ridge forming a more symmetric magmatic taper (distal necking).

f) 131-130Ma (~M4-M2): The observed strain acceleration generating the crustal thin point ends the distal neck. As the South American and African plates drifted apart, the magmatic production was balanced by plates velocity. The magmatic input slowly decreased changing the conditions of emplacement of the extrusives from outer-type 1 SDR to outer-type 2 SDR, (Fig. 18f) ultimately evolving to FLF type sequences.

g) 130-126 Ma (M2-M0): Since 130 Ma (Hauterivian-Barremian transition, Fig. 18g), a more classical oceanic crust emplaced clearly emphasizing the drifting between the two newly formed geodynamic plates.

Acknowledgments

F.C. would like to thank François Euriat, Gaëtan Rimméle, Jonathan Pelletier, Florian Meresse, Sophie Bouscarat, Victoriano Silva, Aurèle Forge, Charlote Nielsen, Frank Despinois, William Vetel, Philippe Werner, Emmanuel Masini, Philippe de Clarens and Jean-Loup Rubino for their technical support, their very helpful advices and critics on the seismic interpretations, but also for their active investment in the completion of this study. ION Geophysical is also thank for providing the seismic data. This work has been financially supported by the UBO-TOTAL Volcanic Margins Research Program. The authors want to express their gratitude towards Laurent Gernigon and an anonymous reviewer which have significantly improved the manuscript by their comments.

References

Abreu, V.S., 1998. Geologic evolution of conjugate volcanic passive margins : Pelotas Basin(Brazil) and Offshore Namibia (Africa); implication for global sea-level changes, Ph.D. Thesis, Rice University, Houston 3.

Abdelmalak, M.M., Planke, S., Faleide, J.I., Jerram, D.A., Zastrozhnov, D., Eide, S., Myklebust, R., 2016a. The development of volcanic sequences at rifted margins: New insights from the structure and morphology of the Vøring Escarpment, mid-Norwegian Margin. J. Geophys. Res. Solid Earth, 121, 5212–5236.6.

Abdelmalak, M.M., Meyer, R., Planke, S., Faleide, J.I., Gernigon, L., Frieling, J., Sluijs, A., Reichart, G.-J., Zastrozhnov, D., Theissen-Krah, S., Said, A., Myklebust, R., 2016b. Pre-breakup magmatism on the Vøring Margin: Insight from new sub-basalt imaging and results from Ocean Drilling Program Hole 642E. Tectonophysics 675, 258–274.

Almeida, J., Dios, F., Mohriak, W.U., Valeriano, C.M., Heilbron, M., Eirado, L.G., Tomazzoli, E., 2013. Pre-rift tectonic scenario of the Eo-Cretaceous Gondwana break-up along SE Brazil–SW Africa: insights from tholeiitic mafic dyke swarms. In: Mohriak, W.U., Danforth, A., Post, P.J., Brown, D.E., Tari, G.C., Nemcok, M., Sinha, S.T. (eds), Conjugate Divergent Margins. Geological Society of London, Special Publications, v. 369, 11-40.

Armitage, J.J., Collier, J.S., Minshull, T.A., 2010. The importance of rift history for volcanic margin formation. Nature, 465, 913–917, https://doi.org/10.1038/nature09063.

Armitage, J.J. and Collier, J.S., 2018. The thermal structure of volcanic passive margins. Petroleum Geoscience, 24, 393-401, https://doi.org/10.1144/petgeo2016-101.

Autin, J., Bellahsen, N., Leroy, S., Husson, L., Beslier, M.-O., d'Acremont, E., 2013. The role of structural inheritance in oblique rifting: insights from analogue models and application to the Gulf of Aden. Tectonophysics, 607, 51-64, http://dx.doi.org/10.1016/j.tecto.2013.05.041.

Baksi, A., 2018. Paraná flood basalt volcanism primarily limited to ~1 Myr beginning at 135 Ma: new $^{40}Ar/^{39}Ar$ ages for rocks from Rio Grande do Sul, and critical evaluation of published radiometric data. J. Volcanol. Geotherm. Res., http://dx.doi.org/10.1016/j.jvolgeores.2017.02.016.

Basei, M.A.S., Frimmel, H.E., Neto, M.daC.C., de Araujo, C.E.G., de Castro, N.A., Passarelli, C.R., 2018. The tectonic history of the southern Adamastor Ocean based on a correlation of the Kaoko and Dom Feliciano Belts. In: S. Siegesmund et al. (eds), Geology of southwest Gondwana, Regional geology reviews, Springer, Heidelberg, 63–85.

Bauer, K., Neben, S., Schreckenberger, B., Emmermann, R., Hinz, K., Fechner, N., Gohl, K., Schulze, A., Trumbull, R. B., Weber, K., 2000. Deep structure of the Namibia continental margin as derived from integrated geophysical studies. *J. Geophys. Res.,* 105(B11), 25829-25853, doi:10.1029/2000JB900227.

Bauer, K., Trumbull, R.B., Vietor, T., 2003. Geophysical images and a crustal model of intrusive structures beneath the Messum ring complex, Namibia. Earth and Plantery Science Letters, 216, 65-80.

Bécel, A., Shillington, D.J., Nedimović, M.R., Webb, S.C., Kuehn, H., 2015. Origin of dipping structures in fast-spreading oceanic lower crust offshore Alaska imaged by multichannel seismic data. Earth and Planetary Science Letters, 424, 26–37.

Becker, K., Franke, D., Schnabel, M., Schreckenberger, B., Heyde, I., Krawczyk, C. M. 2012. The crustal structure of the southern Argentine margin. Geophysical Journal International, 189, 1483–1504. http://dx.doi.org/10.1111/j.1365-246X.2012.05445.x

Becker, K., Franke, D., Trumbull, R. B., Schnabel, M., Heyde, I., Schreckenberger, B., 2014. Asymmetry of high-velocity lower crust on the South Atlantic rifted margins and implications for the interplay of magmatism and tectonics in continental break-up. Solid Earth Discussions, 6(1), 1335–1370, https://doi.org/10.5194/sed-6-1335-2014.

Becker, K., Tanner, D. C., Franke, D., & Krawczyk, C. M., 2016. Fault-controlled lithospheric detachment of the volcanic southern South Atlantic rift. Geochemistry, Geophysics, Geosystems, 17, 887–894, https://doi.org/10.1002/2015GC006081.

Bellahsen N., Husson, L., Autin, J., Leroy, S., d'Acremont, E., 2013. The rffect of thermal weakening and buoyancy forces on rift localization: field evidences from the Gulf of Aden oblique rifting. Tectonophysics, 607, 80–97, doi:10.1016/j.tecto.2013.05.042.

Berndt, C., Planke, S., Alvestad, E., Tsikalas, F., & Rasmussen, T., 2001. Seismic volcanostratigraphy of the Norwegian Margin: constraints on tectonomagmatic break-up processes. Journal of the Geological Society, London, 158, 413–426.

Blaich, O.A., Faleide, J.I., Tsikalas, F., Franke, D. Leon, E., 2009. Crustal-scale architecture segmentation of the Argentine margin and its conjugate off South Africa. Geophysical Journal International, 178, 85–105, http://dx.doi.org/10.1111/j.1365-246X.2009.04171.x.

Blaich, O.A., Faleide, J.I., Tsikalas, F., 2011. Crustal breakup and continent-ocean transition at South Atlantic conjugate margins. Journal of Geophysical Research, 116, B01402, http://dx.doi.org/10.1029/2010jb007686.

Blaich, O.A., Faleide, J.I., Tsikalas, F., Gordon A.C., Mohriak, W., 2013. Crustal-scale architecture and segmentation of the South Atlantic volcanic margin. In: Mohriak, W.U., Danforth, A., Post, P. J., Brown, D.E., Tari, G.C., Nemčok, M., Sinha, S.T. (eds). Conjugate Divergent Margins. Geological Society, London, Special Publications, 369, 167–183. http://dx.doi.org/10.1144/SP369.22.

Broad, D.S., Jungslager, E.H.A., McLachlan, I.R., Roux, J., van der Spuy, D., 2012. South Africa's offshore Mesozoic basins. In: Roberts, D.G. and Bally, A.W. (eds). Phanerozoic Passive Margins, Cratonic Basins and Global Tectonic Maps. pp. 535-564, DOI: 10.1016/B978-0-444-56357-6.00014-7.

Brune, S., Heine, C., Perez-Gussinye, M., Sobolev, S.V., 2014. Rift migration explains continental margin asymmetry and crustal hyper-extension. Nat. Commun., 5 (4014) http://dx.doi.org/10.1038/ncomms5014.

Brune, S., Heine, C., Clift, P.D., Pérez-Gussinyé, M., 2016a. Rifted margin architecture and crustal rheology: Reviewing Iberia-Newfoundland, Central South Atlantic, and South China Sea. Marine and Petroleum Geology, 79, 257-281.

Brune, S., Williams, S.E., Butterworth, N.P., Müller, R.D., 2016b. Abrupt plate accelerations shape rifted continental margins. Nature, 536, doi:10.1038/nature18319.

Buck, W.R., 2017. The role of magmatic loads and rift jumps in generating seaward dipping reflectors on volcanic rifted margins. Earth Planet. Sci. Lett., 466, 62–69, https://doi.org/10.1016/j.epsl.2017.02.041.

Bueno, G. V., Zacharias, A. A., Oreiro, S. G., Cupertino, A. A., Falkenhein, F. U. H., & Neto, M. A. M., 2007. Bacia de Pelotas. Boletim de Geociências da Petrobras, Rio de Janeiro, 15, 551–559.

Buiter, S.J.H. and Torsvik, T.H., 2014. A review of wilson cycle plate margins: a role for mantle plumes in continental break-up along sutures? Gondwana Res., 26, 627–653.

Callot, J.-P., Geoffroy, L., Brun, J.-P., 2002. Development of volcanic passive margins: three-dimensional laboratory models. Tectonics, 21, 1052, https://doi.org/10.1029/2001TC901019.

Cartwright, J., Swart, R., Corner, B., 2012. Conjugate margins of the South Atlantic: Namibia-Pelotas. In: Roberts, D.G. and Bally, A.W. (eds). Phanerozoic Passive Margins, Cratonic Basins and Global Tectonic Maps. pp. 203-221, DOI: 10.1016/B978-0-444-56357-6.00005-6.

Chaboureau, A.-C., Guillocheau, F., Robin, C., Rohais, S., Moulin, M., Aslanian, D., 2013. Paleogeographic evolution of the central segment of the South Atlantic during Early Cretaceous times: paleotopographic and geodynamic implications. Tectonophysics, 604, 191e223. http://dx.doi.org/10.1016/j.tecto.2012.08.025.

Chenin, P., Manatschal, G., Lavier, L.L., Erratt, D., 2015. Assessing the impact of orogenic inheritance on the architecture, timing and magmatic budget of the North Atlantic rift system: a mapping approach. J. Geol. Soc., 172, 711–720, https://doi.org/10.1144/jgs2014-139.

Chernicoff, C.J., Zappettini, E.O., Peroni, J., 2014. The Rhyacian El Cortijo suture zone: Aeromagnetic signature and insights for the geodynamic evolution of the southwestern Rio de la Plata craton, Argentina: Geoscience Frontiers, 5, 43–52.

Christeson, G.L., Goff, J.A., Reece, R.S., 2019. Synthesis of Oceanic Crustal Structure from Two-Dimensional Seismic Profiles, Reviews of Geophysics, https://doi.org/10.1029/2019RG000641

Clemson, J., Cartwright, J., Booth, J., 1997. Structural segmentation and the influence of basement structure on the Namibian passive margin. Journal of the Geological Society, London, 154, 477–482.

Clerc, C., Jolivet, L., Ringenbach, J.-C., 2015. Ductile extensional shear zones in the lower crust of a passive margin. Earth Planet. Sci. Lett., 431, 1–7.

Clerc, C., Ringenbach, J.C., Jolivet, L., Ballard, J.F., 2018. Rifted margins: Ductile deformation, boudinage, continentward-dipping normal faults and the role of the weak lower crust. Gondwana Res., 53, 20–40, https://doi.org/10.1016/j.gr.2017.04.030.

Collier, J.S., McDermott, C., Warner, G., Gyori, N., Schnabel, M., McDermott, K., Horn, B.W., 2017. New constraints on the age and style of continental breakup in the South Atlantic from magnetic anomaly data. Earth Planet. Sci. Lett., 477, 27–40, https://doi.org/10.1016/j.epsl.2017.08.007.

Coltice, N., Phillips, B., Bertrand, H., Ricard, Y., Rey, P., 2007. Global warming of the mantle at the origin of flood basalts over supercontinents. Geology, 35(5) 391-394, https://doi.org/10.1130/G23240A.1.

Corner, B., 2000. Crustal framework of Namibia derived from magnetic and gravity data. Communications of the Geological Survey of Namibia, 12, 13–19

Corner, B., Cartwright, J., Swart, R., 2002. Volcanic passive margin of Namibia: A potential fields perspective. In: Menzies, M. A., Klemperer, S. L., Ebinger, C. J. & Baker, J. (eds) Volcanic Rifted Margins. Geological Society of America Special Papers, 362, 203–220.

Corner, B. and Durrheim, R.J., 2018. An Integrated Geophysical and Geological Interpretation of the Southern African Lithosphere. In: Siegesmund, S., Basei, M.A.S., Oyhantçabal, P., Oriolo, S. (eds), Geology of Southwest Gondwana. Regional Geology Reviews, Springer International Publishing, https://doi.org/10.1007/978-3-319-68920-3_2.

Corti, G., Bonini, M., Mazzarini, F., Boccaletti, M., Innocenti, F., Manetti., P., Mulugeta, G., Sokoutis, D., 2002. Magma-induced strain localization in centrifuge models of transfer zones. Tectonophysics, 348, 205-218.

Corti, G., Bonini, M., Sokoutis, D., Innocenti, F., Manetti., P., Cloetingh, S., Mulugeta, G. 2004. Continental rift architecture and patterns of magma migration: A dynamic analysis based on centrifuge models. Tectonics, 23, TC2012, doi:10.1029/2003TC001561.

Corti, G., Agostini, A., Keir, D., Van Wijk, J., Bastow, I. D., Ranalli, G., 2015. Magma-induced axial subsidence during final-stage rifting: Implications for the development of seaward-dipping reflectors. Geosphere, 11(3), 563–571. https://doi.org/10.1130/ges01076.1

Courtillot, V., Jaupart, C., Manighetti, I., Tapponnier, P., Besse, J., 1999. On causal links between flood basalts and continental breakup. Earth Planet. Sci. Lett., 166 (3–4), 177-195.

Daly, M.C., Chorowicz, J., Fairhead, J.D., 1989. Rift basin evolution in Africa: the influence of reactivated steep basement shear zones. Geol. Soc. Lond. Spec. Publ., 44, 309–334, https://doi.org/10.1144/GSL.SP.1989.044.01.17.

Dauteuil, O., Deschamps, F., Bourgeois, O., Mocquet, A., Guillocheau, F., 2013. Post-breakup evolution and palaeotopography of the North Namibian Margin during the Meso-Cenozoic. Tectonophysics, 589, 103–115.

de Wit, M., Jeffrey, M., Berg, H., Nicolaysen, L., 1988. Geological map of sectors of Gondwana reconstructed to their disposition; 150 Ma. Tulsa, American Association of Petroleum Geologists and University of the Witwatersrand, scale 1:10 000 000.

de Wit, M.J., Stankiewicz, J., Reeves, C., 2008. Restoring Pan-African–Brasiliano connections: more Gondwana control, less Trans-Atlantic corruption. In: Pankhurst, R.J., Trouw, R.A.J., Brito Neves, B.B. & de Wit, M.J. (eds) West Gondwana: Pre-Cenozoic Correlations Across the South Atlantic Region. Geological Society, London, Special Publications, 294, 399–412. DOI: 10.1144/SP294.20.

Dias, J.L., Sad, A.R.E., Fontana, R.L., Feljó, F.J., 1994. Bacia de Pelotas. Boletim de Geociências da Petrobras, Rio de Janeiro, 8(1), 235–245.

Ding, W., Sunc, Z., Dadd, K., Fanga, Y., Lia, J., 2018. Structures within the oceanic crust of the central South China Sea basin and their implications for oceanic accretionary processes. Earth and Planetary Science Letters, 488, 115–125.

Du Toit, A. L., 1937. Our wandering continents. Edinburgh, Oliver and Boyd

Eldholm, O., Gladczenko, T.P., Skogseid, J., Planke, S., 2000. Atlantic volcanic margins: a comparative study. In: Nøttvedt, A. et al. (eds) Dynamics of the Norwegian Margin. Geological Society, London, Special Publications, 167, 411-428.

Eldholm, O., Skogseid, J., Planke, S., Gladczenko, T.P., 1995. Volcanic margin concepts. In: Banda, E., Talwani, M., Turnip, M. (eds) Rifted Ocean-Continent Boundaries. NATO ASI Series. Kluwer, Dordrecht, 1-16.

Elliott, G.M., Berndt, C., & Parson, L.M., 2009. The SW African volcanic rifted margin and the initiation of the Walvis Ridge, South Atlantic. Marine Geophysical Researches, 30(3), 207–214.

Foulger, G.R., 2018. Origin of the South Atlantic igneous province. Journal of Volcanology and Geothermal Research, 355, 2-20, https://doi.org/10.1016/j.jvolgeores.2017.09.004.

Franke, D., 2013. Rifting, lithosphere breakup and volcanism: comparison of magma-poor and volcanic rifted margins. Mar. Petrol. Geol., 43, 63–87, https://doi.org/10.1016/j.marpetgeo.2012.11.003.

Franke, D., Neben, S., Ladage, S., Schreckenberger, B., Hinz, K., 2007. Margin segmentation and volcano-tectonic architecture along the volcanic margin off Argentina/Uruguay, South Atlantic. Mar. Geol., 244, 46–67.

Franke, D., Ladage, D., Schnabel, M., Schreckenberger, B., Reichert, C., Hinz, K., Paterlini, M., de Abelleyra, J., Siciliano, M., 2010. Birth of a volcanic margin off Argentina, South Atlantic. Geochem. Geophys. Geosyst., 11, Q0AB04, https://doi.org/10.1029/2009GC002715.

Frimmel, H. E., Basei, M. S., Gaucher, C., 2011. Neoproterozoic geodynamic evolution of SW-Gondwana: a southern African perspective. Int. J. Earth Sci., 100, 323–354.

Frimmel, H.E., Basei, M.A.S., Correa, V.X., Mbangula, N., 2013. A new lithostratigraphic subdivision and geodynamic model for the Pan-African western Saldania Belt, South Africa. Precam. Res., 231, 218–235.

Frizonde Lamotte, D., Fourdan, B., Leleu, S., Leparmentier, F., de Clarens, P., 2015. Style of rifting and the stages of Pangea breakup, Tectonics, 34, doi:10.1002/2014TC003760.

Fromm, T., Jokat, W., Ryberg, T., Behrmann, J.H., Haberland, C.,Weber M., 2017. The onset of Walvis Ridge: Plume influence at the continental margin. Tectonophysics, 716, 90-107.

Gac, S. and Geoffroy, L., 2009. 3D Thermo-mechanical modelling of a stretched continental lithosphere containing localized low-viscosity anomalies (the soft-point theory of plate break-up). Tectonophysics 468, 158–168.

Graça, M.C., Kusznir, N., Gomes Stanton, N.S., 2019. Crustal thickness mapping of the central South Atlantic and the geodynamic development of the Rio Grande Rise and Walvis Ridge. Marine and Petroleum Geology, doi: https://doi.org/10.1016/j.marpetgeo.2018.12.011.

Geoffroy, L., 2005. Volcanic passive margins. C. R. Geoscience., 337, 1395–1408.

Geoffroy, L., Burov, E.B., Werner, P., 2015. Volcanic passive margins: another way to break up continents. Nature Scientific Reports, 5, 14828, doi: 10.1038/srep14828.

Geoffroy, L., Chauvet, F., Ringenbach, J.-C., Despinois, F., 2019. Continent-Ocean boundaries: a new model. Geophysical Research Abstracts, EGU General Assembly 2019, 21, EGU2019-5923.

Geoffroy, L., Guan, H., Gernigon, L., Foulger, G.R., Werner, P., 2020. The extent of continental material in oceans: C-Blocks and the Laxmi Basin example. Geophys. J. Int., DOI: 10.1093/gji/ggaa215.

Gernigon, L., Lucazeau, F., Brigaud, F., Ringenbach, J-C., Planke, S., Le Gall, B., 2006. A moderate melting model for the Vøring margin (Norway) based on structural observations and a thermo-kinematical modelling: Implication for the meaning of the lower crustal bodies. Tectonophysics, 412, 255–278.

Gibson, I.L. and Love, D., 1989. A Listric Fault Model for the Formation of the Dipping Reflectors Penetrated during the Drilling of Hole 642E, ODP Leg 104, https://doi.org/10.2973/odp.proc.sr.104.195.1989.

Gladczenko, T.P., Hinz, K., Eldholm, O., Meyer, H., Neben, S., Skogseid, J., 1997. South Atlantic volcanic margins: dour. Geol. Soc., London, 154, 465-470.

Gladczenko, T.P., Skogseid, J., Eldholm, O., 1998. Namibia volcanic margin. Mar. Geophys. Res., 20, 313–341.

Gordon, A.C., Mohriak, W.U., Heilbron, M., 2017. From SE Paraná to Pelotas Basin, a geophysical-geological transect traversing two of the world's largest igneous provinces in South America. Fifteenth Internation International Congress of the Brazilian Geophysical Society.

Gordon, A.C. and Mohriak, W. U., 2015. Seismic volcano-stratigraphy in the basaltic complexes on the rifted margin of Pelotas Basin, Southeast Brazil. In P. Coleman, et al. (Eds.), Petroleum Systems in "Rift" Basins 34th Annual GCSSEPM Foundation Perkins-Rosen Research Conference (pp. 748–786). Houston, TX: GCSSEPM Gulf Coast Section SEPM.

Goscombe, B., Foster, D.A., Gray, D., Wade, B., 2018. The evolution of the Damara orogenic system: a record of West Gondwana assembly and crustal response. In: Siegesmund, S., Basei, M.A.S., Oyhantcabal, P., Oriolo, S. (Eds.), Geology of Southwest Gondwana, Regional Geology Reviews. Springer International Publishing Company, pp. 303–352.

Gradstein, F., Ogg, J., Schmitz,M., Ogg, G., 2012. The Geologic Time Scale 2012. Elsevier, 1.

Graça, M.C., Kusznir, N., Gomes Stanton, N.S., 2019. Crustal thickness mapping ofthe central South Atlantic and the geodynamic development of the Rio Grande Rise and Walvis Ridge. Marine and Petroleum Geology, doi: https://doi.org/10.1016/j.marpetgeo.2018.12.011.

Gray, D.R., Foster, D.A., Meert, J.G., Goscombe, B.D., Armstrong, R., Trouw, R.A.J., Passchier, C.W., 2008. A Damara orogen perspective on the assembly of southwestern Gondwana. In: Pankhurst, R.J., Trouw, R.A.J., Brito Neves, B.B., De Wit, M.J. (Eds.), West Gondwana: Pre-Cenozoic correlations across the South Atlantic region. Geol. Soc., London, Spec. Publ., 294, 257–278.

Guan, H., Geoffroy, L., Gernigon, L., Chauvet, F., Grigné, C., Werner, P., 2018. Magmatic ocean-continent transitions. Marine and Petroleum Geology, 104, 438-450.

Hall, S.A., Bird, D.E., McLean, D.J., Towle, P.J., Grant, J.V., Danque, H.A., 2018. New constraints on the age of the opening of the South Atlantic basin. Marine and Petroleum Geology, 95, 50-66.

Hansma, J., Tohver, E., Schrank, C., Jourdan, F., Adams, D., 2016. The timing of the Cape Orogeny : New $^{40}Ar/^{39}Ar$ age constraints on deformation and cooling of the Cape Fold Belt, South Africa. Gondwana Research, 32, 122–137. https://doi.org/10.1016/j.gr.2015.02.005.

Heilbron, M., Valeriano, C.M., Tassinari, C.C.G., Almeida, J., Tupinambá, M., Siga, Jr.O., Trouw, R., 2008. Correlation of Neoproterozoic terranes between the Ribeira Belt, SE Brazil and its African counterpart: comparative tectonic evolution and open questions From: Pankhurst,

R.J., Trouw, R.A.J., Brito Neves, B.B., de Wit, M.J. (eds) West Gondwana: Pre-Cenozoic Correlations Across the South Atlantic Region. Geological Society, London, Special Publications, 294, 211–237, DOI: 10.1144/SP294.12.

Heilbron, M., Cordani, U.G., Alkmim, F.F., 2017. The São Francisco Craton and its margins. In: Heilbron, M. et al. (eds.), São Francisco Craton, Eastern Brazil, Regional Geology Reviews, Springer International Publishing Switzerland, pp. 3-14, DOI 10.1007/978-3-319-01715-0_1.

Hinz, K., 1981. A hypothesis on terrestrial catastrophes; wedges of very thick oceanward dipping layers beneath passive continental margins. Geologisches Jahrbuch Reihe Geophysic, 22, 3–28.

Hinz, K., Neben, S., Schreckenberger, B., Roeser, H. A., Block, M., Goncalves de Souza, K., Meyer, H., 1999. The Argentine continental margin north of 48°S: Sedimentary successions, volcanic activity during breakup. Marine and Petroleum Geology, 16, 1–25.

Hirsch, K.K., Bauer, K., Scheck-Wenderoth, M., 2009. Deep structure of the western South African passive margin – results from a combined approach of seismic, gravity and isostatic investigations. Tectonophysics, 470, 57–70.

Hopper, J.R., Dahl-Jensen, T., Holbrook, W.S., Larsen, H.C., Lizarralde, D., Korenaga, J., Kent, G.M., Kelemen, P.B., 2003. Structure of the SE Greenland margin from seismic reflection and refraction data: Implications for nascent spreading center subsidence and asymmetric crustal accretion during North Atlantic opening. J. Geophys. Res., 108(B5), 2269, doi:10.1029/2002JB001996.

Hueck, M., Oyhantçabal, P., Philipp, R.P., Basei, M.A.S., Siegesmund, S., 2018. The DomFeliciano Belt in southern Brazil and Uruguay. In: Siegesmund, S., Basei, M.A.S., Oyhantcabal, P., Oriolo, S. (Eds.), Geology of Southwest Gondwana, Regional Geology Reviews. Springer International Publishing Company, pp. 267–302.

Husson, L., Conrad, C. P., Faccenna, C., 2012. Plate motions, Andean orogeny, and volcanism above the South Atlantic convection cell. Earth Planet Sci Lett, 317, 126–135, doi:10.1016/j.epsl.2011.11.040.

Jacques, J.M., 2003. A tectonostratigraphic synthesis of the Sub-Andean basins: inferences on the position of South American intraplate accommodation zones and their control on South Atlantic opening. Journal of the Geological Society, London, 160, 703–717.

Jammes, S., Manatschal, G., Lavier, L., Masini, E., 2009. Tectonosedimentary evolution related to extreme crustal thinning ahead of a propagating ocean: example of the western Pyrenees. Tectonics, 28, TC4012, http://dx.doi.org/10.1029/2008TC002406.

Jerram, D. A., Mountney, N., Stollhofen, H., 1999. Facies architecture of the Etjo Sandstone Formation and its interaction with the Basal Etendeka Flood Basalts of northwest Namibia: implications for offshore prospectivity. In: Cameron, N. R., Bate, R. H. & Clure, V. S. (eds) The Oil and Gas Habitats of the South Atlantic. Geological Society, London, Special Publications, London, 153, 367–380, http://dx.doi.org/10.1144/gsl.sp.1999.153.01.22.

Jolivet, L., Menant, A., Clerc, C., Sternai, P., Bellahsen, N., Leroy, S., Pik, R., Stab, M., Faccenna, C., Gorini, C., 2018. Extensional crustal tectonics and crust-mantle coupling, a view from the geological record. Earth-Science Reviews, 185, 1187-1209, https://doi.org/10.1016/j.earscirev.2018.09.010.

Jungslager, E.H.A., 1999. Petroleum habitats of the Atlantic margin of South Africa. In: Cameron, N.R., Bate, R.H., Clure, V.S. (Eds.), The Oil and Gas Habitats of the South Atlantic. Spec. Pub. Geol. Soc., 153, 153–168.

Karner, G.D. and Gambôa, L.A.P., 2007. Timing and origin of the South Atlantic pre-salt sag basins and their capping evaporites. In: Schreiber, B.C., Lugli, S., Babel, M. (eds). Evaporites Through Space and Time. Geological Society, London, Special Publications, 285, 15–35. DOI: 10.1144/SP285.2.

Kjøll, H.J., Andersen T.B., Corfu, F., Labrousse, L., Tegner, C., Abdelmalak, M.M., Planke S., 2019. Timing of breakup and thermal evolution of a pre- Caledonian Neoproterozoic exhumed magma-rich rifted margin. Tectonics,1843-1862. doi: 10.1029/2018TC005375

Klausen, M.B., 2009. The Lebombo monocline and associated feeder dyke swarm: Diagnostic of a successful and highly volcanic rifted margin? Tectonophysics. 468, 42-62

Klausen, M. and Larsen, H.C., 2002. East-Greenland coastparallel dike swarm and its role in continental break-up. In: M.A. Menzies, S. Klemperer, C. Ebinger and J. Baker (Eds.), Volcanic Rifted Margins. Geological Society of America Special Paper. 362, 1-14

Koopmann, H., Franke, D., Schreckenberger, B., Schulz, H., Hartwig, A., Stollhofen, H., di Primio, R., 2014a. Segmentation and volcano-tectonic characteristics along the SW African continental margin, South Atlantic, as derived from multichannel seismic and potential field data. Marine and Petroleum Geology, 50(0), 22–39. https://doi.org/10.1016/j.marpetgeo.2013.10.016.

Koopmann, H., Schreckenberger, B., Franke, D., Becker, K., Schnabel, M., 2014b. The late rifting phase and continental break-up of the southern South Atlantic: The mode and timing of volcanic rifting and formation of earliest oceanic crust. In T. J. Wright, A. Ayele, D. J. Ferguson, T. Kidane, & C. Vye-Brown (Eds.), Magmatic Rifting and Active Volcanism, Geological Society, London, Special Publications, 420, 315–340. https://doi.org/10.1144/sp420.2.

Larsen, H.C., Dahl-Jensen, T., Hopper, J.R., 1998. Crustal structure along the Leg 152 drilling transect. In: Proceedings of the Ocean Drilling Program. Scientific Results, 152. Ocean Drilling Program, Texas A&M University, College Station, TX, 463–475. https://doi.org/10.2973/odp.proc.sr.152.245.1998.

Lehmann, J., Saalmann, K., Naydenov, K.V., Milani, L., Belyanin, G.A., Zwingmann, H., Charlesworth, G., Kinnaird, J.A., 2016. Structural and geochronological constraints on the Pan-African tectonic evolution of the northern Damara belt, Namibia. Tectonics, 35, 103–135.

Lenoir, X., Féraud, G., Geoffroy, L., 2003. High-rate flexure of the East Greenland volcanic margin: constraints from $^{40}Ar/^{39}Ar$ dating of basaltic dykes. Earth and Planetary Science Letters. 214, 515-528.

Linol, B., deWit, M.J., Guillocheau, F., Robin, C., Dauteuil, O., 2015. Multiphase Phanerozoic subsidence and uplift history recorded in the Congo Basin: a complex successor basin. In: deWit, M.J., Guillocheau, F., deWit, M.C.J. (Eds.), Geology and Resource Potential of the Congo Basin. Springer-Verlag, Berlin Heidelberg, pp. 213–227.

Lovecchio, J.P., Rohais, S., Joseph, P., Bolatti, N.D., Kress, P.R., Gerster, R., Ramos, V.A., 2018. Multistage rifting evolution of the Colorado basin (offshore Argentina): Evidence for extensional settings prior to the South Atlantic opening. Terra Nova, 30 , 359–368.

Lovecchio, J.P., Rohais, S., Joseph, P., Bolatti, N.D., Ramos, V.A., 2020. Mesozoic rifting evolution of SW Gondwana: A poly-phased, subduction-related, extensional history responsible for basin formation along the Argentinean Atlantic margin, *Earth-Science Reviews*, https://doi.org/10.1016/j.earscirev.2020.103138.

Matthews, K.J., Müller, R.D., Wessel, P., Whittaker, J.M. 2011. The tectonic fabric of the ocean basins. Journal of Geophysical Research, 116, B12109. https://doi.org/10.1029/2011JB008413.

Maystrenko, Y. P., Scheck-Wenderoth, M., Hartwig, A., Anka, Z., Watts, A. B., Hirsch, K. K., and Fishwick, S., 2013. Structural features of the Southwest African continental margin according to results of lithosphere-scale 3D gravity and thermal modelling. Tectonophysics, 604, 104–121.

McDermott, K., E. Gillbard, Clarke, N., 2015. From basalt to skeletons - the 200 million-year history of the Namibian margin uncovered by new seismic data. First Break, 33, 77-85.

McDermott, C., Lonergan, L., Collier, J. S., McDermott, K. G., Bellingham, P., 2018. Characterization of seaward-dipping reflectors along the South American Atlantic margin and implications for continental breakup. Tectonics, 37.

McMaster, M., Almeida, J., Heilbron, M., Guedes, E., Mane, M.A., Linus, J.H., 2019. Characterisation and tectonic implications of the Early Cretaceous, Skeleton Coast Dyke Swarm, NW Namibia. Journal of African Earth Sciences, 150, 319-336.

McMillan, I., 2003. Foraminiferally defined biostratigraphic episodes and sedimentation pattern of the Cretaceous drift succession (Early Barremian to Late Maastrichtian) in seven basins on the South African and southern Namibian continental margin. South Afr. J. Sci., 99 (11–12), 537–576.

Mittelstaedt, E., Garrett, I., Behn, M.D., 2008. Mid-ocean ridge jumps associated with hotspot magmatism. Earth and Planetary Science Letters, 266, 256–270.

Mittelstaedt, E., Garrett, I., van Hunen, J., 2011. Repeat ridge jumps associated with plume-ridge interaction, melt transport, and ridge migration. J. Geophys. Res., 116, B01102, doi:10.1029/2010JB007504.

Milani, E.J., de Melo, J.H.G., de Souza P.A., Fernandes, L.A., França, A.B., 2007. Bacia do Paraná B. Geoci. Petrobras, Rio de Janeiro, v. 15, n. 2, 265-287.

Milani, E. and de Wit, M.J., 2008. Correlations between the classic Parana and Cape-Karoo sequences of South America and southern Africa and their basin infills flanking the Gondwanides: du Toit revisited. Geological Society, London, Special Publication, 294, 319-342.

Miller, R.McG., 2013. Comparative Stratigraphic and Geochronological Evolution of the Northern Damara Supergroup in Namibia and the Katanga Supergroup in the Lufilian Arc of Central Africa. Geoscience Canada, v. 40, http://dx.doi.org/10.12789/geocanj.2013.40.007.

Milner, S.C., Duncan, A.R., Ewart, A., 1992. Quartz latite rheoignimbrite flows of the Etendeka Formation, north-western Namibia. Bull. Volcanol., 54, 200-219.

Mjelde, R., Raumb, T., Muraic Y., Takanamic, T., 2007. Continent–ocean-transitions: Review, and a new tectono-magmatic model of the Vøring Plateau, NE Atlantic. Journal of Geodynamics, 43, 374-392.

Mohn, G., Manatschal, G., Müntener, O., Beltrando, M., Masini, E., 2010. Unravelling the interaction between tectonic and sedimentary processes during lithospheric thinning in the Alpine Tethys margins. International Journal of Earth Sciences, 99, 75–101.

Mohriak, W.U. and Fainstein, R., 2012. Phanerozoic regional geology of the eastern Brazilian margin. In: Roberts, D.G. and Bally, A.W. (eds). Phanerozoic Passive Margins, Cratonic Basins and Global Tectonic Maps, pp. 223-282, DOI: 10.1016/B978-0-444-56357-6.00006-8.

Mohriak, W.U., Rosendahl, B.R., Turner, J.P., Valente, S.C., 2002. Crustal architecture of South Atlantic volcanic margins. Geological Society of America, Special Paper 362, 159-202.

Mooney, W.D. and Meissner, R., 1992. Multi-genetic origin of crustal reflectivity: a review of seismic reflection profiling of the continental lower crust and Moho, in Continental Lower Crust. D.M. Fountain, R. Arculus and R.W. Kay, editors, Elsevier, Amsterdam, p. 45-79.

Morales, E., Chang, H.K., Soto, M., Corrêa, F.S., Veroslavsky, G., de Santa Ana, H., Conti, B., Daners, G., 2017. Tectonic and stratigraphic evolution of the Punta del Este and Pelotas basins. Petroleum Geoscience, https://doi.org/10.1144/petgeo2016-059.

Morgan, R.L. and Watts, A.B., 2018. Seismic and gravity constraints on flexural models for the origin of seaward dipping reflectors. Geophys. J. Int., 214, 2073–2083. doi: 10.1093/gji/ggy243.

Moulin, M., Aslanian, D., Olivet, J.-L., Contrucci, I., Matias, L., Geli, L., Klingelhoefer, F., Nouzé, H., Réhault, J.-P., Unternehr, P., 2005. Geological constraints on the evolution of the Angolan margin based on reflection and refraction seismic data (ZaïAngo project). Geophys. J. Int., 162, 793–810. doi: 10.1111/j.1365-246X.2005.02668.x

Moulin, M., Aslanian, D., Unternehr, P., 2010. A new starting point of the south and equatorial Atlantic Ocean. Earth Sciences Reviews, 98, 1-37.

Moulin, M., Aslanian, D., Rabineau, M., Patriat, M., Matias, L., 2013. Kinematic keys of the Santos–Namibe basins. In: Mohriak, W.U., Danforth, A., Post, P.J., Brown, D.E., Tari, G.C., Nemčok, M., Sinha, S. T. (eds). Conjugate Divergent Margins. Geological Society, London, Special Publications, 369, 91–107.

Müller, R. D., Cannon, J., Qin, X., Watson, R. J., Gurnis, M., Williams, S., et al. 2018. GPlates: Building a virtual Earth through deep time. Geochemistry, Geophysics, Geosystems, 19. doi:10.1029/2018GC007584.

Mutter, J.C., Talwani, M., Stoffa, P.L., 1982. Origin of seaward-dipping reflectors in oceanic crust off the Norwegian margin by "subaerial sea-floor spreading". Geology, 10, 353–357.

Nirrengarten, M., Gernigon, L., Manatschal G., 2014. Lower crustal bodies in the Møre volcanic rifted margin: Geophysical determination and geological implications. Tectonophysics, 636 143–157.

Nomade, S., Pouclet, A., Chen, Y., 2002. The French Guyana doleritic dykes: geochemical evidence of three populations and new data for the Jurassic Central Atlantic Magmatic Province. Journal of Geodynamics, 34, 595–614.

Norcliffe, J.R., Paton, D.A., Mortimer, E.J., McCaig, A.M., Nicholls, H., Rodriguez, K., Hodgson, N., Van Der Spuy, D., 2018. Laterally Confined Volcanic Successions (LCVS); recording rift-jumps during the formation of magma-rich margins. Earth and Planetary Science Letters, 504, 53-63, https://doi.org/10.1016/j.epsl.2018.09.033.

O'Connor, J.M. and Duncan, R.A., 1990. Evolution of the Walvis Ridge-Rio Grande Rise hot spot system: Implications for African and South American Plate motions over plumes. Journal of Geophysical Research, 95, 17475–17502.

Oriolo, S., Hueck, M., Oyhantçabal, P., Goscombe, B., Wemmer, K., Siegesmund, S., 2018. Shear zones in Brasiliano-Pan-African belts and their role in the amalgamation and break-up of Southwest Gondwana. In: S. Siegesmund et al. (eds), Geology of southwest Gondwana, Regional geology reviews, Springer, Heidelberg, pp 593–613.

Pángaro, F. and Ramos, V.A., 2012. Paleozoic crustal blocks of onshore and offshore central Argentina: new pieces of the southwestern Gondwana collage and their role in the accretion of Patagonia and the evolution of Mesozoic south Atlantic sedimentary basins. Marine and Petroleum Geology, 37, 162–183.

Pankhurst, R.J., Rapela, C.W., Fanning, C.M., Márquez, M., 2006. Gondwanide continental collision and the origin of Patagonia. Earth Sci. Rev., 76, 235–257. doi.org/10.1016/j.earscirev.2006.02.001.

Paton, D.A., Mortimer, E.J., Hodgson, N., van der Spuy, D., 2016. The missing piece of the South Atlantic jigsaw: when continental break-up ignores crustal heterogeneity. In: Sabato Ceraldi, T., Hodgkinson, R. A. & Backe, G. (eds) Petroleum Geoscience of the West Africa Margin. Geological Society, London, Special Publications, 438, http://doi.org/10.1144/SP438.8.

Paton, D.A., Pindell, J., McDermott, K., Bellingham, P., Horn, B., 2017. Evolution of seaward-dipping reflectors at the onset of oceanic crust formation at volcanic passive margins: insights from the South Atlantic. Geology, 45, 439–442, https://doi.org/10.1130/G38706.1.

Peace, A., McCaffrey, K. J. W., Imber, J., van Hunen, J., Hobbs, R., Wilson, R., 2018. The role of pre-existing structures during rifting, continental breakup and transform system development, offshore West Greenland. Basin Research, 30(3), 373-394. https://doi.org/10.1111/bre.12257.

Peate, D.W., Hawkesworth, C.J., Mantovani, M.S.M., Shukowsky, W., 1990. Mantle plumes and flood-basalt stratigraphy in the Paraná, South America. Geology, 18, 223–1226.

Peate, D.W., Hawkesworth, C.J., Mantovani, M.S.M., 1992. Chemical stratigraphy of the Paraná lavas (South America): classification of magma types and their spatial distribution. Bull. Volcanol., 55, 119–139.

Pérez-Díaz, L. & Eagles, G. 2014. Constraining South Atlantic growth with seafloor spreading data. Tectonics, 33, 1848–1873, https://doi.org/10.1002/2014tc003644.

Petersen, K.D. and Schiffer, C., 2016. Wilson cycle passive margins: Control of orogenic inheritance on continental breakup. Gondwana Research 39, 131–144.

Phillips, T.B., Jackson, C.A.-L., Bell, R.E., Duffy, O.B., 2018. Oblique reactivation of lithosphere-scale lineaments controls rift physiography - the upper-crustal expression of the Sorgenfrei-Tornquist Zone, offshore southern Norway. Solid Earth, 9(2), 403.

Pindell, J., Graham, R., Horn, B., 2014. Rapid outer marginal collapse at the rift to drift transition of passive margin evolution, with a Gulf of Mexico case study. Basin Res., 26, 701–725. https://doi.org/10.1111/bre.12059

Planert, L., Behrmann,J., Jokat, W., Fromm, T., Ryberg, T., Weber, M., Haberland, C., 2017. The wide-angle seismic image of a complex rifted margin, offshore North Namibia: Implications for the tectonics of continental breakup. Tectonophysics, 716, 130-148.

Planke, S., Symonds, P.A., Alvestad, E., Skogseid, J., 2000. Seismic volcanostratigraphy of large-volume basaltic extrusive complexes on rifted margins. J. Geophys. Res., 105, 19335–19351.

Planke, S., Millett, J.M., Maharjan, D., Jerram, D.A., Abdelmalak, M.M., Groth, A., Hoffmann, J., Berndt, C., Myklebust, R., 2017. Igneous seismic geomorphology of buried lava fields and coastal escarpments on the Vøring volcanic rifted margin. Interpretation.

Quirk, D.G., Shakerley, A., Howe, M.J., 2014. A mechanism for construction of volcanic rifted margins during continental breakup. Geology, 42(12), 1079–1082, https://doi.org/10.1130/g35974.1.

Rabinowitz, P. D. and LaBrecque, J., 1979. The Mesozoic South Atlantic Ocean and evolution of its continental margins. Journal of Geophysical Research, 84(B11), 5973–6002. https://doi.org/10.1029/JB084iB11p05973.

Ranero, C.R. and Pérez-Gussinyé, M., 2010. Sequential faulting explains the asymmetry and extension discrepancy of conjugate margins. Nature, 468, doi:10.1038/nature09520.

Renne, P.R., Ernesto, M., Pacca, I.G., Coe, R.S., Glen, J., Prev, M., Perrin, M., 1992. The age of Paraná flood volcanism, rifting of Gondwanaland, and the Jurassic-Cretaceous boundary. Science. 258, 975–979

Renne, P.R., Deckart, K., Ernesto, M., Piccirillo, E., 1996a. Age of the Ponta Grossa dike swarm (Brazil), and implications to Paraná flood volcanism. Earth Planet. Sci. Lett. 144, 199–211

Renne, P.R., Glen, J.M., Milner, S.C., Duncan, A.R., 1996b. Age of Etendeka flood volcanism and associated intrusions in southwestern Africa

Reuber, K., Mann, P., Pindell, J., 2019. Hotspot origin for asymmetrical conjugate volcanic margins of the austral South Atlantic Ocean as imaged on deeply-penetrating seismic reflection images. Interpretation, DOI: 10.1190/int-2018-0256.1.

Reuber, K. and Mann, P., 2019. Control of Precambrian-to-Paleozoic orogenic trends on along-strike variations in early Cretaceous continental rifts of the South Atlantic Ocean. Intepretation, DOI: 10.1190/int-2018-0257.1.

Rohde, J.K., van den Bogaard, P., Hoernle, K., Hauff, F., Werner, R., 2013. Evidence for an age progression along the Tristan-Gough volcanic track from new $^{40}Ar/^{39}Ar$ ages on phenocryst phases. Tectonophysics, 604, 60-71, http://dx.doi.org/10.1016/j.tecto.2012.08.026.

Ryberg, T., Haberland, C., Haberlau, T., Weber, M.H., Bauer, K., Behrmann, J.H., Jokat, W., 2015. Crustal structure of northwest Namibia: evidence for plume-rift-continent interaction. Geology, 43, 739–742. http://dx.doi.org/10.1130/G36768.1.

Salomon, E., Passchier, C., Koehn, D., 2017. Asymmetric continental deformation during South Atlantic rifting along southern Brazil and Namibia. Gondwana Res., 51, 170–176.

Sapin, F., Ringenbach, J.-C., Clerc, C., submitted. Rifted margins archetypes: first order geometries, tentative classification and forcing parameters.

Schiffer, C., et al., 2019. Structural inheritance in the North Atlantic. Earth-Science Reviews, https://doi.org/10.1016/j.earscirev.2019.102975.

Schnabel, M., Franke, D., Engels, M., Hinz, K., Neben, S., Damm, V., Grassmann, S., Pelliza, H., Dos Santos, P. R., 2008. The structure of the lower crust at the Argentine continental margin, South Atlantic at 44°S. Tectonophysics, 454, 14–22.

Senkans, A., Leroy, S., d'Acremont, E., Castilla, R., Despinois, F., 2019. Polyphase rifting and break-up of the central Mozambique margin. Marine and Petroleum Geology, 100, 412–433.

Simon, K., Huismans, R.S., Beaumont, C., 2009. Dynamical modelling of lithospheric extension and small-scale convection: implications for magmatism during the formation of volcanic rifted margins. Geophys. J. Int., 176, 327–350.

Smith, L.K., White, R.S., Kusznir, N.J. and iSIMM Team, 2005. Mantle plume influence on the Hatton-Rockall Basin and adjacent continental margin, in Petroleum Geology: North-West Europe and Global Perspectives. Proceedings of the 6th Petroleum Geology Conference, edited by A.G. Doré and B.A. Vining, pp. 947–956, Geol. Soc., London.

Smith, R.M.H. and Swart, R., 2002. Changing fluvial environments and vertebrate taphonomy in response to climatic drying in a Mid-Triassic rift valley fill: the Omingonde Formation (Karoo Supergroup) of central Namibia. Palaios, 17, 249–267.

Soto, M., Morales, E., Veroslavsky, G., de Santa Ana, H., Ucha, N., Rodríguez, P., 2011. The continental margin of Uruguay: crustal architecture and segmentation. Mar. Pet. Geol., 28, 1676-1689.

Stica, J.M., Zalan, P.V., Ferrari, A.L., 2014. The evolution of rifting on the volcanic margin of the Pelotas Basin and the contextualization of the Paraná–Etendeka LIP in the separation of Gondwana in the South Atlantic. Marine Petroleum Geology, 50, 1–21.

Stoakes, F.A., Campbell, C.V., Cass, R., Ucha, N., 1991. Seismic stratigraphic analysis of the Punta del Este Basin, offshore Uruguay, South America. Bulletin American Association of Petroleum Geologists, 75, 219–240.

Sutra, E., Manatschal, G., Mohn, G., Unternehr, P., 2013. Quantification and restoration of extensional deformation along the Western Iberia and Newfoundland rifted margins. Geochemistry, Geophysics, Geosystems 14, 2575-2597.

Tankard, A., Welsink, H., Aukes, P., Newton, R., Stettler, E., 2012. Geodynamic interpretation of the Cape and Karoo basins, South Africa. In: Roberts, D.G. and Bally, A.W. (eds). Phanerozoic Passive Margins, Cratonic Basins and Global Tectonic Maps, pp. 869-945, DOI:10.1016/B978-0-444-56357-6.00022-6.

Taposeea, C.A., Armitage, J.J., Collier, J.S., 2017. Asthenosphere and lithosphere structure controls on early onset oceanic crust production in the southern South Atlantic. Tectonophysics, 716, 4-20, https://doi.org/10.1016/j.tecto.2016.06.026.

Tavella, G.F. and Wright, C.G., 1996. Cuenca del Salado [Salado Basin]. In: Ramos, V.A. and Turic, M.A. (eds). Geología y Recursos Naturales de la Plataforma Continental Argentina. Capitulo, 6, 95–116.

Theunissen, T. and Huismans, R.S., 2019. Long-term coupling and feedback between tectonics and surface processes during non-volcanic rifted margin formation. Journal of Geophysical Research: Solid Earth., 124, 12,323–12,347. https://doi.org/10.1029/2018JB017235.

Torsvik, T.H., Rousse, S., Labails, C., Smethurst, M.A., 2009. A new scheme for the opening of the South Atlantic Ocean and the dissection of an Aptian salt basin, Geophys. J. Int., 177, 1315–1333, doi:10.1111/j.1365-246X.2009.04137.x.

Tugend, J., Manatschal, G., Kusznir, N.J., Masini, E., 2015. Characterizing and identifying structural domains at rifted continental margins: application to the Bay of iscay margins and

its Western Pyrenean fossil remnants. In: Gibson, G.M., Roure, F. & Manatschal, G. (eds). Sedimentary Basins and Crustal Processes at Continental Margins: From Modern Hyper-extended Margins to Deformed Ancient Analogues. Geological Society, London, Special Publications, 413, 171–203. https://doi.org/10.1144/SP413.3.

Tugend, J., Gillard, M., Manatscha, G., Nirrengarten, M., Harkin, C., Epin, M.-A., Sauter, D., Autin, J., Kusznir, N., McDermott, K., 2018. Reappraisal of the magma-rich versus magma-poor rifted margin archetypes In: McClay, K.R. and Hammerstein, J.A. (eds). Passive Margins: Tectonics, Sedimentation and Magmatism. Geological Society, London, Special Publications, 476. https://doi.org/10.1144/SP476.9.

Turner, S., Regelous, M., Kelley, S., Hawkesworth, C., Mantovani, M., 1994. Magmatism and continental break-up in the South Atlantic: High precision ^{40}Ar-^{39}Ar geochronology. Earth and Planetary Science Letters, 121, 333–348.

Ucha, N., de Santa Ana, H., Veroslavsky, G., 2004. La Cuenca Punta del Este: geología y potencial hidrocarburífero. In: Veroslavsky, G., Ubilla, M. & Martínez, S. (eds). Cuencas Sedimentarias de Uruguay: Geología, Paleontología y recursos naturales – Mesozoico. DIRAC, Montevideo, Uruguay, 173–192.

Uriz, N., Cingolani, C., Chemale Jr., F., Macambira, M., Armstrong, R., 2011. Isotopic studies on detrital zircons of Silurian-Devonian siliciclastic sequences from Argentinean North Patagonia and Sierra de la Ventana regions: comparative provenance. International Journal of Earth Sciences (Geol Rundsch), 100, 571-589.

Uriz, N.J., Cingolani, C.A., Basei, M.A.S., Blanco, G., Abre, P., Portillo, N.S., Siccardi, A., 2016. Provenance and paleogeography of the Devonian Durazno Group, southern Parana Basin in Uruguay. Journal of South American Earth Sciences, 66, 248-267.

Van Wijk, J.W. and Cloetingh, S.A.P.L., 2002. Basin migration caused by slow lithospheric extension. Earth and Planetary Science Letters 198, 275-288.

Veroslavsky, G., Ana, Santa, de, H., Rossello, E.A., 2004. Origen y evolución tectosedimentaria de los depósitos juroeocretácicos de la región meridional del Uruguay: su vinculación con el Lineamiento Santa Lucía-Aiguá-Merín. In: Veroslavsky, G., Ubilla, M., Martínez, S. (Eds.), Cuencas sedimentarias de Uruguay: Geología, paleontología y recursos minerales, Mesozoico 2da. Edición. Ediciones DIRAC, Facultad de Ciencias, Universidad de la República, Montevideo, Uruguay, pp. 117E142.

Waichel, B. L., de Lima, E. F., Lubachesky, R., Sommer, C. A., 2006. Pahoehoe flows from the central Paraná Continental Flood Basalts. Bulletin of Volcanology, 68(7–8), 599–610. https://doi.org/10.1007/s00445-005-0034-5

Wanke, A., Stollhofen, H., Stanistreet, I.G., Lorenz, V., 2000. Karoo unconformities in NW-Namibia and their tectonic implications. Communs geol. Surv. Namibia, 12, 291-301.

Will, T.M., Frimmel, H.E., Gaucher, C., Bossi, J., 2014. Geochemical and isotopic composition of Pan-African metabasalts from southwestern Gondwana: evidence of Cretaceous South Atlantic opening along a Neoproterozoic back-arc. Lithos, 202–203, 363–381.

Will, T.M., Frimmel, H.E., Pfänder, J.A., 2016. Möwe Bay Dykes, Northwestern Namibia: Geochemical and geochronological evidence for different mantle source regions during the Cretaceous opening of the South Atlantic. Chem. Geol., http://dx.doi.org/10.1016/j.chemgeo.2016.08.040.

Will, T.M., and Frimmel, H.E., 2018. Where does a continent prefer to break up? Lessons from the South Atlantic margins. Gondwana Res., 53, 9–19.

White, R.S. and McKenzie, D., 1989. Magmatism at rift zones: the generation of volcanic continental margins and flood basalts. J. Geophys. Res., 94, 7685-7729.

White, R.S. and Smith L.K., 2009. Crustal structure of the Hatton and the conjugate east Greenland rifted volcanic continental margins, NE Atlantic. J. Geophys. Res., 114, B02305, doi:10.1029/2008JB005856.

White, R.S., White, D., O'Nions, R.K., 1992. Oceanic crustal thickness from seismic measurements and rare earth element inversions. J. Geophys. Res., 97, 19,683–19,715. https://doi.org/10.1029/92JB01749.

Wickens, H.deV. and McLachlan, I.R., 1990. The stratigraphy and sedimentology of the reservoir interval of the Kudu 9A-2 and 9A-3 boreholes. Communications of the Geological Survey of Namibia, 6, 9–23.

Wrona, T., Fossen, H., Lecomte, I., Eide, C.H., Gawthorpe, R., 2019. Seismic expression of shear zones: insights from 2-D convolution seismic modelling. https://doi.org/10.31223/osf.io/5ypzg

Yamasaki, T. and Gernigon, L., 2009. Styles of lithospheric extension controlled by underplated mafic bodies. Tectonophysics 468, 169–184.

Yamasaki, T. and Gernigon, L., 2010. Redistribution of the lithosphere deformation by the emplacement of underplated mafic bodies: implications for microcontinent formation. Journal of the Geological Society, London, 167, 961-971. doi: 10.1144/0016-76492010-027.

Zerfass, H., Chemale Jr., F., Lavina, E.L., 2005. Tectonic control of the Triassic Santa Maria Supersequence of the Paraná Basin, southernmost Brazil, and its correlation to the Waterberg Basin, Namibia. Gondwana Research, 8, 163–176.

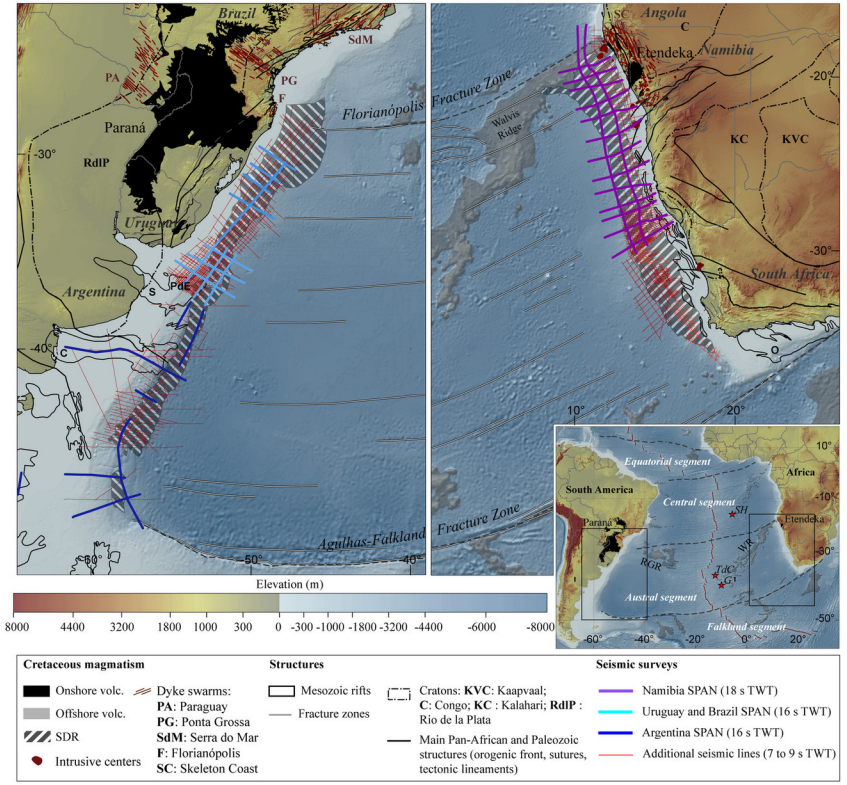

Figure 1. Map of the SDR extend (this study) with the 2D seismic surveys used to define the crustal architecture of the South Atlantic conjugate volcanic margins.
Background data: topography/bathymetry ETOPO1 grid. The South Atlantic oceanic segments and related morphostructures are reported on the inset map (from Moulin et al., 2005). WR/RGR: Walvis Ridge/Rio Grande Rise, Islands: SH: Saint Helena, TdC: Tristan da Cunha, G: Gough. The oceanic fracture zones are from Matthews et al. (2011). The dyke swarms are from Almeida et al. (2013) and McMaster et al. (2019). Mesozoic basins: C: Colorado Basin, S: Salado Basin, PdE: Punta del Este Basin, O: Outeniqua Basin. See Fig. 3 for the legend of the onshore geological background.

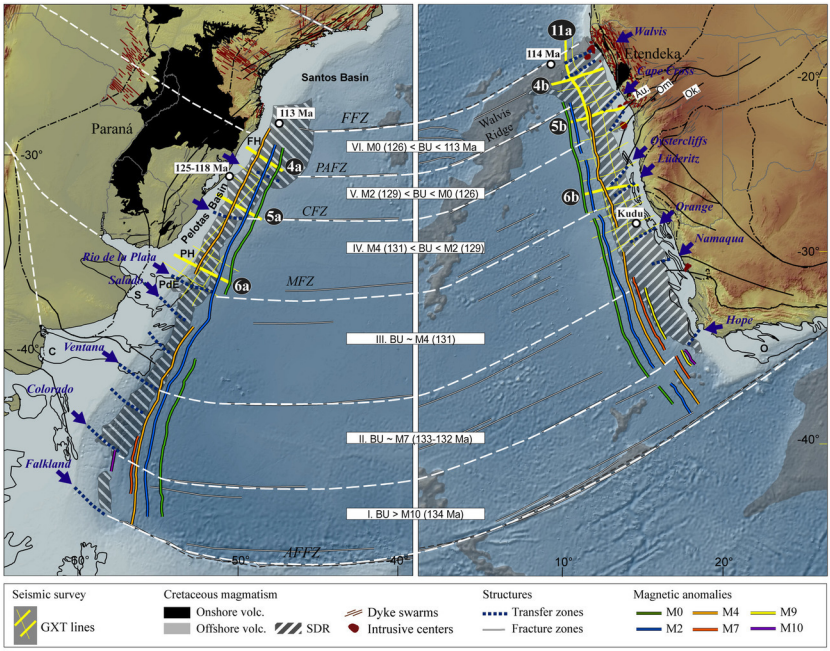

Figure 2. Map of the SDR extend (this study) with the conjugate profiles interpreted in Figs. 4, 5 & 6 (the thick yellow lines). The sub-segment ages are from magnetic anomalies (Rabinowitch & LaBrecque, 1979; Moulin et al., 2010; Koopmann et al., 2014b; Hall et al., 2018; Collier et al., 2017).
The first- and second-order along strike segmentation of the margin is figured with the major transfer zones (blue dotted lines and related arrows) recognized by Clemson et al. (1997), Franke et al. (2007), Blaich et al. (2009), Koopmann et al. (2014a), Soto et al. (2011) and Stica et al. (2014). In the Pelotas basin, they refer to the facing oceanic fracture zones (Chuí and Porto Alegre FZ in Stica et al., 2014). Microplates limits from the kinematic model of Moulin et al. (2010) are reported with onshore white dashed lines. The first-order segmentation of the South American margin is extrapolated to the conjugate plate (offshore white dashed lines), by following the oceanic fracture zones from Matthews et al. (2011). The indications for the break-up age in each first-order segment corresponds to the age (according to the timescale of Gradstein et al., 2012) of the first magnetic anomaly resting on a constant thickness crust (this study). Note the M9 and M4 anomalies overlapping the SDR. The ages in white boxes correspond to the available Ar-Ar datings obtained on Brazilian SDR sequences and on a Walvis Ridge volcano (see text for references). Fracture Zones: FFZ: Florianópolis Fracture Zone, PAFZ: Porto Alegre FZ, CFZ: Chuí FZ, MFZ: Meteor FZ, AFFZ: Aguhlas-Falkland FZ. Basement highs: PH: Polonio High, FH: Florianópolis High. . The Pan-African structures reactivated during the South Atlantic opening (from Corner & Durrheim, 2018): Au.: Autsieb, Om.: Omaruru, Ok.: Okahandja. See Fig. 3 for the legend of the onshore geological background.

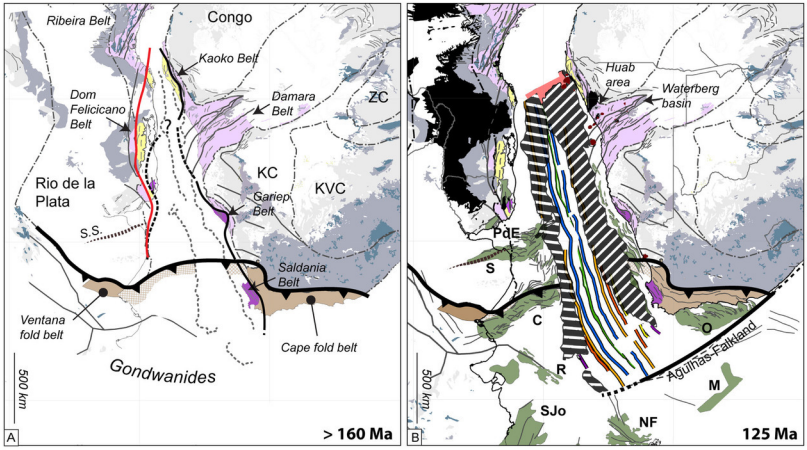

Sediments

- Mesozoic - Cenozoic
- Late Jurassic - Early Cretaceous rifts
  - > PdE : Punta del Este
  - > S : Salado
  - > C : Colorado
  - > V : Valdes
  - > R : Rawson
  - > SJo : San Jorge
  - > NF : North Falkland
  - > M : Malvinas
  - > O: Outeniqua
- Late Carboniferous to Middle Jurassic
- Precambrian to Devonian

Magmatism

- Walvis Ridge volcanism
- SDR
- Paraná-Etendeka traps
- Pre-Cretaceous magmatism
- Igneous intrusive centers (Messum, Brandberg, Cape Cross, Etc.)
- The onset of Cretaceous SDR plotted in the reconstruction at 160 Ma

Basement

Paleozoic

- Onshore and offshore fold belts (Cape & Ventana)

Neoproterozoic to Cambrian (0.65 - 0.45 Ga) tectono-stratigraphic domains

- Back arc domain (inferred extension in dashed line)
- Continental magmatic arc
- Brasiliano / Pan-African orogenic belt undifferentiated

Cratonic areas (Proterozoic and Archean)

- KVC : Kaapvaal; ZC : Zimbabwe; KC : Kalahari

- S.S. : Salado suture (2.1.Ga)
- Structural lineaments
- Main Pan-African suture
- Gondwanides deformation front

Ocean

Magnetic anomalies	GTS12 (Ma)
M0 (Moulin et al., 2010)	126.3-125.9
M2max (Moulin et al., 2010)	129.1-128.6
M4 (Moulin et al., 2010)	131.4-130.6
M7 (Moulin et al., 2010)	132.5-132
M9 (Koopmann et al., 2014b)	133.6-133
M10 (Collier et al., 2017)	134.2-133.6

Figure 3. A: Pre-opening reconstruction of the SW Gondwana (kinematic model from Moulin et al., 2010); B: Reconstruction at 126 Ma (~M0) with the magnetic anomalies identified in the South Atlantic Ocean and the SDR domains mapped in this study. The trans-Atlantic connections between analogous tectono-stratigraphic units are from and Pangaro & Ramos (2012), Frimmel et al. (2013) and Paton et al. (2016). Mesozoic rifts are from Parsiegla et al. (2009), Becker et al. (2012), Lovecchio et al. (2018) and this study. GTS12: time scale from Gradstein et al. (2012).

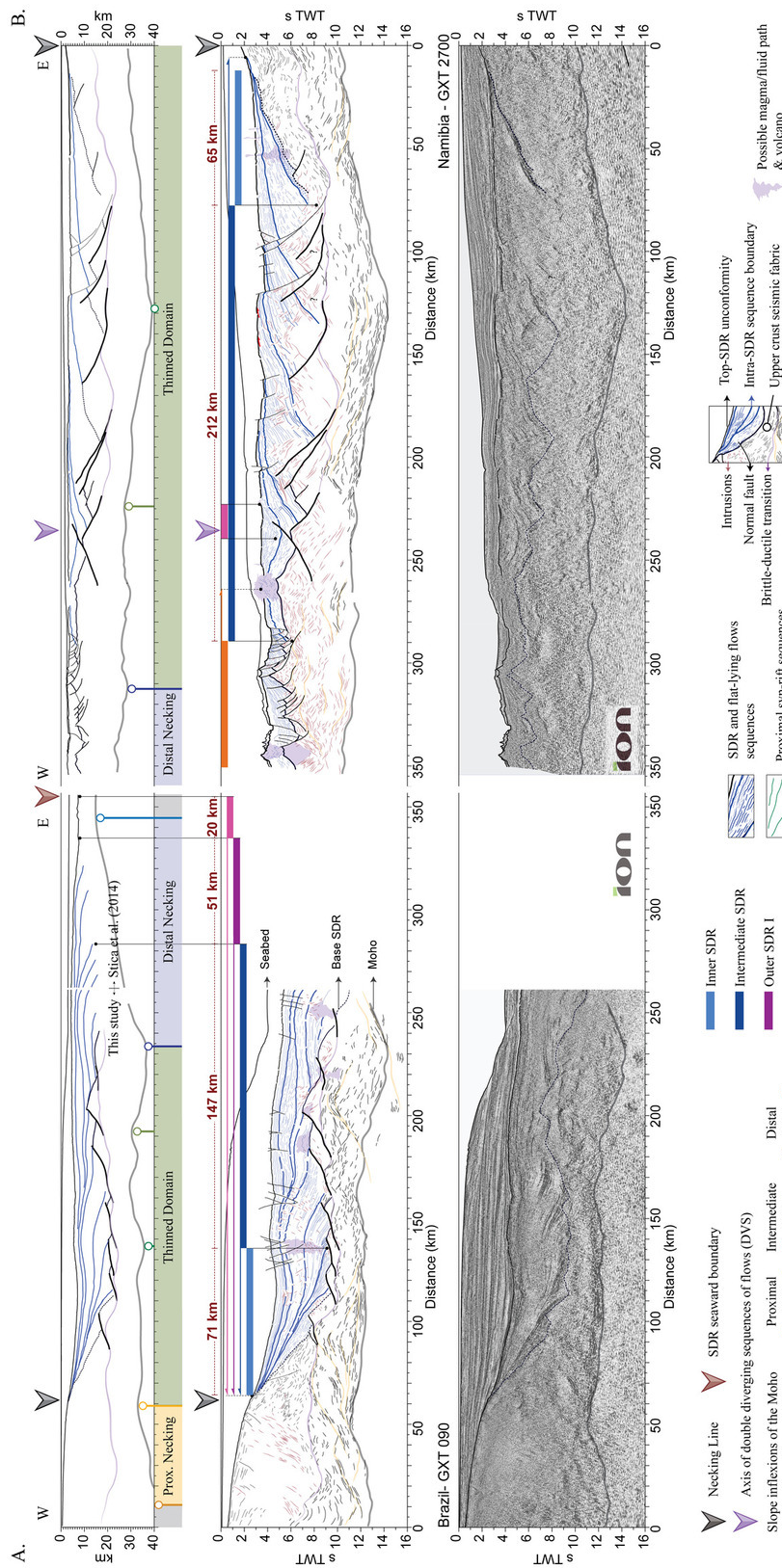

Figure 4. Conjugate 090 vs. 2700 ION GXT lines line drawing and interpretation with corresponding time-depth conversion. The conjugate lines are located in the segment VI of Fig. 2.

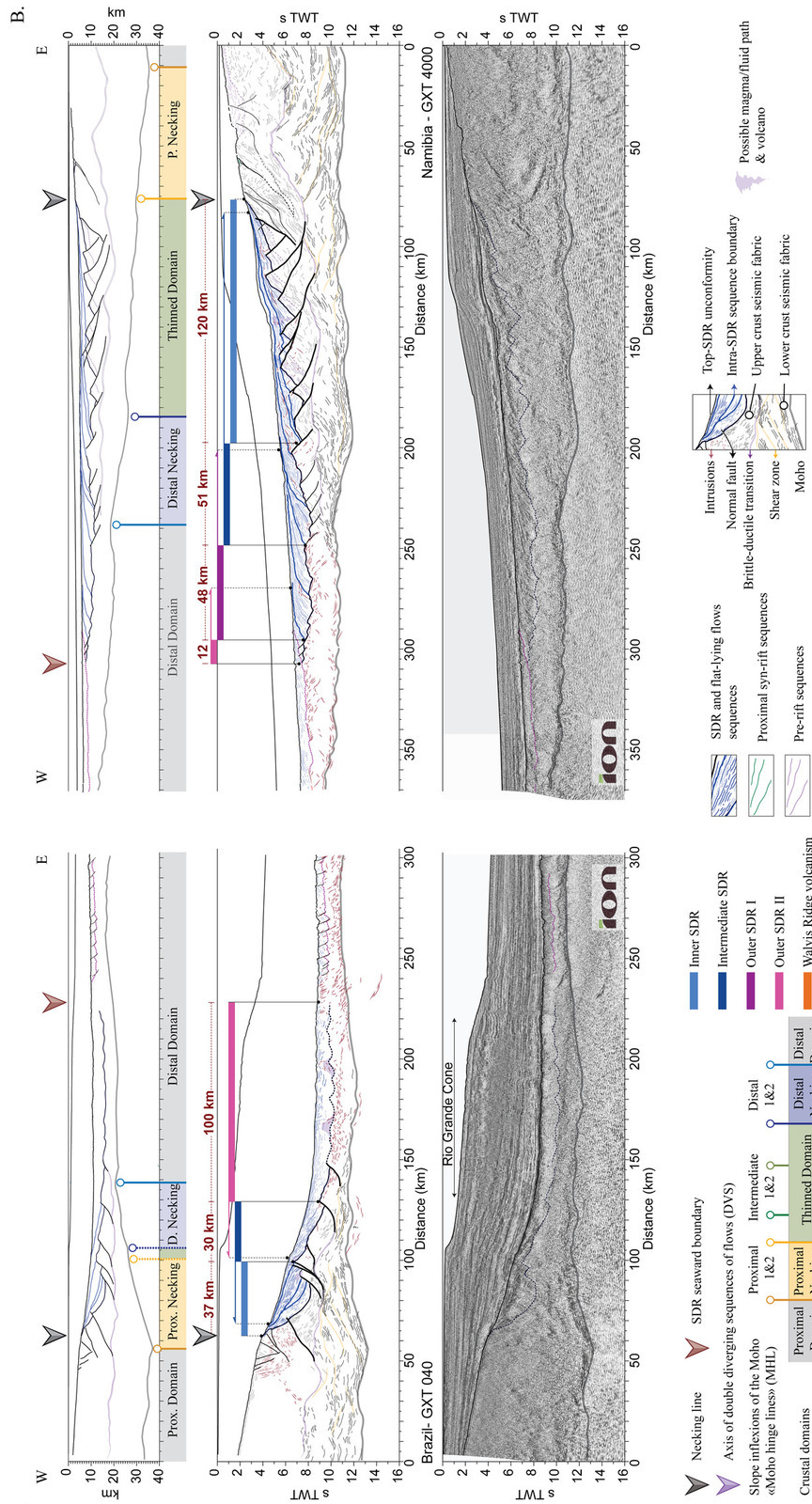

Figure 5. Conjugate 040 vs. 4000 ION GXT lines line drawing and interpretation with corresponding time-depth conversion. The conjugate lines are located in the segment V of Fig. 2.

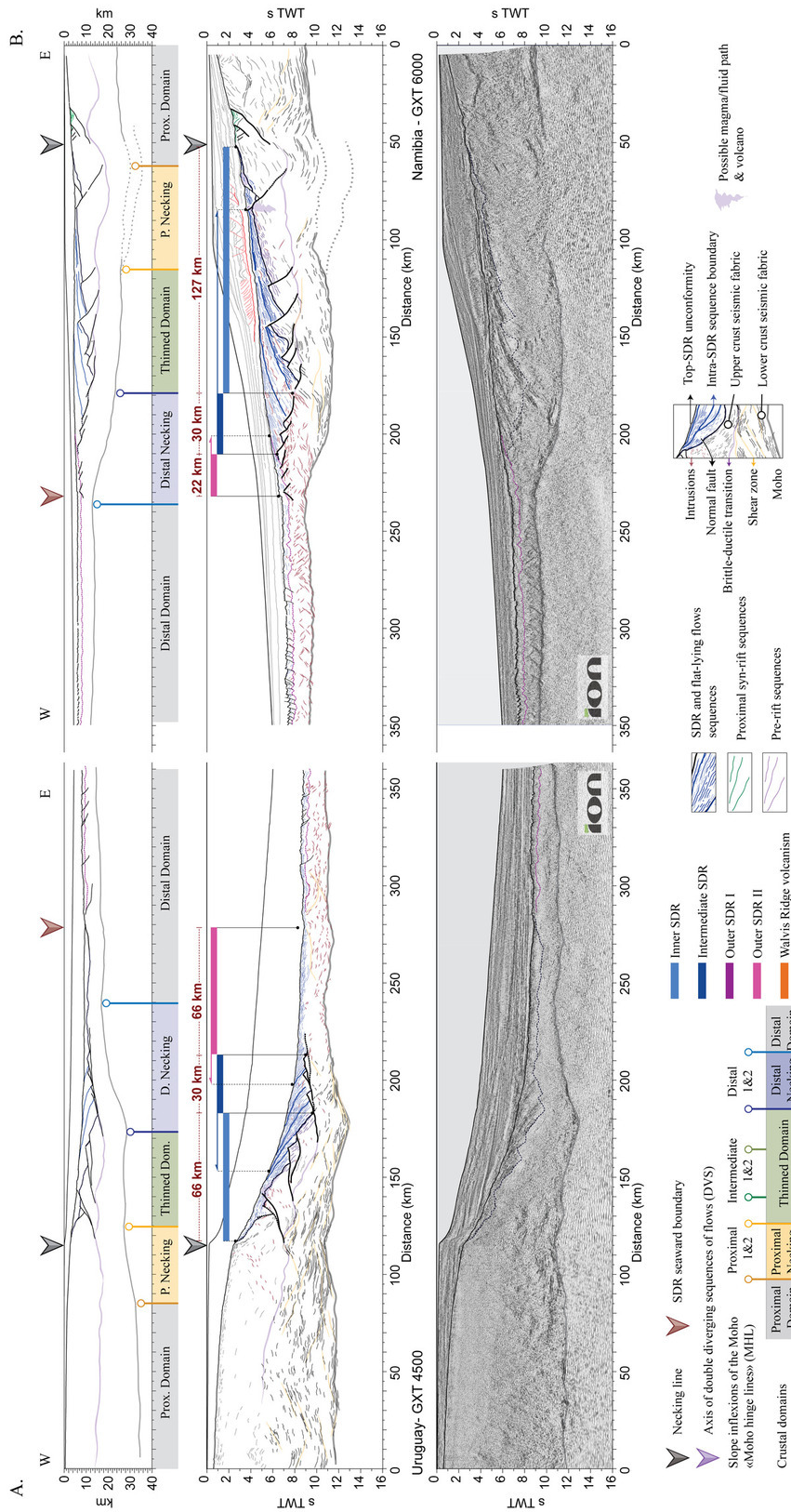

Figure 6. Conjugate 4500 vs. 6000 ION GXT lines line drawing and interpretation with corresponding time-depth conversion. The conjugate lines are located in the segment IV of Fig. 2.

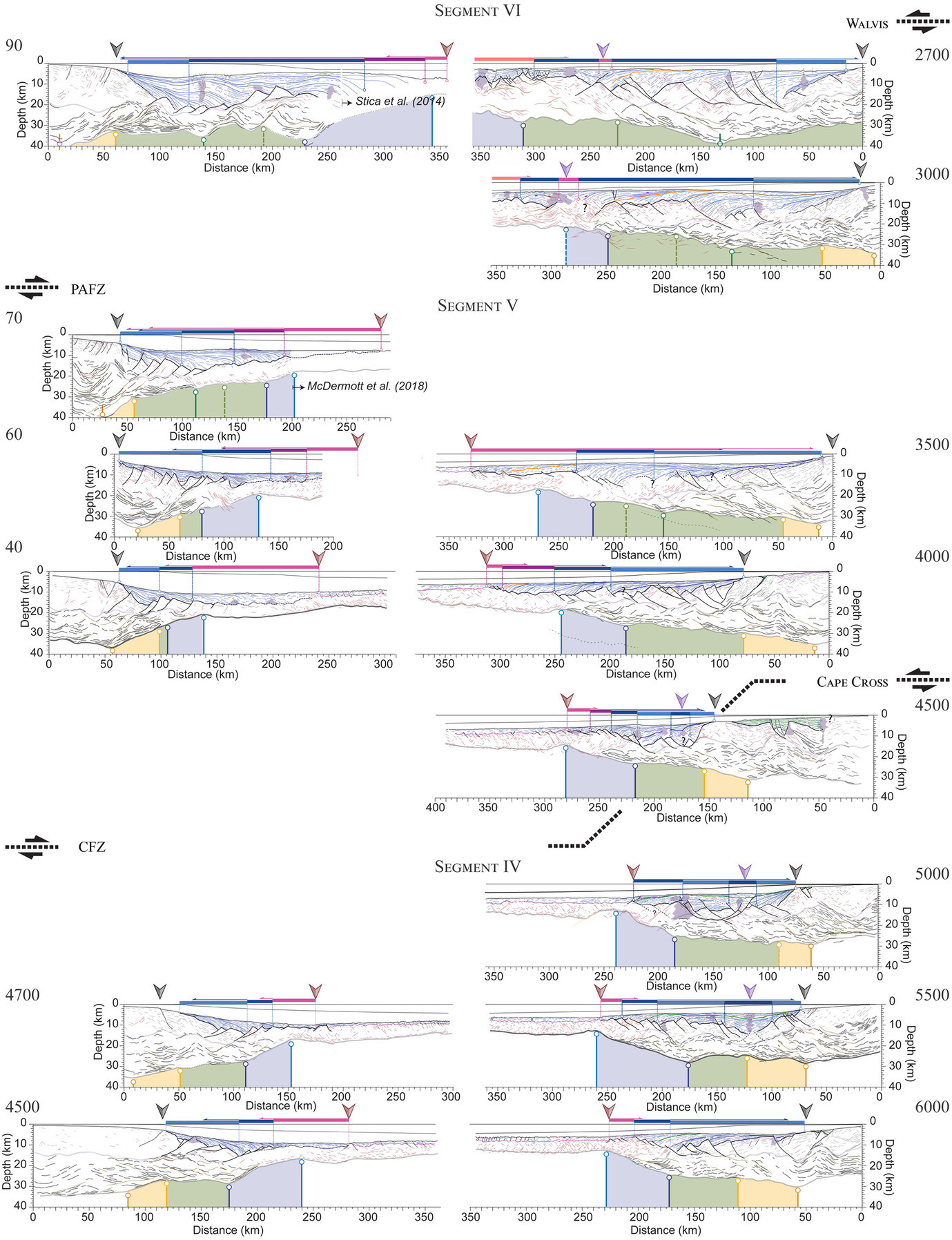

Figure 7. Interpretations of the depth-converted seismic profiles for the entire 2D ION survey (location in Fig. 2). The inset map displays the seismic survey reconstructed at 126 Ma and 133 Ma according to the Moulin et al. (2010) kinematic model. The conjugate lines displayed in Figs. 4 to 6 are underlined in yellow.

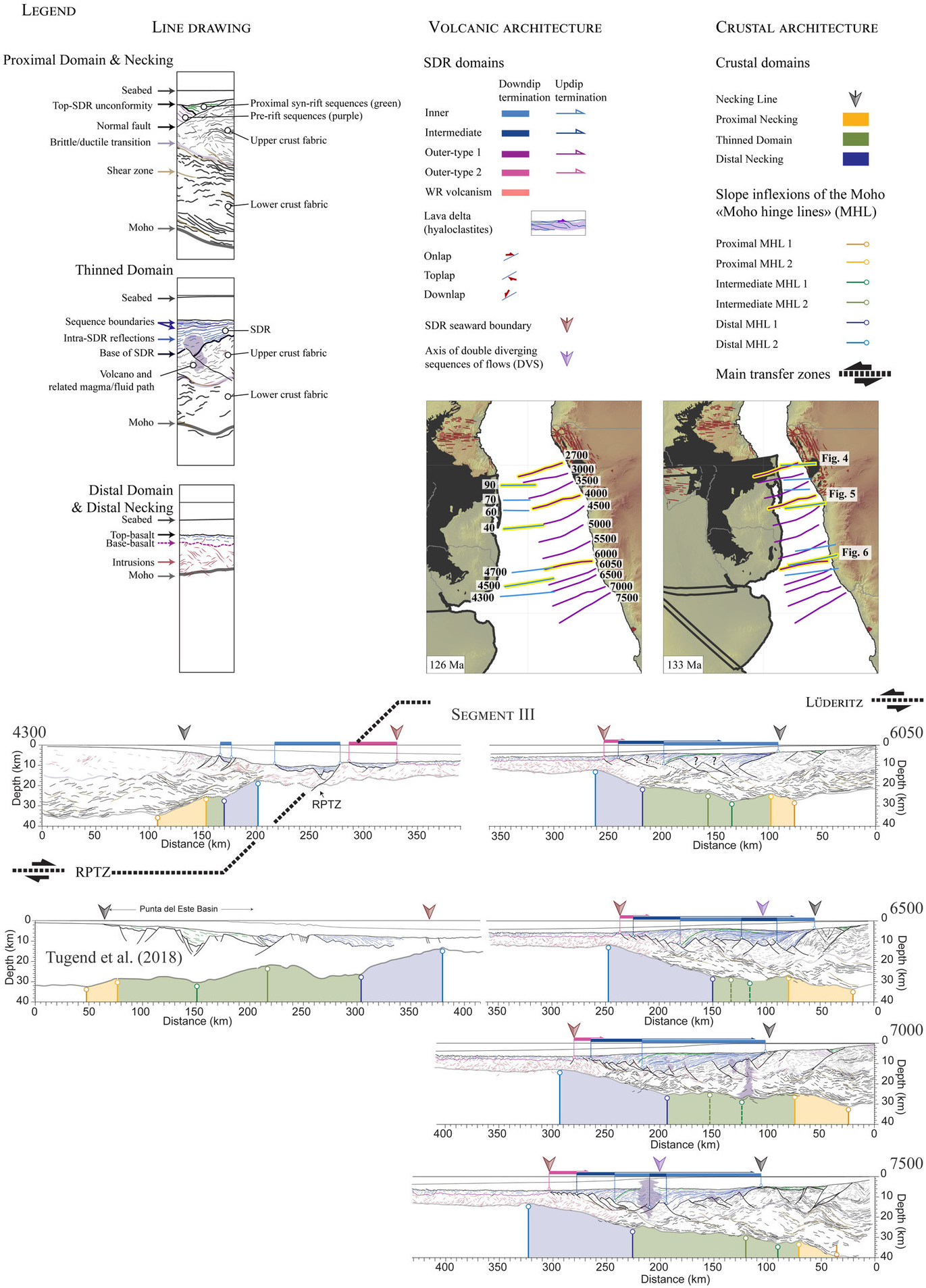

Figure 7. (continue)

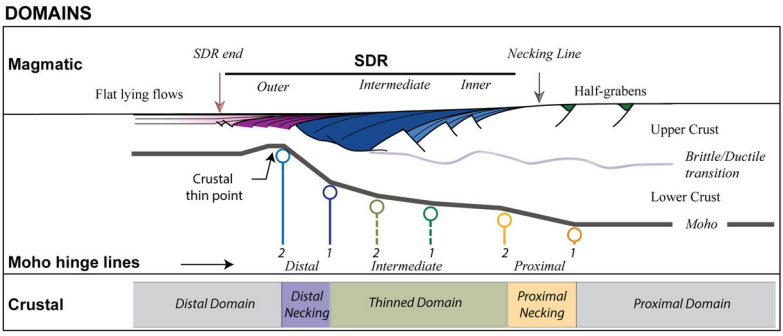

Figure 8. Synthetic scheme illustrating the distribution of the main structures and of the different magmatic and crustal domains as observed on the South Altantic conjugate VPM (Fig. 7).

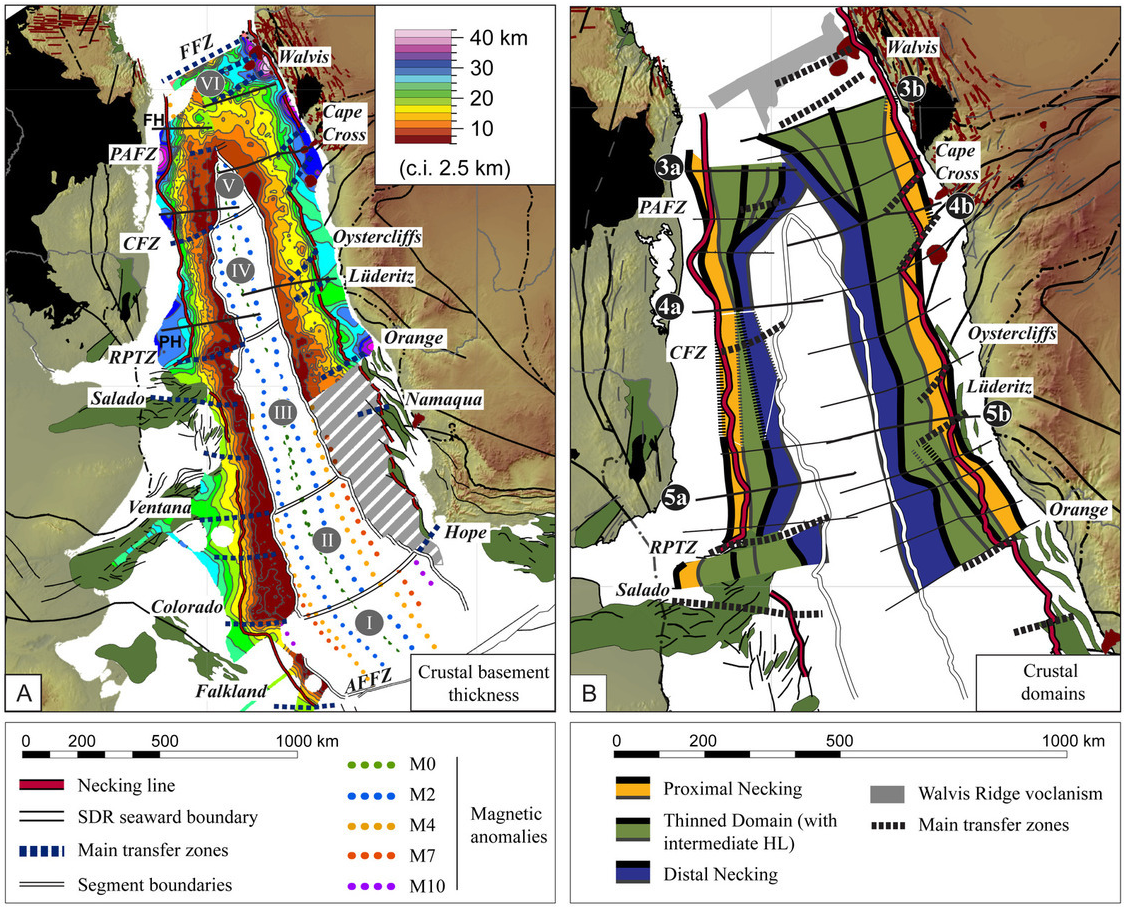

Figure 9. Maps reconstructed at 126 Ma (M0). See Fig. 3 for the legend of the geological background. A: Thickness of the crust preserved beneath the SDR. PH: Polonio High, FH: Florianópolis High. B: Location of the main crustal domains and Moho hinge lines. In A., the first-order oceanic segments corresponds to those of the displayed in Fig. 2.

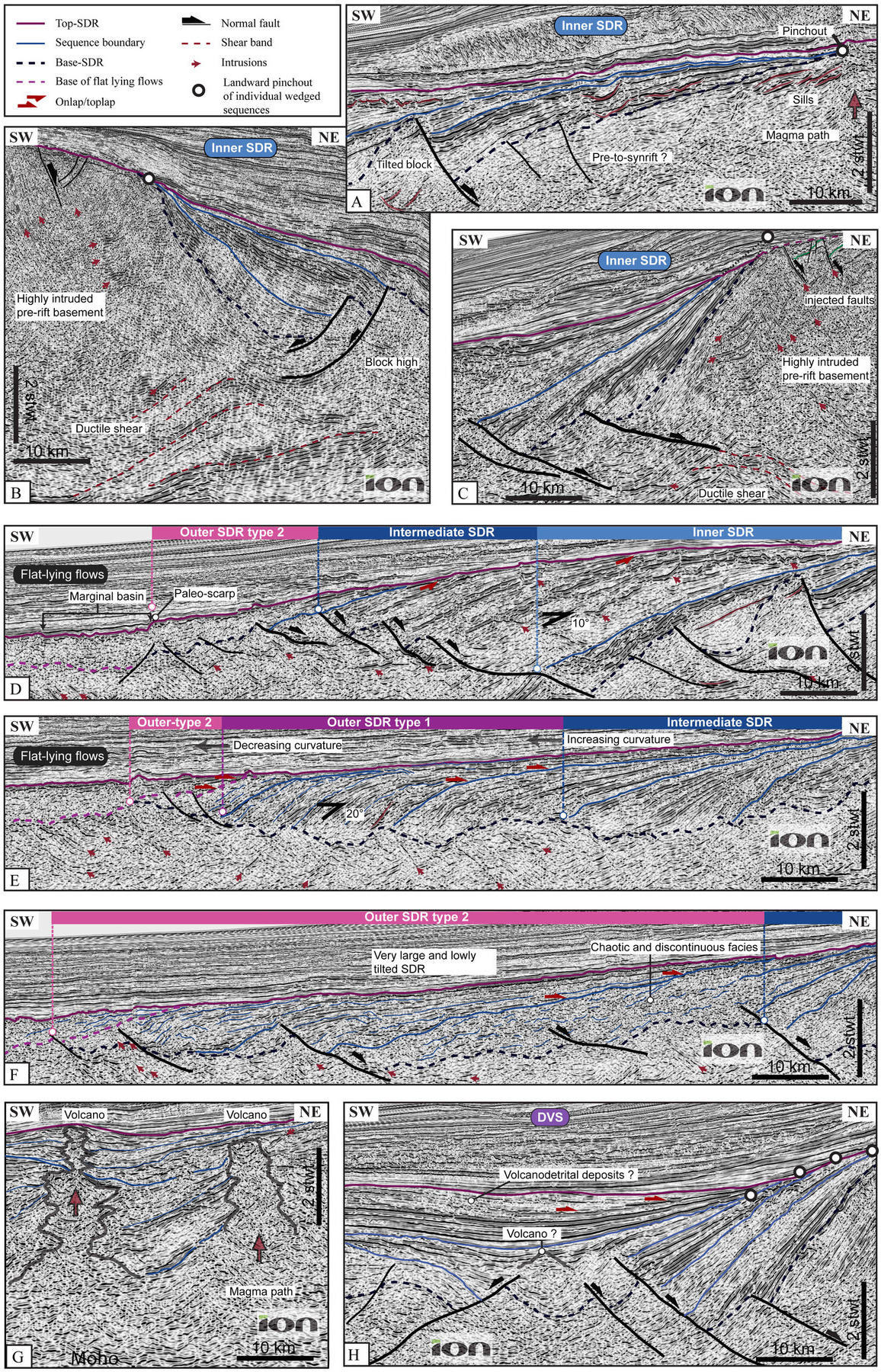
Top-SDR
Sequence boundary
Base-SDR
Base of flat lying flows
Onlap/toplap
Normal fault
Shear band
Intrusions
Landward pinchout of individual wedged sequences
SW
NE
Inner SDR
Pinchout
Sills
Magma path
Pre-to-synrift ?
Tilted block
2 sTWT
10 km
A
Highly intruded pre-rift basement
Block high
Ductile shear
B
injected faults
C
Outer SDR type 2
Intermediate SDR
Flat-lying flows
Marginal basin
Paleo-scarp
10°
D
Outer-type 2
Outer SDR type 1
Decreasing curvature
Increasing curvature
20°
E
Very large and lowly tilted SDR
Chaotic and discontinuous facies
F
Volcano
G
Moho
DVS
Volcanodetrital deposits ?
Volcano ?
H

Figure 10. Illustration of the main structure types and of seismic facies encountered within the SDR domain. A-B-C: Inner-type SDR: Different examples of inner SDR forming a planar-diverging wedge related to continent-ward dipping normal faults. Note the important lateral and vertical variations of the reflectivity within these seismic units. D: Intermediate-type SDR: Large and thick wedge with slightly arcuate-diverging reflections (up to 10° dip). Up-dip terminations display seaward migrating pinchout of successive wedges. The base of the wedge lies on an unclear surface which appears intensively intruded (red arrows) and cut up by a complex network of continentward-dipping faults. This SDR is overlain by a slightly thickening seaward-dipping sequence of planar-diverging reflectors (above the pink dotted line). This ultimate sequence of flows (outer-type 2) oversteps the hanging wall of the underlying SDR and laterally merges with a sequence of flat-lying flows. Toward the continent, the intermediate-type wedge overlies a set of shorter and over-tilted inner-type wedges (bottom right). The intermediate-type SDR develops above a 11 km thick highly intruded basement. Note the numerous figures of intrusions in the interior of the wedge (red arrows). E: Outer-types 1 and 2: The outer-type 1 is characterized by a set of strongly arcuate-diverging sequences of reflectors deflected above a sub-horizontal to slightly continent-ward dipping basal surface. This outer SDR forms a 5-6km thick wedge of seaward-dipping sequences flows. The reflections tend to onlap the previously emplaced sequences with a backstepping pattern which suggests a coeval subsidence of the inner-more domain. The last emplaced sequence of flows (outer-type 2) onlap a residual topography formed by the previous SDR sequence flexure. They overly a highly injected basement which underwent a very limited extension. F: 100 km long and 4 km thick outer-type 2 SDR showing a planar-diverging pattern with a slightly tectonized substratum and a low lateral thickening (cf. line 3500 in Fig. 7). G: Evidences for deep-seated volcanic constructions emplaced throughout the inner SDR of the Namibian margin (line 4500 in Fig. 7). Note the « vertical column » of highly disrupted seismic facies. This disturbed acoustic facies is likely due to a magma and/or fluid extensive impregnation of the basement. H: Example of double verging sequences of SDR wedges.

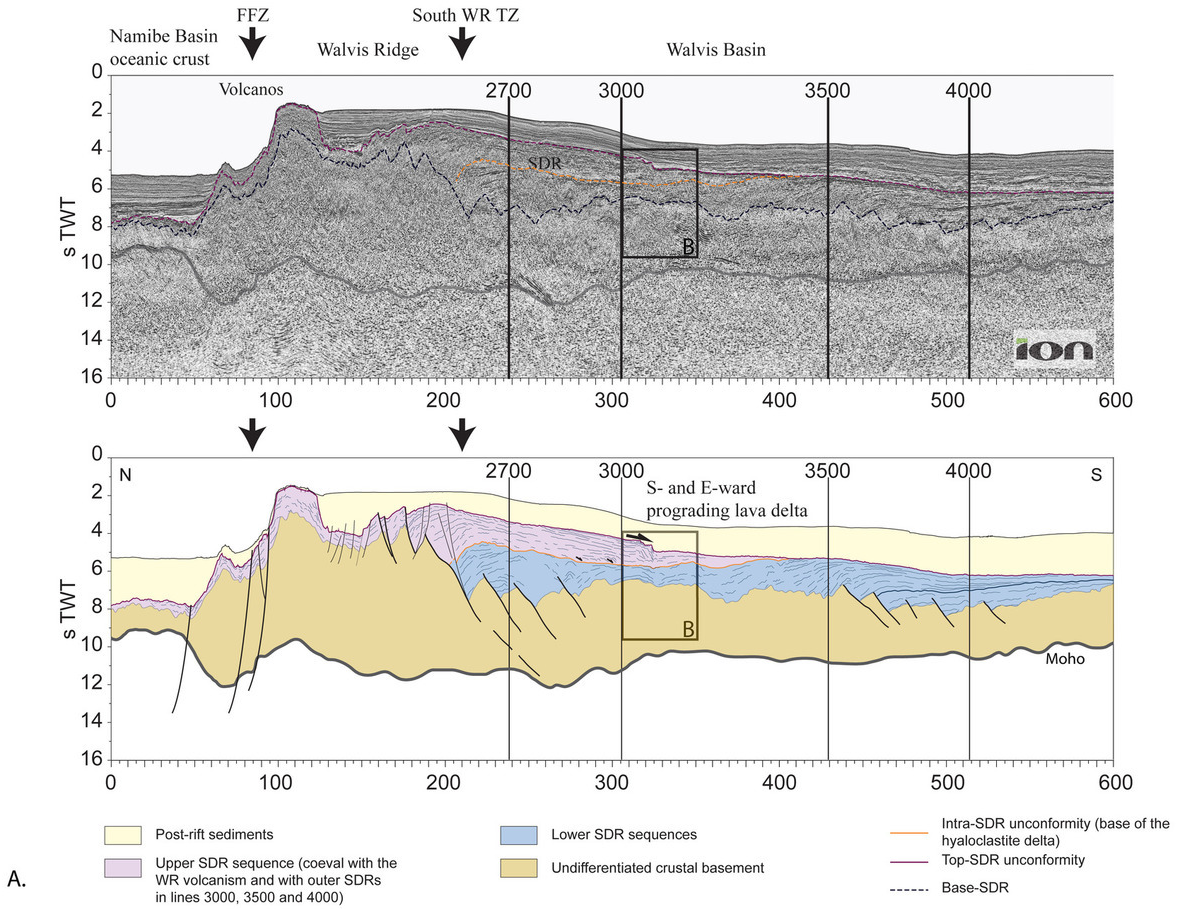

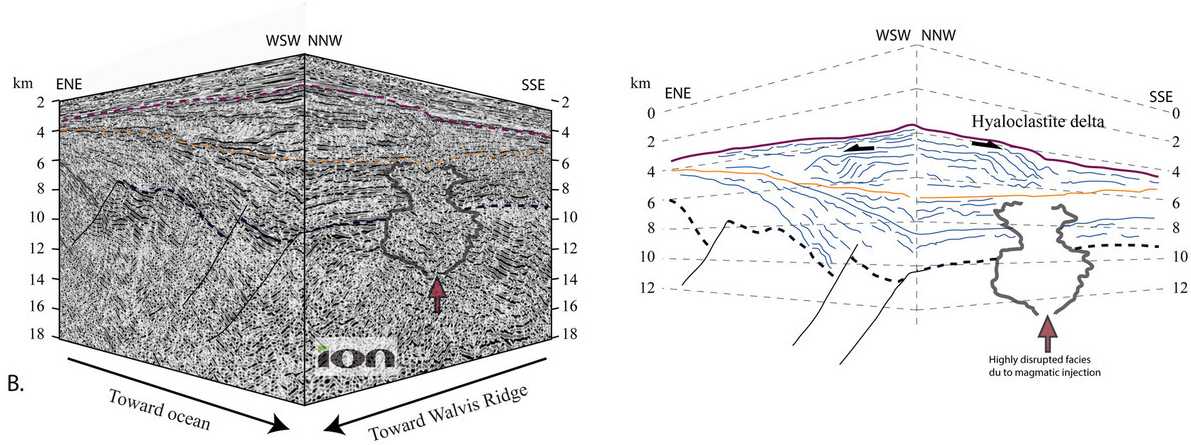

Figure 11. A: Margin parallel profile (location in Fig. 2) and corresponding schematic interpretation illustrating the crustal and volcanic architecture of the northern Namibian VPM and Walvis Ridge. Two superimposed sequences of SDR, separated by a major unconformity (orange marker, also in Fig. 7). The youngest SDR (pink) are correlatable with the sequences that lie at the top of the Walvis Ridge and which are likely intra-Aptian (see text for explanation). The two SDR sequences dip and thicken northward, against an E-W transfer zone (Walvis TZ in Fig. 2), and westward (see in-dip profiles in Figs. 4 & 5). A lava delta is interpreted southeastward, down-lapping the orange marker (cf B). B: Intersecting seismic profiles showing the 3D architecture of the southeastward prograding lava delta. The subaqueous volcano-detrital construction develops against the southern flank of Walvis Ridge and within a subsiding down to 1000m depth basin. This indicates that the margin central segment (n° V, Fig. 2) south of Walvis Ridge has started its subsidence and is drowning whereas subaerial flows continue to develop SDR wedges toward the N and the W.

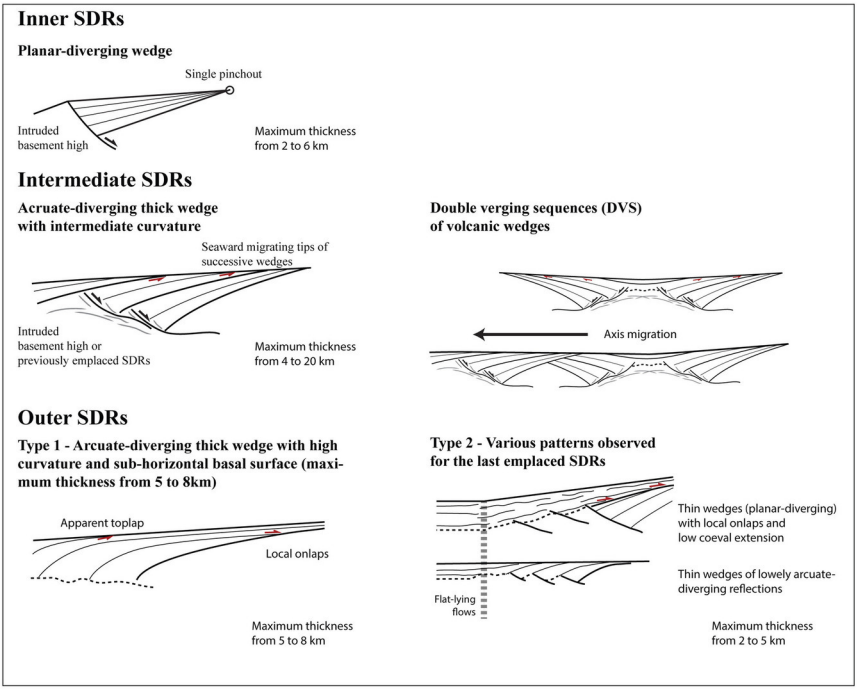

Figure 12. Typology applied to the SDR domain and based on the structural diversity of the SDR successive wedges (modified from Planke et al., 2000).

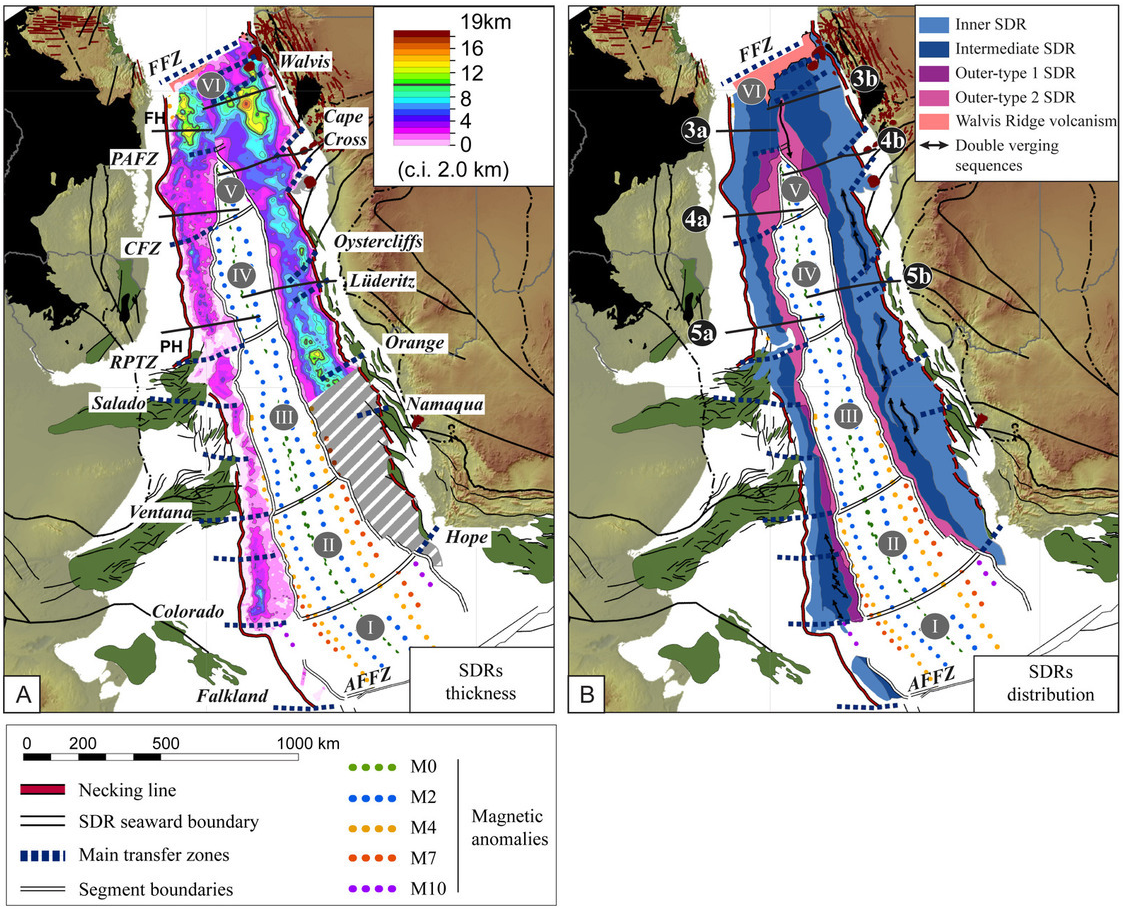

Figure 13. Maps reconstructed at 126 Ma (M0). See Fig. 3 for the legend of the geological background. A: Total SDR thickness. B: Distribution of the different types of SDR. The first-order oceanic segments corresponds to those of the displayed in Fig. 2.

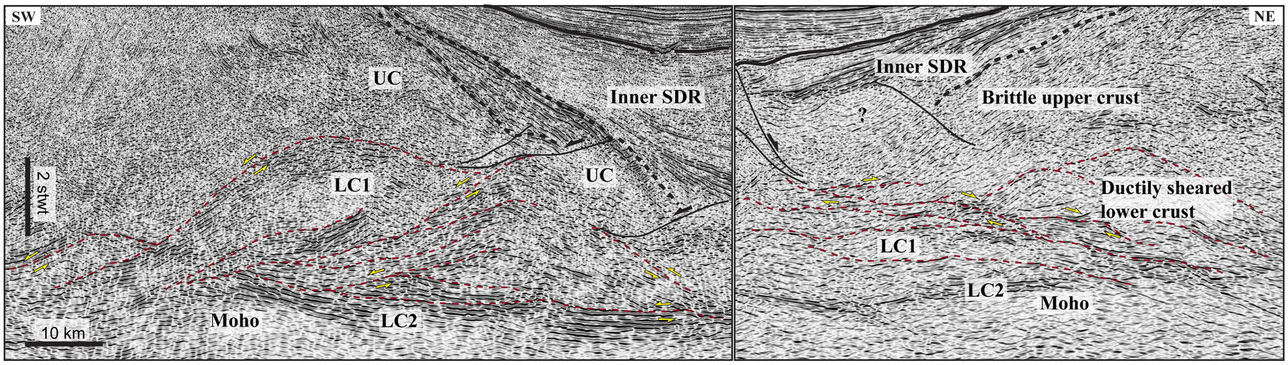

Figure 14. Conjugate view of the ductile and pervasive deformation within the lower crust. Shear bands (red dotted lines) are distributed through the reflective lower crust. The internal fabric display folds and dome-shape structures which is also diagnostic for a solide-state flow of the deep part of the VPM. Not the apparent sense of shear is consistent with continentward-dipping normal faults crosscutting the upper crust (UC) and the seaward tilt of the overlying SDR. See the text for explanation of LC1 and LC2 lower crust.

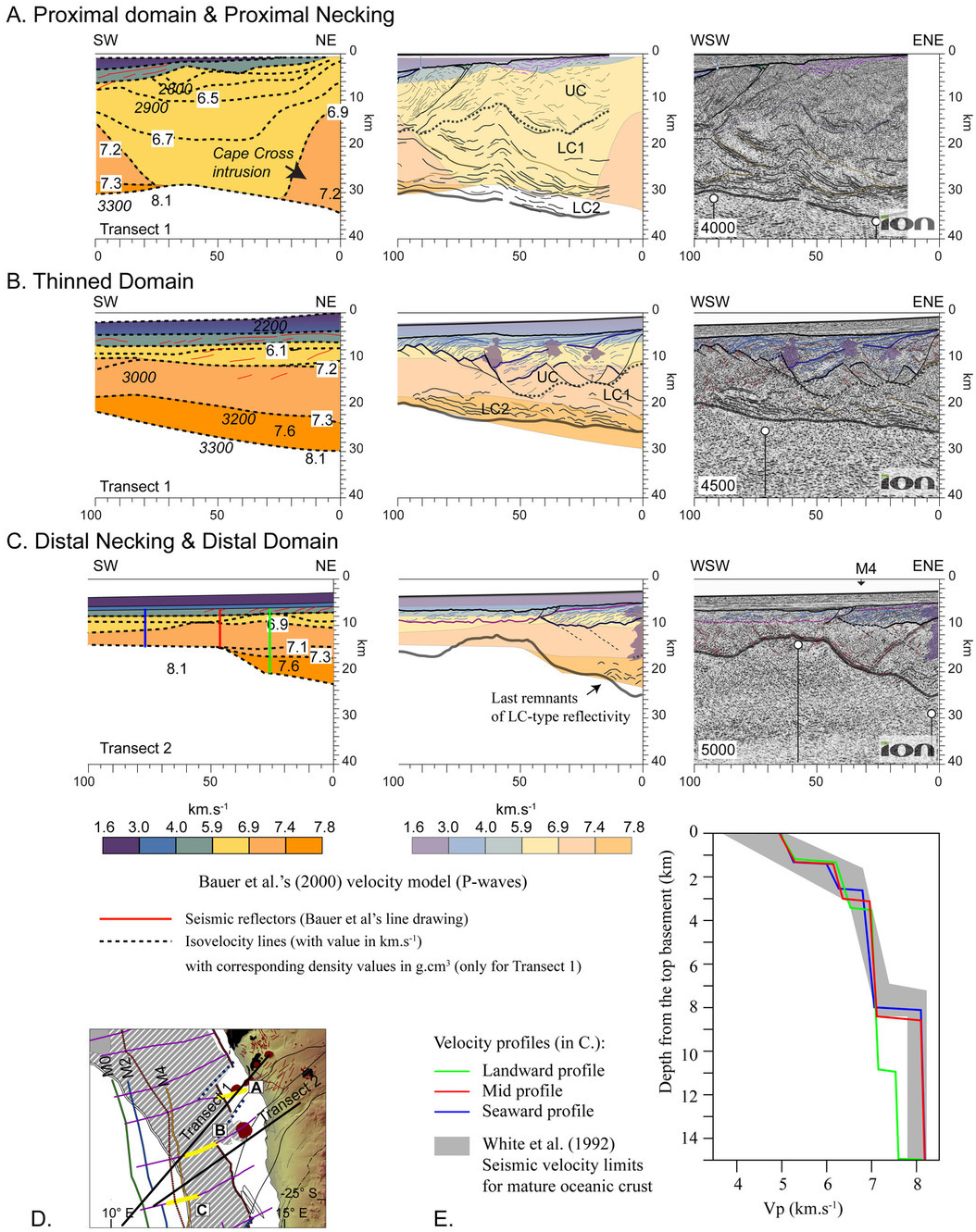

Figure 15. Velocity structure of the Namibian volcanic margin. Bauer et al. (2000) refraction profile (Transect 1 & 2, in left column) plot on top (on central column) of the closest seismic lines (4000 in A, 4500 in B and 5000 in C). A: Velocity model (Transect 1) projected on the Proximal Domain of the line 4000 (location in D). B: Velocity model (Transect 1) projected on the Thinned Domain of the line 4500 (location in D). C: Velocity model (Transect 2) projected on the Distal Necking and Distal Domain of the line 5000 (location in D). D: Map of the location of the displayed seismic (yellow lines) and refraction (thick black lines) data. The undifferentiated SDR domain is plotted in grey-whites strippes together with the magnetic anomalies as picked by Moulin et al (2010) and the Necking Line and the SDR-seaward boundary. E: Depth-Vp plot for the three profiles shown in C. and the seismic velocity limits for mature oceanic crust (grey shading) from White et al. (1992). This diagramm is from Taposeea et al. (2017, redrawn).

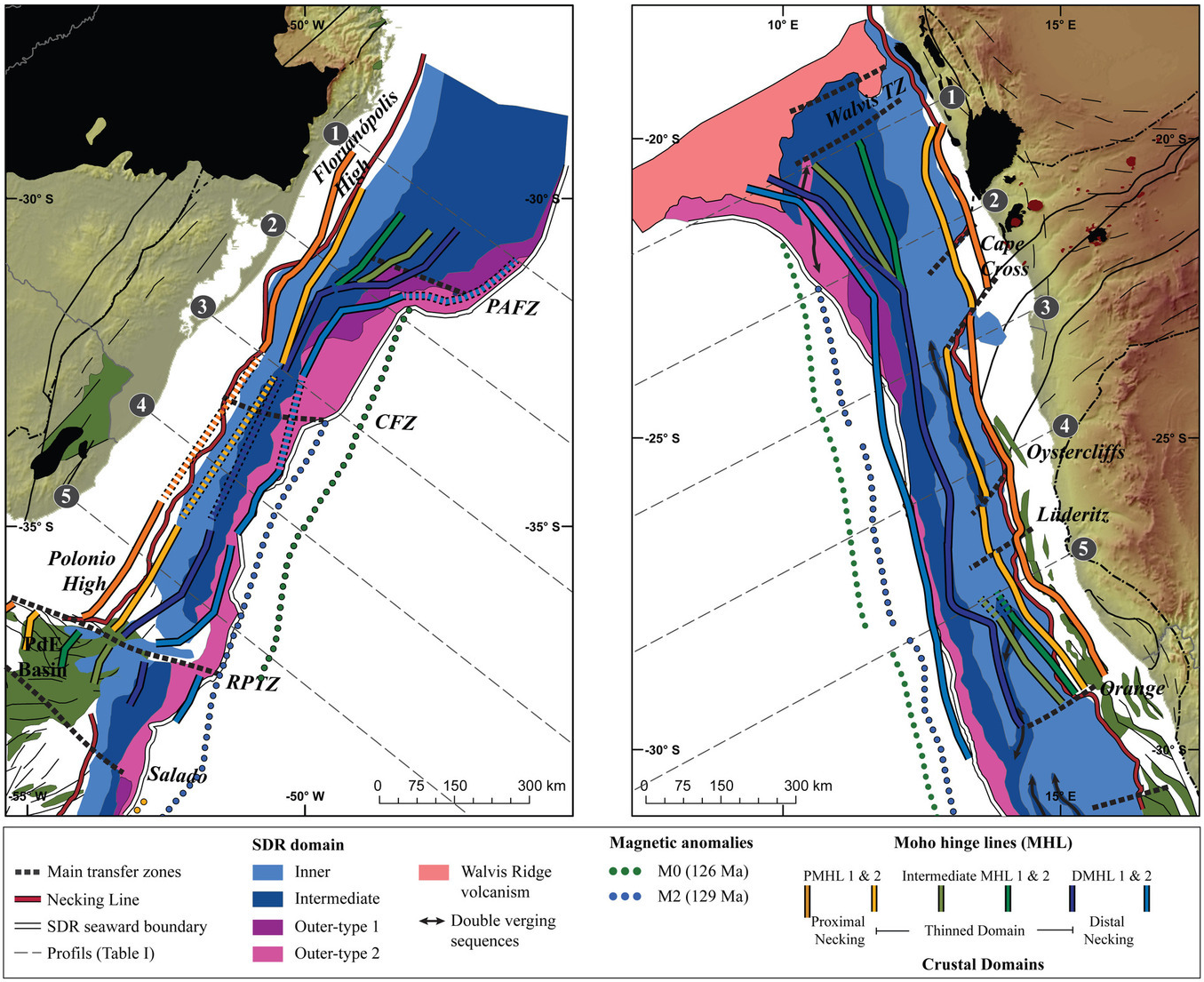

Figure 16. Location of the main crustal domains and related Moho hinge lines over the distribution of the SDR in Uruguay-SE Brazil and Namibia conjugate VPM. The conjugate profiles in dashed lines refer to the measures reported in Table I.

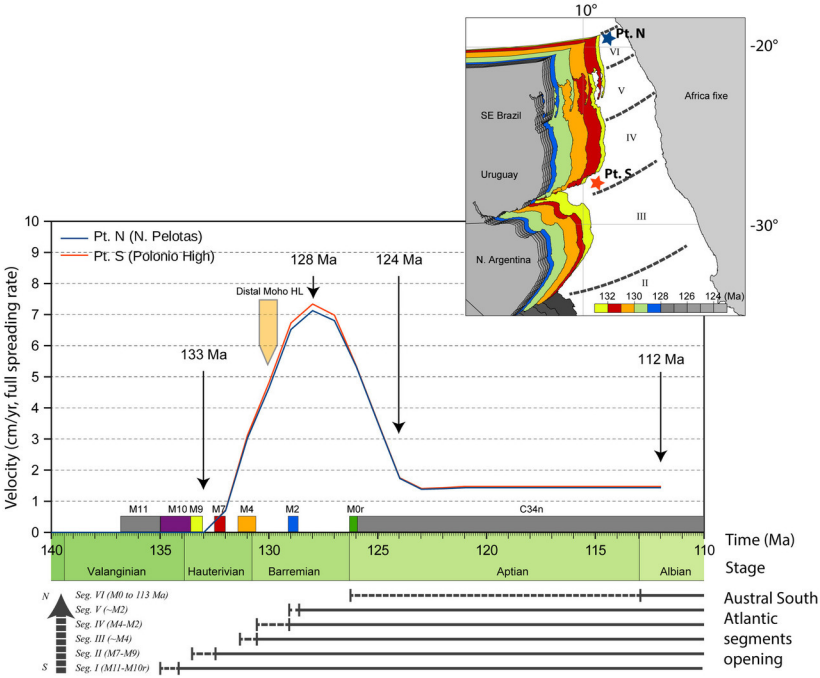

Figure 17. Full spreading rates evolution in austral South Atlantic according to Moulin et al.'s (2010) rotation poles and kinematic model. The two velocities curves are calculated for the N and S extremities of the "la Plata" microplate (Uruguay-SE Brazil) of Moulin et al. (2010) (see the inset map for location). It is noteworthy that no significant difference is observed between these two reference points. The main velocity changes are pointed with an arrow. The age indicated for the distal Moho hinge line 2 and associated crustal thin point is inferred, assessing it corresponds to an isochron located between M4 and M2 anomalies (Fig. 16). The successive openings of the six major SA segments are reported below the graph, in accordance with the data and studies quoted in Fig. 2. The dotted lines segments illustrate the incertitudes related magnetic anomalies duration. The inset map show an animation of the SW-ward drift of the South American microplates of Moulin et al. (2010), between 133 Ma and 124 Ma, relatively to a fixed Africa.

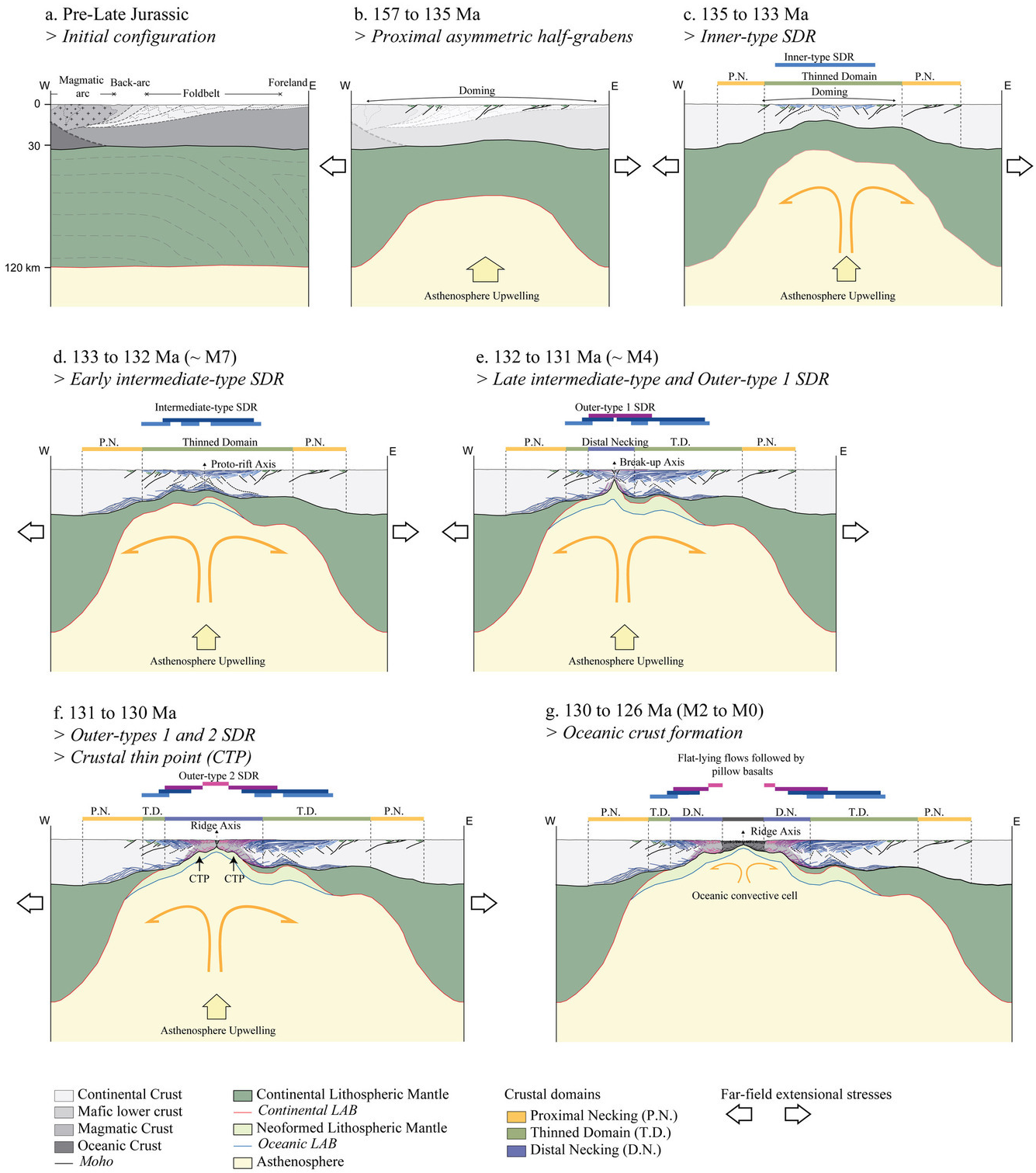

Figure 18. Conceptual evolution of South Atlantic austral segment VPM. The initial stage structural domains from Panafrican belt are redrawn from Basei et al. (2018). LAB: Lithosphere-Asthenosphere Boundary. The proposed timing is adapted for the tectono-magmatic development of the segments IV and V (Fig. 2 for location and Fig. 17 for timing constraints).

Profiles number (from N to S)	Margin width (km)		Inner (km)		Intermediate (km)		Outer-type 1 (km)		Outer-type 2 (km)	
	Ur-Br	**Na**	**Ur-Br**	**Na**	**Ur-Br**	**Na**	**Ur-Br**	**Na**	**Ur-Br**	**Na**
1	300	310	51	100	180	140	40	-	20	99
2	123	244	44	168	60	60	43	30	25	60
3	84	150	32	72	38	27	-	34	88	-
4	97	193	42	136	40	40	-	-	25	9
5	131	172	55	100	41	49	-	-	63	20
Average ± S.D. (all)	147 ± 88	213 ± 64	45 ± 9	115 ± 37	72 ± 61	63 ± 45	42 ± 2	32 ± 3	44.2 ± 30	47 ± 41
Average ± S.D. (2 to 5)	109 ± 22	190 ± 40	43 ± 9	119 ± 42	45 ± 10	44 ± 14	43 ± 9	32 ± 3	50 ± 31	30 ± 27

Table I. Comparison of conjugate profiles based on the criteria of the width of the margin (column 1) and of the width of the different SDR domains (columns 2 to 5). See Fig. 16 for location of e

each profile.